UFL/COEL-89/024

PREDICTION OF SHORELINE CHANGES NEAR TIDAL INLETS

by

Barry D. Douglas

Thesis

1989

PREDICTION OF SHORELINE CHANGES NEAR TIDAL INLETS

By

BARRY D. DOUGLAS

A THESIS PRESENTED TO THE GRADUATE SCHOOL
OF THE UNIVERSITY OF FLORIDA IN
PARTIAL FULFILLMENT OF THE REQUIREMENTS
FOR THE DEGREE OF MASTER OF SCIENCE

UNIVERSITY OF FLORIDA

1989

ACKNOWLEDGEMENTS

I would like to thank my advisor Dr. Robert G. Dean for all of his assistance in completing this thesis; I value him as both a teacher and a friend. The assistance of my other committee members, Dr. Ashish Mehta and Dr. Max Sheppard, is greatly appreciated.

This work was sponsored by Florida Sea Grant; their continued support of the study of coastal problems is appreciated. The data used in this investigation was furnished by the Florida Department of Natural Resources; without this data this study would not have been possible.

I would like to acknowledge my parents for their love and support. They have always encouraged me, even if they did not understand why or what I was doing.

Greg and Margo, Dananimal, Howie, and Bro J are appreciated for their continued friendship. Everyone at the "G": Sue, Kim, Jode, Michelle, Steverino, Rich, Don Juan, Disco, and Will were my family in Gainesville. Thanks for sharing all the good times and bad times. Dud's, the Porp, and Farrah's are appreciated for providing a means to keep my sanity while in school. My fellow coastal students were a source of friendship and help Paul, Steve, Ahn, Kyu-Nam, and Jei. Special thanks go to my fellow LAS members: Sam, Gusty, and Jeff.

Finally, I would like to dedicate this thesis to Orville and Ethel Douglas, and Frank and Roberta Soper. They were not afforded many opportunities in their lives. But because of their hard work and the love they instilled in their families, I have been able to live my life to its fullest extent. I hope they would like what I have achieved so far.

TABLE OF CONTENTS

LIST OF FIGURES

LIST OF TABLES

Abstract of Thesis Presented to the Graduate School
of the University of Florida in Partial Fulfillment of the
Requirements for the Degree of Master of Science

PREDICTION OF SHORELINE CHANGES NEAR TIDAL INLETS

By

BARRY D. DOUGLAS

December 1989

Chairman: Dr. Robert G. Dean
Major Department: Coastal and Oceanographic Engineering

It is well known that tidal inlets tend to cause accretion on updrift shorelines and erosion on downdrift shorelines. This study documented the shoreline changes near several tidal inlets along Florida's east and west coasts. An analytical and a numerical method were used to attempt to predict the shoreline changes downdrift of these inlets.

The analytical method is based on Pelnard-Considere's solution for the combined continuity and transport equation. This solution used simple boundary conditions and a constant breaking wave height and wave direction. It was found that this solution could predict shoreline changes associated with rapidaly eroding downdrift shorelines. If refraction over offshore shoals of diffraction around jetties influenced the downdrift shorelines, this solution could not predict accurately the shoreline changes.

An implicit numerical model was developed that used monthly wave heights and wave directions to model transport reversals. The model also contained diffraction and refraction routines. It was found that the best results were obtained for Ft. Pierce Inlet for an offshore bathymetry which represented the pre- and post-inlet cutting contours. This model could not predict accurately a sheltered zone adjacent to the south jetty due to a lack of wave breaking on the offshore shoal.

A detailed qualitative analysis of the effects of refraction due to tidal currents on the net longshore transport was also completed. It was found that the currents affect the net longshore transport for a considerable distance updrift and downdrift of the inlet. The currents tend to increase updrift accretion and decrease downdrift erosion.

CHAPTER 1
INTRODUCTION

1.1 Purpose of Study

The Florida coastline consists of long, narrow barrier islands separated by inlets, maintained by tidal flows. These inlets are openings which connect sheltered areas behind the barrier islands to the open ocean. This thesis presents methods to predict shoreline changes near tidal inlets, with emphasis placed on shorelines downdrift of the inlets. Tidal inlets are dynamic features which in most cases affect adjacent shorelines. The inlet is dynamic because of changing conditions of tidal flow, wave action, sediment transport, and human modifications for navigation purposes. The inlet and associated processes interfere with the natural movement of the longshore transport of sediment. The usual result, for jettied inlets, is that the downdrift shorelines experience erosion and the updrift shorelines experience accretion. This results in shorelines in the vicinity of inlets to be subject to considerable change as compared to shorelines on the open coast away from the influences of inlets. Reported rates of shoreline erosion near inlets indicate that they can be on the order of one to two times higher than areas remote from inlets (Walton and Adams, 1976). This study investigated methods to predict the erosion of the downdrift shorelines, and further understand the natural processes affecting the inlet.

The first method used is an analytical solution developed by Pelnard-Considere. This solution was adapted to fit the case of an inlet which would block a net longshore transport. This solution uses a constant wave height and wave direction, and assumes simple boundary conditions. The second method used is a numerical model with very specific boundary conditions. This model incorporates refraction and diffraction. Monthly wave heights from wave gages and wave directions from littoral drift roses are also used as inputs. Many inlets

are studied and comparisons are made for inlets with different coastal processes affecting them.

1.2 Background

Along Florida's eastern coast there are 19 tidal inlets from St. Mary's Entrance at the Florida-Georgia border to Government Cut at Miami beach. Along Florida's west coast there are a total of 37 inlets from Pensacola Bay Entrance near the Alabama border to Caxambas Pass at the south end of Marco Island. On the east coast the predominant drift is to the south and generally decreases from north to south, along the west coast transport varies in magnitude and direction.

At natural inlets shallow, wide offshore bars exist which act like sand bridges that allow the sediment to flow across the inlet mouths. A quasi-equilibrium exists at these natural inlets, between the updrift and downdrift shorelines. An inlet would stay open in a location where the tidal flow was sufficient to maintain the opening against longshore transport which acts to close the inlet (Bruun and Gerritsen, 1959). Natural inlets migrated and posed serious navigation hazards, most of these inlets have been modified for navigation or water quality purposes. These modifications include deepening of entrance channels, construction of jetties, and dredging. All of these modifications are intended to maintain a deepened fixed channel. While maintaining the inlet, these modifications interfered with the quasi-equilibrium that existed at the natural inlet, resulting in changes to the adjacent shorelines. The modified inlet interrupts the longshore transport and can act as a sediment sink.

The maintenance of navigational channels will also affect the adjacent shorelines. Deepened channels cut through the natural offshore bar which transferred sand across the inlet mouth. The inlet system will attempt to refill the channel and return to its quasi-equilibrium state. Sediment which is deposited in this deepened channel is removed from the longshore transport system. This removed sand results in a deficit of sand from the adjacent shores; erosion will have to occur to make up for this deficit. Often dredging is used to maintain

the channel, if the dredged material is not reintroduced to the system downdrift of the inlet, erosion will also occur to account for the deficit of material.

Jetties also affect the inlet and adjacent shorelines. All the inlets on the east coast except Nassau Sound and Matanzas Inlet have been jettied. Jetties generally cause an impoundment of sand updrift of the structure and erosion downdrift. The jetties decrease the amount of sediment entering the inlet and also move sediment offshore. The effect is the same as mentioned above, a sediment deficit occurs which will result in downdrift erosion to account for the missing volume of sand.

The above-mentioned modifications work together with other factors such as shoals and transport reversals to make an inlet and adjacent shores a very complex physical system.

CHAPTER 2
APPROACH

2.1 Shoreline Change Data

The Division of Beaches and Shores of the Florida Department of Natural Resources (DNR) maintains permanent monuments along counties with predominantly sandy shorelines. These monuments are spaced approximately every 1000 feet along the shoreline, a total of 3,428 monuments have been established. As an example, figure 2.1 shows St. Lucie County with the locations of the DNR monuments noted. Surveys using these monuments were started in 1971 and continue up to the present. Historic shoreline maps and aerial photos which pre-date 1971 have been digitized and combined to yield shoreline positions referenced to the DNR monuments. The resulting data base available from DNR consists of shoreline positions given in state plane coordinates which date back to before the turn of the century and continue up to the present.

These DNR shoreline change data were compared to analytical and numerical results in this study. Shoreline changes were calculated using the first post cut survey and the most current pre-nourishment survey. Shoreline positions were referenced with the inlet center as $x = 0.0, y = 0.0$. Shoreline positions from this reference were determined for each survey. These positions were then interpolated to common evenly spaced intervals. The resulting data were a set of shoreline changes at evenly spaced longshore increments with the origin at the inlet.

2.2 One Line Theory

Both the analytical and numerical models presented in this paper are based on what is known as one line theory. The beach profile is assumed to maintain its equilibrium form.

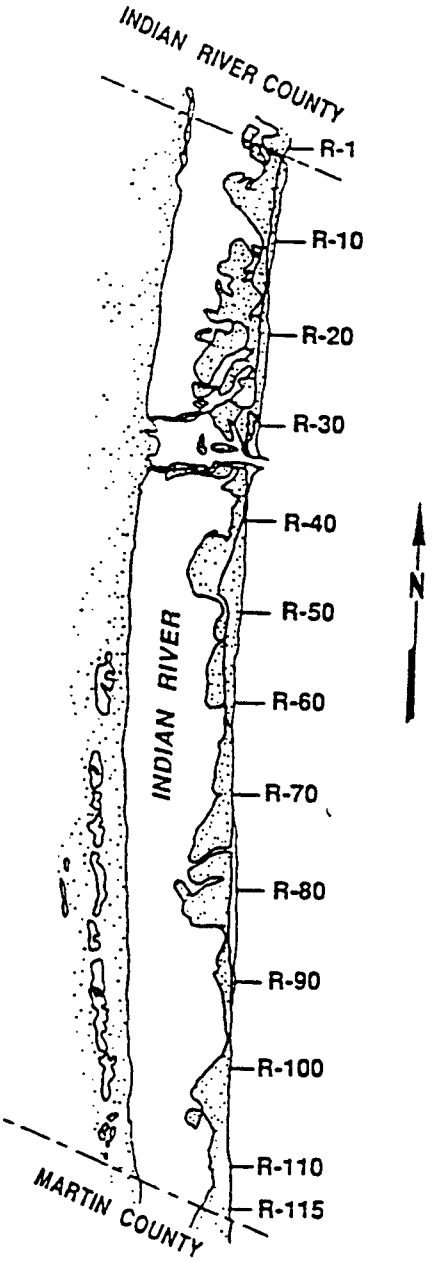

Figure 2.1: DNR Monuments Located in St. Lucie County

This implies that the profile is displaced horizontally without change of form. The entire profile moves uniformly when responding to changes, therefore only "one line," usually taken as the shoreline needs to be considered. One line theory attempts to describe long term variations in shoreline positions.

One line theory can not predict accurately short term variations such as storm conditions which are regarded as disturbances superimposed on the long-term general trend.

2.3 Pelnard-Considere Solution

The analytical solution used in this study is adapted from a solution to the combined transport and continuity equation first developed by Pelnard-Considere (Pelnard-Considere, 1956). The Pelnard Considere formulation can be applied to the prediction of the accumulation of sand updrift of a littoral barrier extending perpendicularly from an initially straight and uniform shoreline. Waves of uniform height and direction arrive obliquely to the shoreline and cause a transport of sediment. At the littoral barrier the transport equals zero, trapping all sediment up to bypassing. This requires the local shoreline at the barrier to be oriented parallel to the incoming wave crests. At large distances updrift and downdrift of the barrier the shoreline is unaffected by the presence of the structure.

Figure 2.2 shows the resulting shoreline evolution of accumulation updrift and erosion downdrift with increasing time. Note that the planforms on the two sides of the barrier are antisymmetric, at all times the accreted volume of material updrift of the barrier equals the eroded volume of material downdrift of the barrier. This is an indication that the Pelnard Considere solution is an odd solution and has no even component.

This solution was used to predict shoreline positions downdrift of an inlet. It was assumed that an inlet acts very similar to a littoral barrier by interrupting the longshore transport. The boundary condition was interpreted to be that no transport would pass through the inlet; this would be analogous to an infinitely long littoral barrier which never achieves bypassing. The same restriction, that at large distance away the shoreline would be unaffected by the presence of the inlet remained, and the local shoreline at the inlet

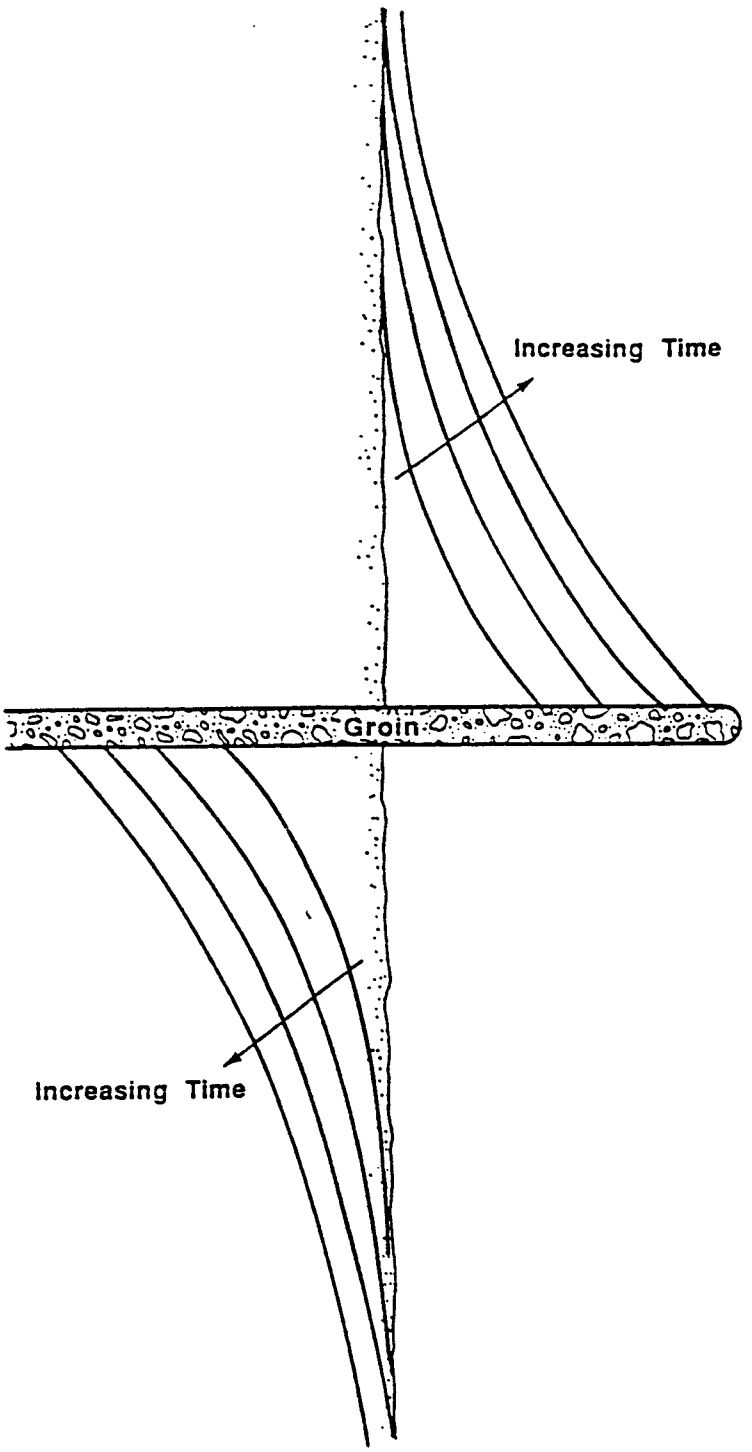

Figure 2.2: Shoreline Near Littoral Barrier

would be parallel to incoming wave crests. The positive accretional shoreline change values for the littoral barrier are equal to the negative erosional values downdrift of an inlet.

2.4 Numerical Modeling

Shoreline evolution can be predicted by the use of a finite difference numerical model. It is not possible to develop analytical solutions for the full equations of transport and continuity. The analytical solution mentioned previously was also limited by very broad or general boundary conditions. Physical parameters such as variable wave direction and height, sediment loss to the inlet, and diffraction could not be accounted for with the analytical solution. Also the solution was odd, resulting in the updrift and downdrift shorelines being antisymmetric images of each other. The use of a finite difference technique to approximate the governing equations allows arbitrary boundary conditions and inputs.

The simplest form of a shoreline evolution model is the explicit model, in which the transport and continuity equations are solved sequentially. The region of interest is divided up into an incremental longshore grid system (see fig. 2.3). Shoreline positions are determined at the grid centers and the transport values are calculated for the grid lines. Transport is calculated using two adjoining grid mid points to determine the local shoreline orientations from the previous time step. The shoreline positions at the grid midpoints for the present time step are calculated using these transport values with the continuity equation. Simply stated, if the transport leaving a grid is greater than the transport entering the grid the shoreline position erodes, and if the transport leaving the grid is less than the transport entering the grid the shoreline accretes.

Since the explicit model relies on information from the previous time step, it can be susceptible to stability problems. If the time step is large a substantial shoreline change can occur for a relatively small difference in transport values. This large change in shoreline position will result in an offset from the adjacent grids. These offsets would tend to transport sediment in the opposite direction during the next time step, thus leading to the possibility of an oscillating unstability. With successive time steps the displacement would grow and

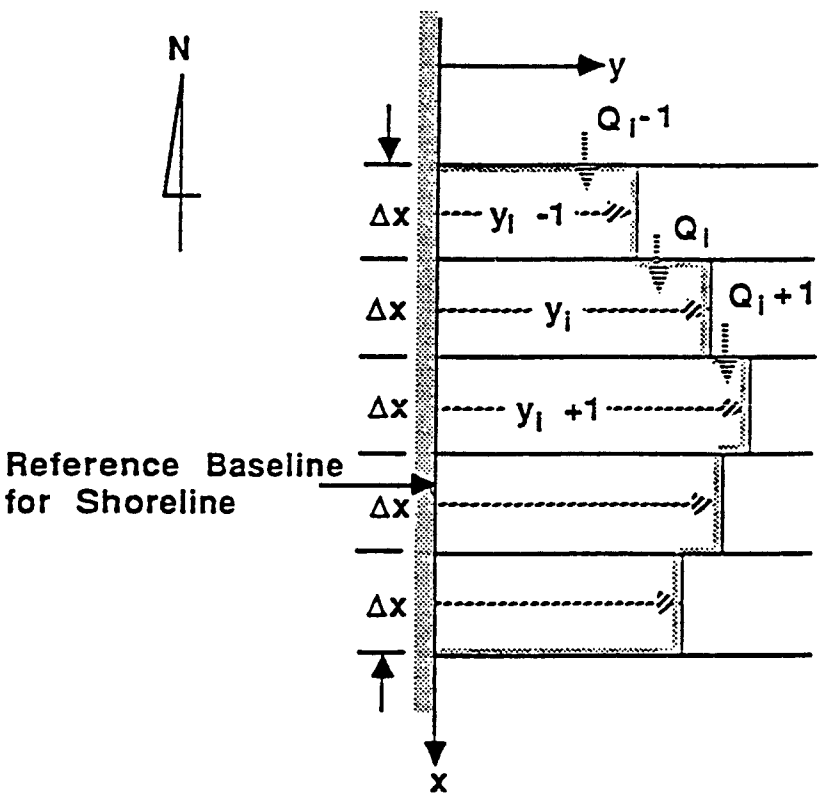

Figure 2.3: Numerical Model Grid System

alternate as accretion and erosion. This oscillation will tend to propagate throughout the grid system and cause the entire region to become unstable. To prevent this instability from occurring there are limits to the size of time step and the length of the incremental grid spacing that can be used.

An implicit model does not have the stability problem of an explicit model and therefore has no restrictions on grid spacing or time step used in the model. The major difference between the implicit and explicit model is that the implicit model solves the transport and continuity equations simultaneously instead of sequentially. The continuity equation is expressed in terms of the average of the transport for the present time step and the next time step. The transport equation is expressed in terms of the average shoreline positions for the present and next time step. Both of these equations then can be represented as an expression of known quantities at the present time step, equated to unknown quantities of the next time step. The result is four unknowns and two equations. With the introduction of two auxiliary equations and appropriate boundary conditions a double sweep algorithm can be used to solve simultaneously the transport and continuity equations.

2.5 Refraction

Wave celerity is dependent upon the water depth in which the wave propagates. Wave speed and wave length decrease as the depth decreases, while the wave period remains constant. When a wave moves over varying bathymetry, the wave crests which pass over the shallower depths will slow down. This decrease in wave speed will cause the waves to bend, becoming more parallel to the bottom contours. This bending of waves is known as refraction. The change in depth will also cause a change in wave height through the process of wave shoaling. These changes result in a convergence or divergence of wave energy.

At inlets a common feature is an offshore shoal. Incoming waves, regardless of direction, will refract around the shoal. The resulting longshore currents will be directed towards the region centered behind the shoal, causing a accumulation of sediment in this region. If the waves are sufficiently large relative to the water depth over the shoal, wave breaking will

occur resulting in a local sheltering of the shoreline. Wave interaction with currents can also cause refraction to occur. If currents interact with waves, the refraction has similar effects of altering wave height and direction.

2.6 Diffraction

Diffraction of water waves is an event in which energy is transferred laterally along a wave crest. It is most common when a regular train of waves is interrupted by a barrier such as a jetty or a breakwater. If transfer of energy did not occur, straight waves passing the tip of the barrier would leave an unaffected calm region in the lee of the barrier. Past the edge of the barrier the waves would travel unchanged, creating a line of discontinuity. Diffraction will alter both the wave height and wave direction.

When waves approach a jetty at an angle, a shadow zone will be created in the lee of the structure as shown in figure 2.4. This shadow zone will be an area of sheltering, with decreased wave energy and altered wave direction and reduced longshore transport.

2.7 Shoaling Processes at a Tidal Inlet

The tidal flows which keep an inlet open are the ebb tide which directs tidal currents seaward and the flood tide which directs tidal currents landward. The flood tide removes material from the longshore drift and deposits it in the calm bay or lagoon behind the inlet. The ebb tide pushes material back through the inlet, also removing sediment from the longshore drift, and deposits it seaward of the inlet.

The ebb flow pushes sediment offshore, while wave attack tends to drive material back towards the inlet. This material is usually deposited in a crescent or kidney shape planform. The ebb currents have a central core with a high velocity, producing an ebb jet which can carrying sediment a considerable distance offshore. Jetties and deepened channels concentrate the ebb flow and move the ebb shoal even farther offshore (Marino and Mehta, 1989). The net longshore currents will move the sediment downdrift from the inlet. The resulting feature is an offshore shoal which is offset offshore and downdrift from the inlet.

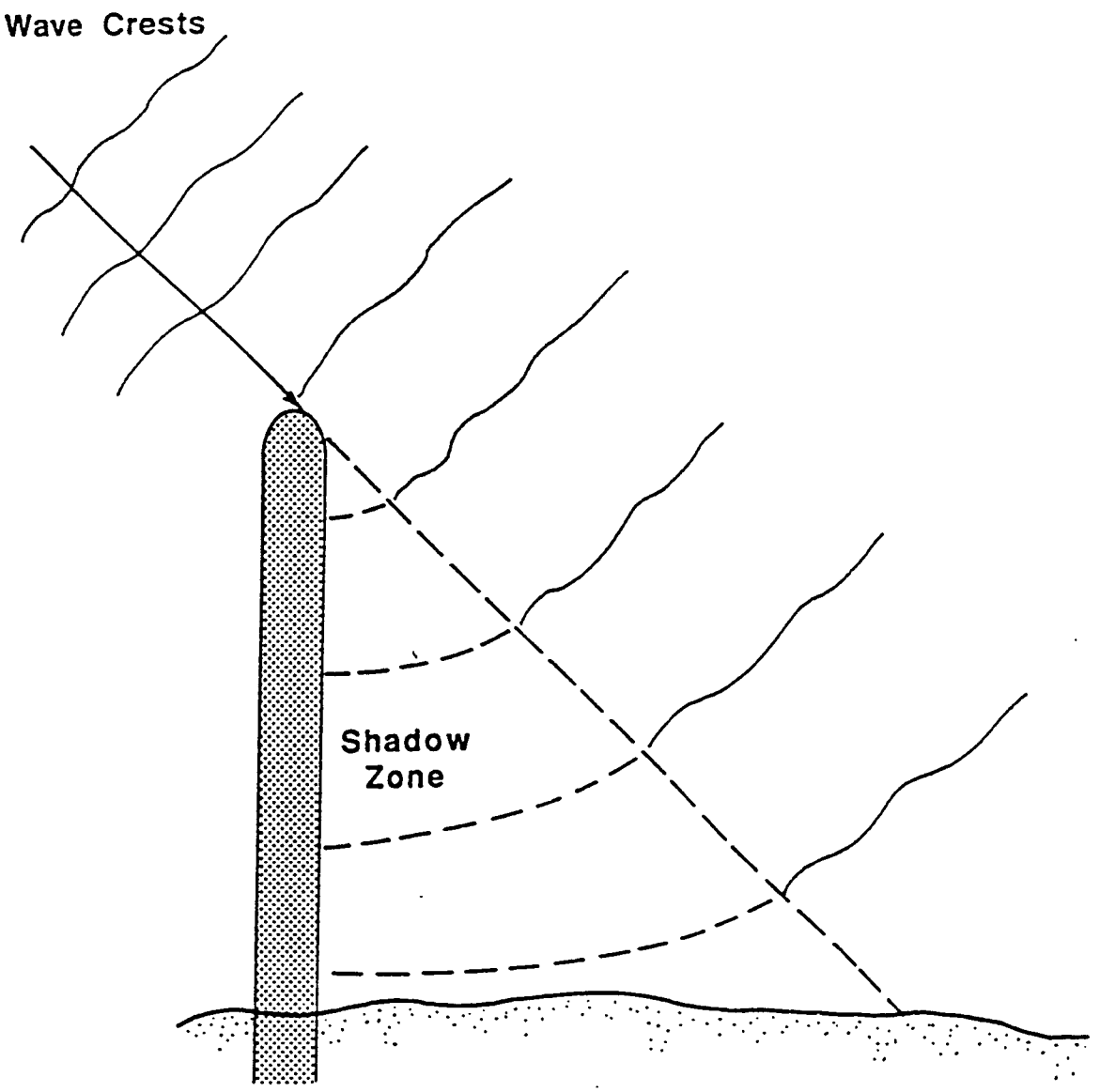

Figure 2.4: Diffraction Patterns Behind a Jetty

The local longshore currents adjacent to the inlet are directed towards the inlet during both flood tide and ebb tide (O'Brien, 1966). On the flood tide, sediment is moved towards the inlet from all directions. On the ebb tide, the momentum of the strong ebb jet entrains adjacent waters forming eddies. These eddies cause circulation cells which move sediment towards the inlet, even though the ebb flow is directed away from the inlet. The currents associated with the ebb and flood tide are shown in figures 2.5, 2.6. Refraction around this outer bar will also move sediment towards the inlet from both sides. The ebb shoal alters incoming waves and tidal currents in such a way to affect the transport systems near an inlet. The presence of the ebb shoal is important in investigating the shoreline evolution near inlets.

The shoaling that occurs at inlets is due to the forces of tidal currents and wave action. After a period of time these forces become somewhat balanced and an equilibrium shoal system will be formed. In an area of high wave energy the offshore shoal volume will be relatively small, while in areas of small wave energy the shoal volumes will tend to be larger (Dean and Walton, 1973). Marino and Mehta (1989) have estimated that 420 10^6 $meters^3$ of material is stored in ebb shoals along Florida's east coast. The general trend is for decreasing shoal size from the Georgia border south towards Government Cut. This also corresponds to decreasing shelf width, decreasing wave energy and decreasing longshore transport. These authors also reported that most of the volume is stored in shoals north of St. Lucie Inlet.

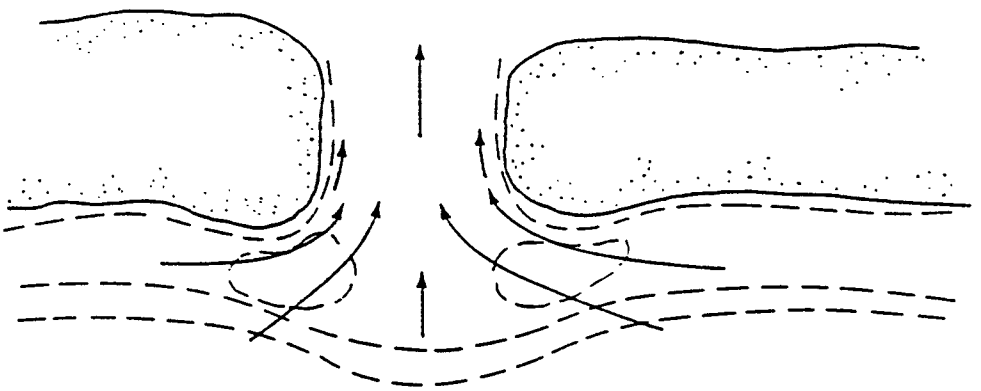

Figure 2.5: Flood Current at an Inlet

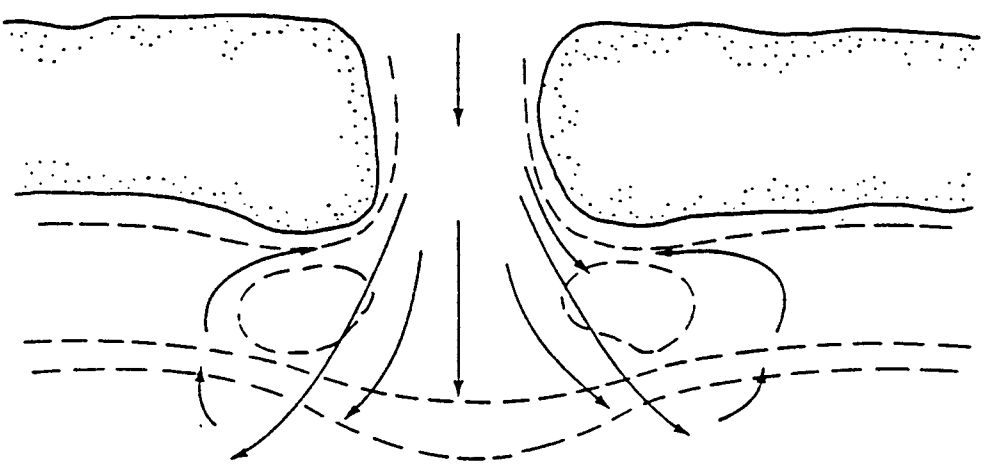

Figure 2.6: Ebb Current at an Inlet

CHAPTER 3
ANALYTICAL METHODOLOGY

3.1 Combined Continuity and Transport Equation

The analytical method used in this study is a solution to the combined continuity and transport equations. As shown in figure 3.1 for an incremental length, Δx, of shoreline the change in volume of sand can be expressed as the product of the change in transport through the region, ΔQ, and time. This change in volume is

$$\Delta V = (\Delta Q)(\Delta t) \tag{3.1}$$

This change in volume can also be expressed as a product of the length dimensions of the region.

$$\Delta V = (\Delta x)(\Delta y)(D) \tag{3.2}$$

In this equation Δy is the change in shoreline position, and D is the vertical dimension of the active profile.

These two expressions (eqns. 3.1 and 3.2) both represent the same change in volume and when equated, the one-line continuity equation results (eqn. 3.3).

$$-\frac{1}{D}\frac{\partial Q}{\partial x} = \frac{\partial y}{\partial t} \tag{3.3}$$

The other equation needed to form the combined continuity, dynamic equation is the equation for transport, a common expression for transport is equation 3.4.

$$Q = Q_o \sin(2\theta) \tag{3.4}$$

where

$$Q_o = \frac{K H_b^{5/2} \sqrt{g/\kappa}}{16(s-1)(1-p)} \tag{3.5}$$

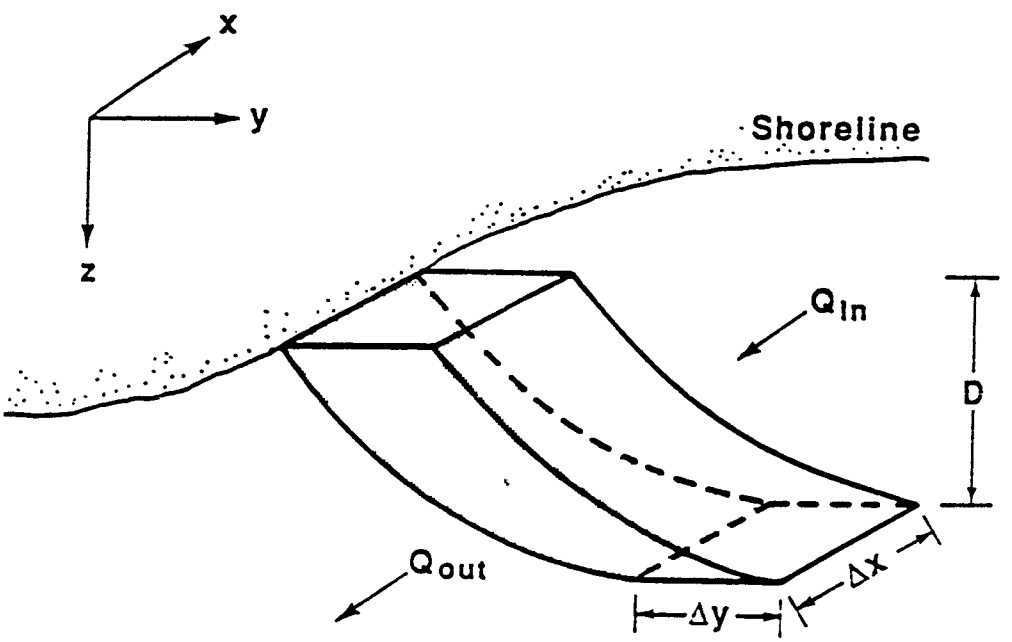

Figure 3.1: Control Volume Along the Shoreline

K =0.77, sediment transport factor

g =acceleration due to gravity

H_b =breaking wave height

κ =0.78, the ratio of breaking wave height to breaking depth

s =2.65, specific gravity of sediment

p =0.35, porosity of the sediment

θ =angle between wave crests and the shoreline

The angle between the breaking wave crests and the shoreline can be expressed as the difference between, β the shoreline orientation, and α_b the breaking wave angle.

$$\theta = \beta - \alpha_b \tag{3.6}$$

The shoreline orientation, β can be expressed as the change in the local shoreline position, as shown in figure 3.2.

$$\beta = -\tan^{-1}\left(\frac{\partial y}{\partial x}\right) \tag{3.7}$$

Substituting this into the transport equation (eqn. 3.5),

$$Q = Q_o \sin\left[2\left(-\tan^{-1}\left(\frac{\partial y}{\partial x}\right) - \alpha_b\right)\right] \tag{3.8}$$

If the angles involved are small the inverse tangent term can be approximated by equation 3.9.

$$\beta = -\frac{\partial y}{\partial x} \tag{3.9}$$

The continuity equation (eqn. 3.3) contains the derivative of transport with respect to the longshore direction. This derivative can be expressed as the following:

$$\frac{\partial Q}{\partial x} = Q_o 2 \cos\left[2\left(\beta - \alpha_b\right)\right]\frac{\partial \beta}{\partial x} \tag{3.10}$$

If the cosine term is assumed to be unity for small angles the derivative can be simplified.

$$\frac{\partial Q}{\partial x} = Q_o(2)(-\frac{\partial^2 y}{\partial x^2}) \tag{3.11}$$

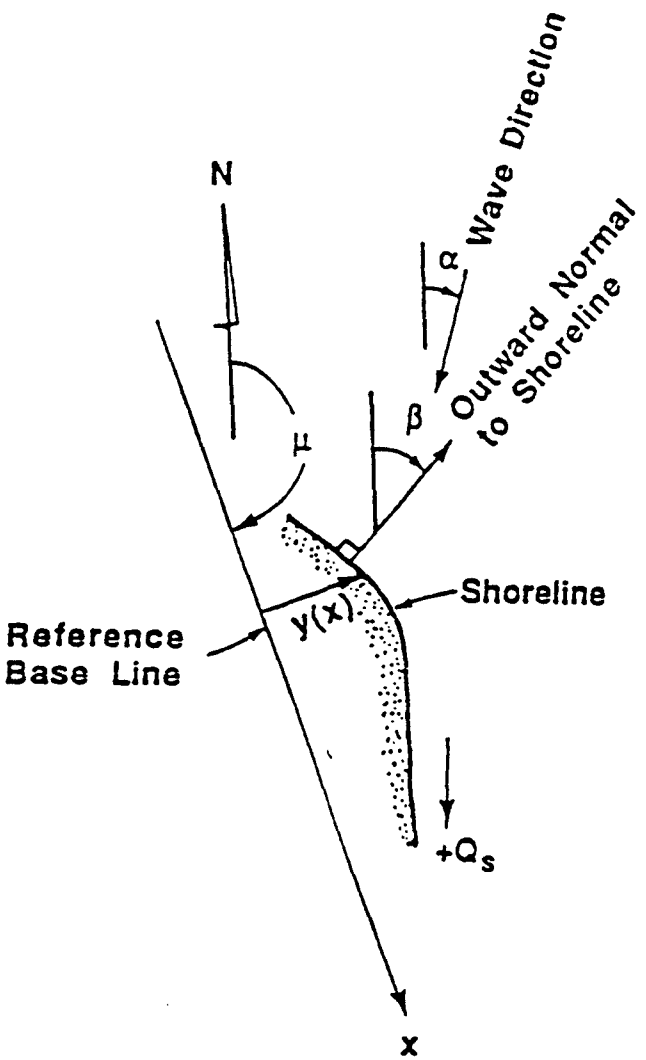

Figure 3.2: Shoreline Orientation and Wave Angle

Substituting this derivative into the continuity equation (eqn. 3.3) results in the linearized combined continuity and dynamic equation.

$$\frac{\partial y}{\partial t} = G\frac{\partial^2 y}{\partial x^2} \tag{3.12}$$

$$G = \frac{2Q_o}{D} = \frac{K H_b^{5/2}\sqrt{g/\kappa}}{8(s-1)(1-p)D} \tag{3.13}$$

Equation 3.12 is the heat conduction equation for solids, also known as the diffusion equation. G has the dimensions of length squared per unit time, and expresses the time scale of shoreline change. In the english unit system G has the value of $0.0214(H_b^{5/2})\text{ft}^2/\text{sec}$, for a closure depth of 27 feet. This equation has many solutions depending on the boundary and initial conditions used. The solution by Pelnard Considere, mentioned earlier, has the following form and is valid up to the occurrence of bypassing around the structure.

$$y(x,t) = \frac{\tan\theta}{\sqrt{\pi}}\left[\sqrt{4Gt}\exp\left(\frac{-x^2}{4Gt}\right) - x\sqrt{\pi}\,\text{erfc}\left(\frac{x}{\sqrt{4Gt}}\right)\right] \tag{3.14}$$

The last term contains erfc, which is the co-error function and is defined as the following.

$$\text{erfc} = 1 - \text{erf} \tag{3.15}$$

$$\text{erf}(z) = \frac{2}{\sqrt{\pi}}\int_0^z \exp(-u^2)\,du \tag{3.16}$$

The error function equals zero when the argument is zero, and approaches unity for large arguments.

The boundary conditions are that at points far updrift and downdrift of the barrier the shoreline remains unaffected, $y = 0.0$ at $x = \pm\infty$. The initial condition is that the shoreline is straight and uniform. The shoreline at the barrier is parallel to incoming wave crests.

This condition can be seen by taking the derivative of equation 3.14 with respect to x. The derivative of the error function with respect to its argument is the following.

$$\frac{\mathrm{d}\,\text{erf}(z)}{\mathrm{d}u} = \left(\frac{2}{\sqrt{\pi}}\right)\left(\frac{\mathrm{d}z}{\mathrm{d}u}\right)\exp(-z^2) \tag{3.17}$$

The derivative of y with respect to x is the following.

$$\frac{\partial y}{\partial x} = \frac{\tan\theta}{\sqrt{\pi}}\left[\frac{-2x}{\sqrt{4Gt}}\exp\left(\frac{-x^2}{4Gt}\right) - \sqrt{\pi}\,\text{erfc}\left(\frac{x}{4Gt}\right) + \frac{x}{2Gt}\exp\left(\frac{-x}{4Gt}\right)^2\right] \tag{3.18}$$

By substituting zero for x in equation 3.18 the derivative will equal the slope of the shoreline at the barrier.

$$\left(\frac{\partial y}{\partial x}\right)_{x=0} = \frac{\tan\theta}{\sqrt{\pi}}[0.0 - \sqrt{\pi} + 0.0] \tag{3.19}$$

$$(\frac{\partial y}{\partial x})_{x=0} = -\tan\theta \tag{3.20}$$

Thus showing that the shoreline at the barrier is parallel to incoming wave crests.

3.2 Predicted Results

Equation 3.14 presented in the last section was used to predict shoreline changes which were compared to measured DNR data for several inlets. The comparisons of predicted results and measured data were made for shoreline change values; not actual shoreline positions. This method was used because the analytical solution assumes a straight and uniform initial shoreline and then determines shoreline change from this initially straight shoreline. Thus only a change from the shoreline at the time of the cut could be computed. The comparison procedure was to compute the shoreline changes between two post-cut DNR surveys and to determine predicted shoreline changes using equation 3.14 for the corresponding time spans. For example, St. Lucie Inlet was cut in 1892 and the surveys used are for 1928 and 1970. The 42 year shoreline change , $y_{measured}$, was determined as the change in shoreline position from 1928 to 1970.

The predicted shoreline change, $y_{predicted}$, was determined as the difference between the shoreline computed for 1970 and the computed shoreline for 1928.

$$\Delta y_{predicted} = y(x, 78_{years}) - y(x, 36_{years}) \tag{3.21}$$

Where the zero reference time in the above equation is 1892. The form of the solution used produces negative or erosional shoreline positions, therefore the change is represented by its difference from 1970 to 1928.

The measured DNR data were in the form of northing and easting positions for each monument, an azimuth of the survey, and a northing and easting position of the mean high water line.

3.3 Least Squares Analysis

The last step needed to compare the measured data to the predicted results was to determine the proper values of G and $\tan\theta$ to be used in the analytical solution. This solution uses a constant G and θ for a specified time value to predict the shoreline position. The only unknowns in this equation are G and $\tan\theta$, and these unknowns are held constant. G is a function of the wave height to the 5/2 power; small changes in the breaking wave height cause large fluctuations of this constant. It was found that the solution was very sensitive to changes in either G or θ. Figure 3.3 shows three predicted shoreline planforms about a littoral barrier for a time span of ten years with no bypassing. The updrift shore is represented by negative distances, and the downdrift shoreline is represented by positive values. A shoreline was calculated for a constant G for a wave height of 1 foot and a θ of 5 degrees, for the second case the θ was held constant and the wave height increased to 2 feet. The last case examined used a G for a wave height of 1 foot and increased the breaker angle θ to 10 degrees. By increasing the variables, drastically different shorelines resulted. Doubling the wave height increased the G constant by a factor of approximately 5.5, and doubling the wave direction doubles the $\tan\theta$ constant. It can be seen that by doubling either variable increased the shoreline change at the barrier by more than a factor of two. Accurate values of G and $\tan\theta$ were needed to predict the shoreline change.

One G value and one θ value had to be chosen to represent the entire shoreline region for the entire time span studied for each inlet. It was decided that determining a net wave height and direction for large time spans of up 50 years would be very inaccurate and a better approach would be to determine best fit values of G and $\tan\theta$. A non-linear least squares method was developed to determine a G, $\tan\theta$ pair that would yield the best fit possible for the predicted results.

An iterative procedure was used that assumed the predicted shoreline position was the position of the last iteration plus an increment due to the $tan\theta$ and another increment due

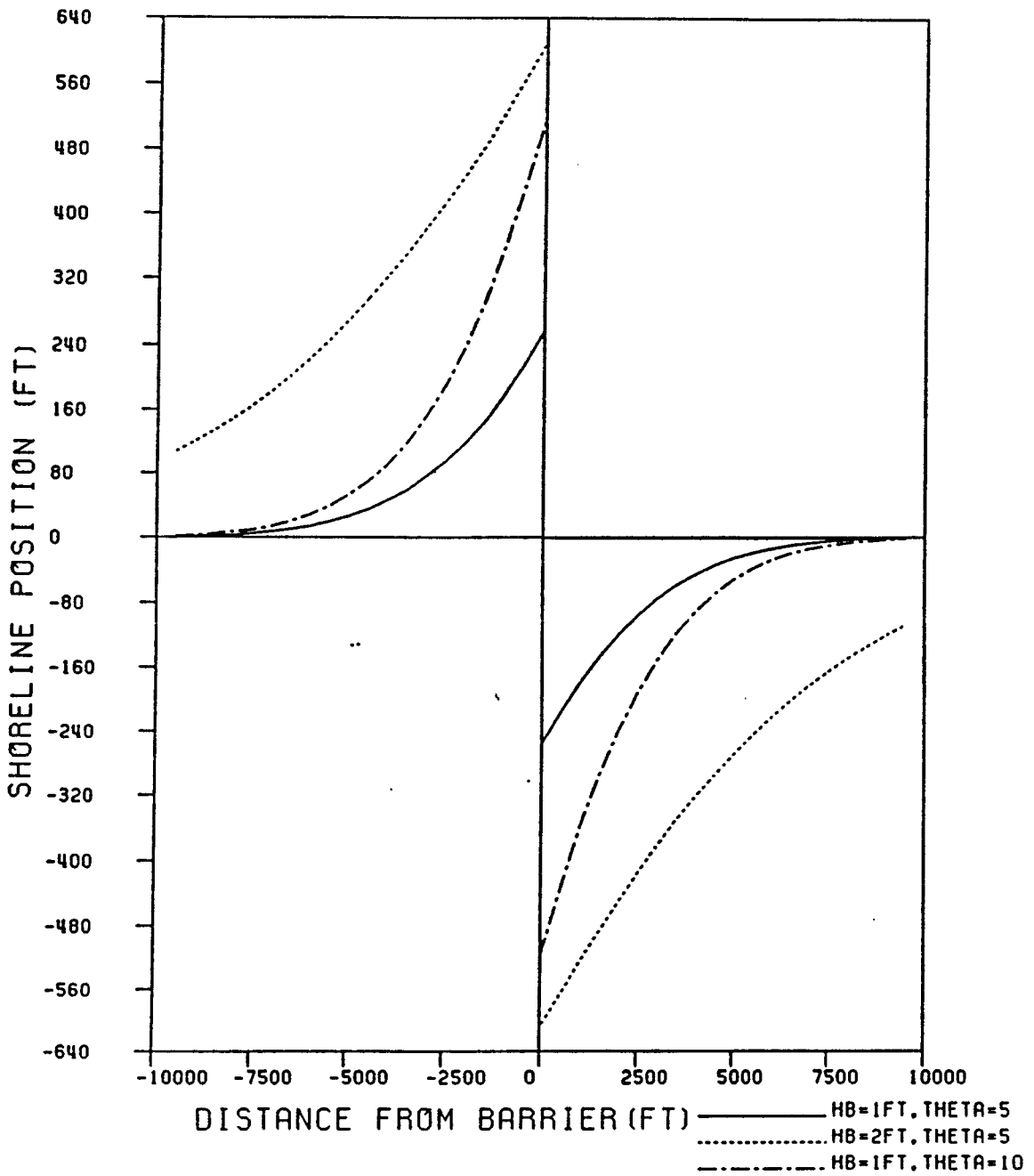

Figure 3.3: Comparison of Shorelines for Different G and $\tan\theta$ Values

to the G constant (eqn. 3.22).

$$y^{k+1} = y^k + \frac{\partial y^k}{\partial G}\Delta G + \frac{\partial y^k}{\partial \tan\theta}\Delta(\tan\theta) \tag{3.22}$$

In equation 3.22 the superscript k denotes the iteration level. The least squares error then becomes the following.

$$\varepsilon^2 = \frac{1}{I}\sum\left[\left(y_{p_i}^k + \frac{\partial y_{p_i}^k}{\partial G}\Delta G + \frac{\partial y_{p_i}^k}{\partial \tan\theta}\Delta\tan\theta\right) - y_{measured}\right]^2 \tag{3.23}$$

I denotes the total number of points and k represents the iteration, and the unknowns are ΔG and $\Delta\tan\theta$.

An initial G and $\tan\theta$ value had to be assumed. Using these values, derivatives of y with respect to G and $\tan\theta$ were calculated. These derivatives were then used to compute ΔG and $\Delta\tan\theta$. The next step was to calculate the new G and $\tan\theta$ to be used to determine $y_{predicted}$ values. This was an iterative process and ceased when the least squares error from two successive iterations differed by less than a specified value.

The least squares expression (eqn. 3.23) was differentiated with respect to ΔG and $\Delta\tan\theta$, these derivatives were set equal to zero to determine minimum error values. The derivative with respect to ΔG follows.

$$\frac{\partial\varepsilon^2}{\partial\Delta G} = \sum\left(y_p\frac{\partial y_p}{\partial G}\right) + \Delta G\sum\left(\frac{\partial y_p}{\partial G}\frac{\partial y_p}{\partial G}\right) + \Delta\tan\theta\sum\left(\frac{\partial y_p}{\partial\tan\theta}\frac{\partial y_p}{\partial G}\right) - \sum\left(y_m\frac{\partial y_p}{\partial G}\right) \tag{3.24}$$

This is minimized by setting the derivative equal to zero, resulting in an equation of two unknowns; ΔG and $\Delta\tan\theta$. The subscripts p and m denote predicted and measured shoreline positions. Equation 3.24 can be rewritten with the known quantities set equal to the unknowns.

$$\Delta G\sum\left(\frac{\partial y_p}{\partial G}\right)^2 + \Delta\tan\theta\sum\left(\frac{\partial y_p}{\partial\tan\theta}\frac{\partial y_p}{\partial G}\right) = \sum\left[(y_m - y_p)\frac{\partial y_p}{\partial G}\right] \tag{3.25}$$

if this same procedure is applied for the derivative of the error with respect to $\Delta\tan\theta$ a second equation results which can be solved simultaneously with equation 3.25 to determine

ΔG and $\Delta \tan\theta$. This second equation is

$$\Delta G \sum \left(\frac{\partial y_p}{\partial G} \frac{\partial y_p}{\partial \tan\theta} \right) + \Delta \tan\theta \sum \left(\frac{\partial y_p}{\partial \tan\theta} \right)^2 = \sum \left[(y_m - y_p) \frac{\partial y_p}{\partial \tan\theta} \right] \tag{3.26}$$

As stated earlier, ΔG and $\Delta \tan\theta$ are the only unknowns, y_p is computed from the previous step. Equations 3.25 and 3.26 are solved with G and $\tan\theta$ values from the previous iteration. The measured shoreline change,$y_{measured}$, is known and the predicted values are computed from the G and $\tan\theta$ from the previous step. The derivatives of $y_{predicted}$ with respect to G and $\tan\theta$ must be known to solve for ΔG and $\Delta \tan\theta$; expressions for these derivatives follow:

$$\frac{\partial y_p}{\partial G} = \frac{\tan\theta}{\sqrt{\pi}} \left[\frac{1}{2} \sqrt{4t/G} \exp\left(\frac{-x^2}{4Gt}\right) \right] \tag{3.27}$$

$$\frac{\partial y_p}{\partial \tan\theta} = \frac{1}{\sqrt{\pi}} \left[\sqrt{4Gt} \exp\left(\frac{-x^2}{4Gt}\right) - x\sqrt{\pi}\,\mathrm{erfc}\left(\frac{x}{\sqrt{4Gt}}\right) \right] \tag{3.28}$$

This process is repeated until the error converges to a minimum value. Figure 3.4 shows a contour plot of error for different values of G and $tan\theta$, used to fit the analytical solution to data for St. Lucie Inlet.

3.4 Even and Odd Analysis

The shoreline changes about the inlet were analyzed to determine an odd and an even component of the net change. An even signal is symmetric about its mid-point; at points equidistant from the center the even component has the same magnitude and sign. An odd signal is antisymmetric and at points equidistant from the origin the signal has the same magnitude but opposite signs. As examples, the sine is an odd function and the cosine is an even function. Figures 3.5 and 3.6 show other examples of purely odd and even functions.

Any function, $f(t)$, regardless of its form can be written as the sum of odd and even components. An even function is defined as any function which satisfies the following condition

$$f(-t) = f(t) \tag{3.29}$$

and a function is odd if

$$f(-t) = -f(t) \tag{3.30}$$

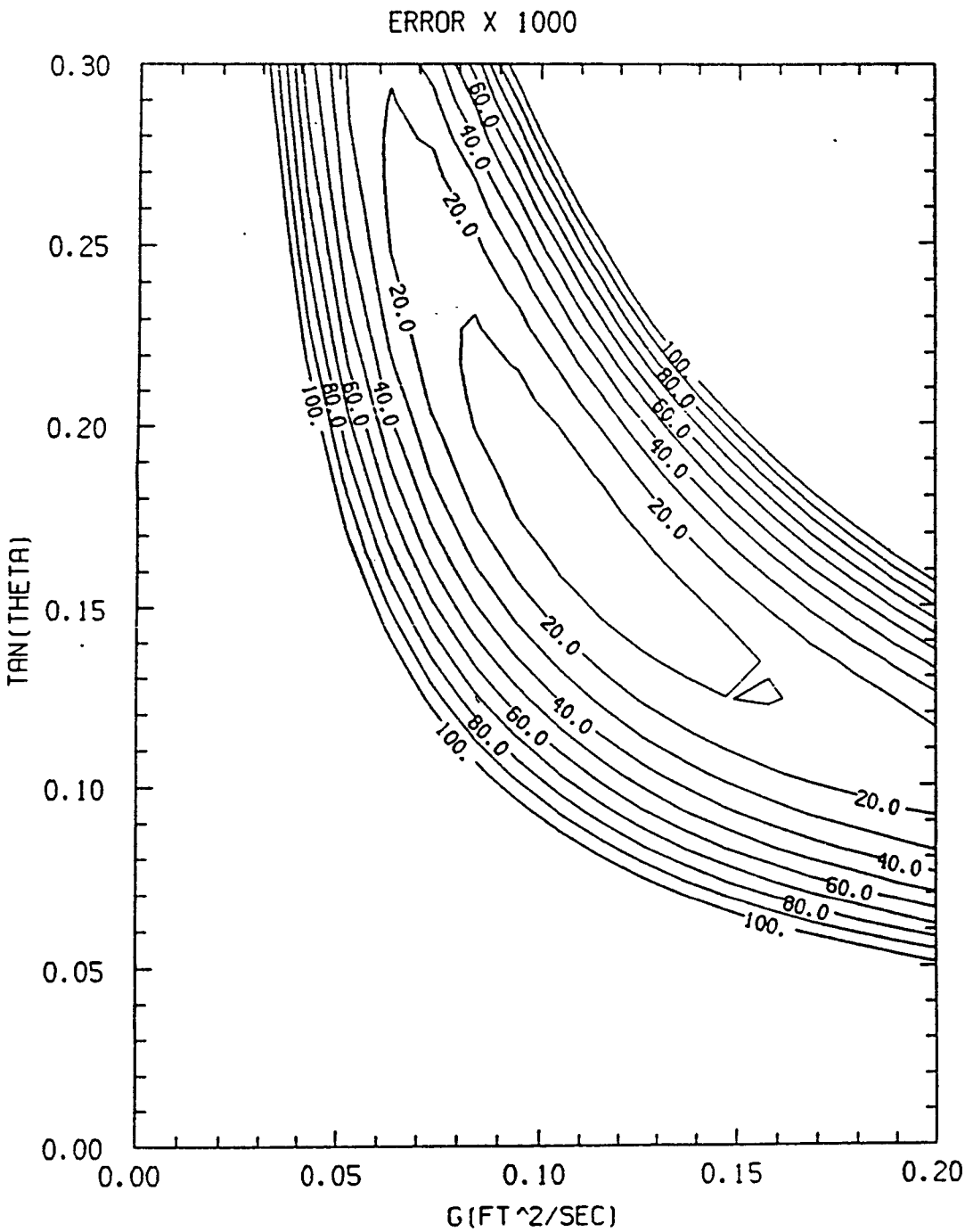

Figure 3.4: Contour Plot of Error for St. Lucie Inlet 1928 to 1970

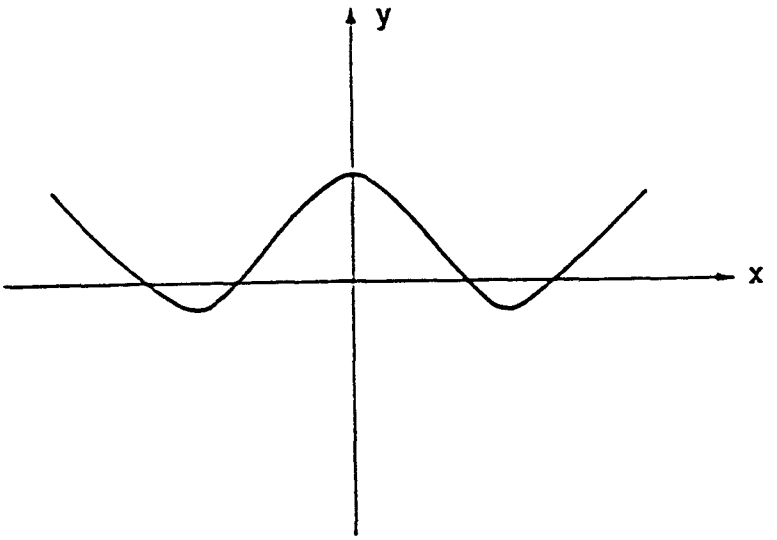

Figure 3.5: Even Function

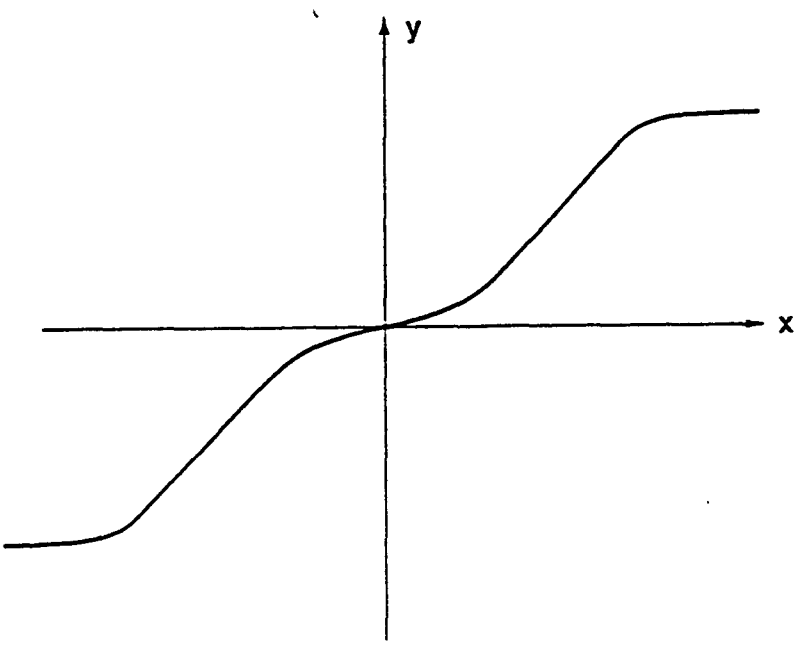

Figure 3.6: Odd Function

The net, $f_n(t)$, is the sum of the odd , $f_o(t)$, and the even, $f_e(t)$.

$$f_n(t) = f_e(t) + f_o(t) \tag{3.31}$$

For a negative value of t, the net would equal

$$f_n(-t) = f_e(-t) + f_o(-t) \tag{3.32}$$

Equation 3.32 can be rewritten as

$$f_n(-t) = f_e(t) - f_o(t) \tag{3.33}$$

Equations 3.31 and 3.33 are solved simultaneously with $f_e(t)$ and $f_o(t)$ as unknowns and $f_n(t)$ and $f_n(-t)$ as known quantities. The solutions for the even and odd components in terms of the net function are

$$f_e(t) = \frac{f_n(t) + f_n(-t)}{2} \tag{3.34}$$

$$f_o(t) = \frac{f_n(t) - f_n(-t)}{2} \tag{3.35}$$

The measured shoreline change was used as the net function, $f_n(t)$, and equations 3.34 and 3.35 were used to determine odd and even components of the net. The inlet midpoint was used as the origin, with the downdrift shore as positive x and the updrift shore as negative x. The least squares analysis discussed in the last section was performed on the odd component to determine a best fit predicted odd component.

An example of an even component of shoreline change could be the background rate of erosion. If the background rate of erosion is constant over a certain region, the shoreline will be affected by the same change. Figure 3.7 shows the shoreline about a littoral barrier predicted by the analytical solution with a background rate of erosion of two feet per year. By adding in the background erosion the shoreline is no longer antisymmetric about the barrier. The odd and even components of the net change have also been plotted . The odd component is the predicted shoreline without the background rate. The even component is a straight line at minus 20 feet which represents the background erosion.

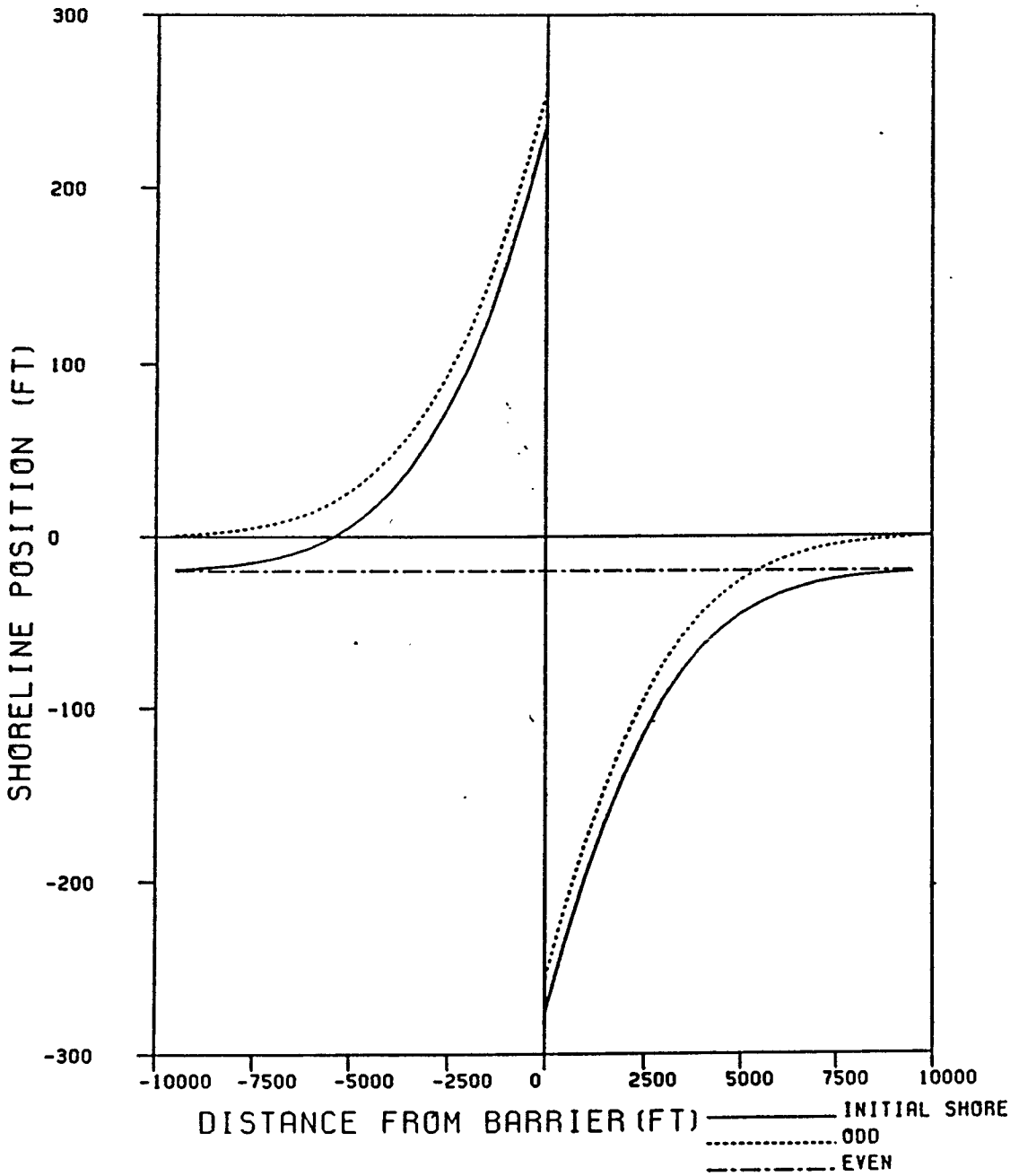

Figure 3.7: Predicted Solution with Background Rate of Erosion

CHAPTER 4
NUMERICAL METHODOLOGY

4.1 Explicit Model

Numerical procedures can be used to solve the continuity and transport equations. Numerical methods have the advantage of being able to model specific physical processes such as refraction or diffraction. Numerical models also have much greater flexibility with boundary conditions and model inputs. Variable wave heights or irregular shorelines are examples of this flexibility. The derivation of the equations for the numerical method will follow.

Derived earlier was the continuity equation

$$\frac{\partial y}{\partial t} = -\frac{1}{D}\frac{\partial Q}{\partial x} \tag{4.1}$$

Using a grid system set up along the shoreline with y at the midpoints this equation can be represented as the following:

$$\frac{\Delta y_i}{\Delta t} = -\frac{1}{D}\frac{(Q_{i+1} - Q_i)}{\Delta x_i} \tag{4.2}$$

The change in shoreline position, Δy_i, then can be written as

$$\Delta y_i = -\frac{(Q_{i+1} - Q_i)(\Delta t)}{(D\ \Delta x_i)} \tag{4.3}$$

The transport is determined using the transport equation of the previous chapter, computing the shoreline angle β referenced to north, from the shoreline position.

$$\beta = \frac{\pi}{2} - \tan^{-1}\left(\frac{y_i - y_{i-1}}{\Delta x_i}\right) \tag{4.4}$$

$$Q_i = \frac{K\sqrt{g/\kappa}}{16(s-1)(1-p)} H_b^{5/2} \sin 2\left[\frac{\pi}{2} - \tan^{-1}\left(\frac{y_i - y_{i-1}}{\Delta x_i}\right) - \alpha_b\right] \tag{4.5}$$

The initial shoreline positions are input as the initial y_i values. Then transport is computed using appropriate wave heights and wave angles. These transport values are used to compute the change in shoreline position, Δy, for the specified time step. This procedure is repeated for the time interval desired. Boundary conditions are that the transport, at a barrier such as an inlet, is either zero or some specified value. Another boundary condition could be a specified shoreline change value at an outer grid point.

These two equations (eqns. 4.3, 4.5) are solved sequentially making this an explicit model. Explicit models have an inherent stability limit, due to this sequential procedure. The stability parameter is

$$\frac{G\,\Delta t}{(\Delta x)^2} < \frac{1}{2} \tag{4.6}$$

If this relationship approaches one half, the shoreline position values start to oscillate. To satisfy this stability condition grid spacing must be large or the time step must be made small. A large grid spacing will not show detailed shoreline evolution, therefore to ensure stability the explicit model must use a small time step. Small time steps have the obvious disadvantage of taking considerably more computer time.

4.2 Implicit Model

The implicit solution used here is based after Perlin (1982), and solves for continuity and transport simultaneously. The method consists of determining four equations to solve for four unknowns; Δy_i^{n+1}, Δy_{i-1}^{n+1}, Q_{i+1}^{n+1}, and Q_i^{n+1}. The superscript n denotes time step. Continuity is expressed in terms of the forward difference of the transport, averaged for the present and the next time steps.

$$\Delta y_i^{n+1} = -\frac{\Delta t}{\Delta x_i}\frac{1}{D}\left[\frac{Q_{i+1}^{n+1}+Q_{i+1}^{n}}{2} - \frac{Q_i^{n+1}+Q_i^{n}}{2}\right] \tag{4.7}$$

This equation is then rewritten to equate unknown quantities at time step $n+1$ to time step n.

$$\left(\frac{\Delta t}{2\,\Delta x D}\right) Q_{i+1}^{n+1} + (1)\;\Delta y_i^{n+1} - \left(\frac{\Delta t}{2\,\Delta x D}\right) Q_i^{n+1} = \left[\frac{\Delta t}{2\,\Delta x D}\,(Q_i^n - Q_{i+1}^n)\right] \tag{4.8}$$

This equation can be expressed as

$$A_i Q_{i+1}^{n+1} + B_i \Delta y_i^{n+1} + C_i Q_i^{n+1} = D_i \tag{4.9}$$

where

$$A_i = \frac{\Delta t}{2\,\Delta x D} \tag{4.10}$$

$$B_i = 1 \tag{4.11}$$

$$C_i = -A_i \tag{4.12}$$

$$D_i = \frac{\Delta t}{2\,\Delta x D}\left(Q_i^n - Q_{i+1}^n\right) \tag{4.13}$$

The transport is expressed as the sum of the transport for the previous time step plus an increment due to time.

$$Q_i^{n+1} = Q_i^n + \frac{\partial Q_i^n}{\partial t}\Delta t \tag{4.14}$$

Expanding the partial derivative of Q with respect to time and neglecting higher order terms, results in the following:

$$\frac{\partial Q_i^n}{\partial t}\Delta t = \frac{\partial Q_i^n}{\partial y_i}\frac{\Delta y_i^{n+1}}{\partial t}\Delta t + \frac{\partial Q_i^n}{\partial y_{i-1}}\frac{\Delta y_{i-1}^{n+1}}{\partial t}\Delta t \tag{4.15}$$

The transport can now be expressed as

$$Q_i^{n+1} = Q_i^n + \frac{\partial Q_i^n}{\partial y_i}\Delta y_i^{n+1} + \frac{\partial Q_i^n}{\partial y_{i-1}}\Delta y_{i-1}^{n+1} \tag{4.16}$$

where

$$\frac{\partial Q_i^n}{\partial y_i} = \left[\frac{K\sqrt{g/\kappa}\,H_b^{5/2}}{16(s-1)(1-p)}\right]\frac{2\cos 2\left[\pi/2 - \tan^{-1}\left(\frac{y_i - y_{i-1}}{\Delta x}\right) - \alpha_b\right]}{\Delta x\left[1 + \left(\frac{y_i - y_{i-1}}{\Delta x}\right)^2\right]} \tag{4.17}$$

$$\frac{\partial Q_i^n}{\partial y_{i-1}} = -\frac{\partial Q_i^n}{\partial y_i} \tag{4.18}$$

As with the continuity equation, the transport equation can be expressed in terms of coefficients.

$$A_i^* \Delta y_i^{n+1} + B_i^* Q_i^{n+1} + C_i^* \Delta y_{i-1}^{n+1} = D_i^* \tag{4.19}$$

where

$$A_i^* = -\frac{\partial Q_i}{\partial y_i} \tag{4.20}$$

$$B_i^* = 1 \tag{4.21}$$

$$C_i^* = -A_i^* \tag{4.22}$$

$$D_i^* = Q_i^n \tag{4.23}$$

There are now four unknowns and two equations. The solution procedure used is known as a double sweep (Abbot,1971) and introduces two auxiliary equations. The two auxiliary equations used were:

$$\Delta y_i^{n+1} = E_i Q_i^{n+1} + F_i \tag{4.24}$$

$$Q_i^{n+1} = E_i^* \Delta y_{i-1}^{n+1} + F_i^* \tag{4.25}$$

Solving these four equations (eqns. 4.9, 4.19, 4.24, 4.25) simultaneously yields the following results for E, F, E^*, and F^*.

$$E_i = -\frac{C_i}{A_i E_{i+1}^* + B_i} \tag{4.26}$$

$$F_i = \frac{D_i - A_i F_{i+1}^*}{A_i E_{i+1}^* + B_i} \tag{4.27}$$

$$E_i^* = -\frac{C_i^*}{A_i^* E_i + B_i^*} \tag{4.28}$$

$$F_i^* = \frac{D_i^* - A_i^* F_i}{A_i^* E_i + B_i^*} \tag{4.29}$$

During the first sweep, the coefficients E, F, E^*, and F^* are conditioned. Sweeping from large values of i to smaller values, the coefficients are determined. These coefficients are then used in the auxiliary equations 4.24 and 4.25 to solve for Δy and Q by sweeping from small values of i to large values of i.

The grid system places, $i = imax$, at the inlet. This results in , $i = 1$, being the farthest grid point away from the inlet. Q_{imax+1} is the transport entering the grid closest to the inlet, and assumed zero. This allows no transport across the inlet regardless of transport direction. For the downdrift shore studied here, this boundary condition allows no southerly transport across the inlet, and traps all northerly transport. Using this boundary condition, E_{imax}^* and F_{imax}^* were determined from equation 4.25.

$$E_{imax}^* \Delta y_{imax-1}^{n+1} + F_{imax}^* = Q_{imax}^{n+1} = 0.0 \tag{4.30}$$

therefore

$$E^*_{imax} = 0.0 \tag{4.31}$$

$$F^*_{imax} = 0.0 \tag{4.32}$$

If E^* and F^* are known for grid $i+1$, then E and F can be determined for grid i (see eqns. 4.26 and 4.27). The transport boundary condition at $imax$ has yielded E^*_{imax} and F^*_{imax}, now E_{imax-1} and F_{imax-1} can be determined. This procedure continues to determine the coefficients as i decreases. After the first sweep has been completed, the second boundary condition allows the auxiliary equations to be solved. The second boundary condition assumes that at grid $i = 1$ the shoreline is unaffected by the presence of the inlet, or Δy_1 is equal to zero. By substituting this in equation 4.25, the transport can be calculated for grid $i = 2$, then Δy_2 can be determined using equation 4.24. This sweep is continued up to $imax$, solving for all the transports and shoreline changes.

$$Q_2^{n+1} = F_2^* \tag{4.33}$$

$$\Delta y_2^{n+1} = E_2 Q_2^{n+1} + F_2 \tag{4.34}$$

This implicit method does not have the stability problems of the explicit procedure and allows for both large and small time steps and grid spacings. A continuity check was introduced, to verify that the stored volume of sediment over the computational domain as calculated from the change in shoreline positions equaled the accumulative difference in transport at $i = imax$ and $i = 1$.

4.3 Wave Refraction

As a wave approaches the shoreline, changes in depth cause the wave crests to bend. The waves tend to become parallel with the bottom contours, and the changing depth also will cause a change in wave height because of shoaling. These changes in wave direction and wave height were incorporated into the model through a wave refraction routine.

The two governing equations for the refraction routine were irrotationality of wave number (eqn. 4.35) and conservation of wave energy flux (eqn. 4.36).

$$\vec{\nabla} \times \vec{k} = 0 \tag{4.35}$$

$$\vec{\nabla} \cdot \left[E\vec{C_g}\right] = 0 \tag{4.36}$$

Expansion of the governing equations results in the following two expression which were solved by finite difference schemes.

$$\frac{\partial (k \sin\theta)}{\partial x} - \frac{(\partial \cos\theta)}{\partial y} = 0 \tag{4.37}$$

$$\frac{\partial (EC_g \cos\theta)}{\partial x} + \frac{\partial (EC_g \sin\theta)}{\partial y} = 0 \tag{4.38}$$

The development of the solution of the refracted wave angle for each grid point will follow, the solution for the wave height is similar and only the final solution will be presented.

A grid system is developed for offshore bathymetry, the longshore direction is represented by the i axis and the offshore direction is represented by the j axis. The finite differenced form of the solution uses eight adjacent grid points to the point of interest,(i,j) (see figure 4.1). Equation 4.37 can be rewritten as the following expression in finite difference form.

$$\begin{aligned}\frac{(k\cos\theta)_{i,j+1} - (k\cos\theta)_{i,j}}{\Delta y} &= \frac{1}{2}\left(\left[\frac{(k\sin\theta)_{i+1,j} - (k\sin\theta)_{i-1,j}}{2\,\Delta x}\right] + \right. \\ &\left. \left[\frac{(k\sin\theta)_{i+1,j+1} - (k\sin\theta)_{i-1,j+1}}{2\,\Delta x}\right]\right)\end{aligned} \tag{4.39}$$

Solving for $(k\cos\theta_{i,j})$ results in

$$\begin{aligned}(k\cos\theta)_{i,j} &= (k\cos\theta)_{i,j+1} - \frac{1}{2}\left(\frac{\Delta y}{2\,\Delta x}\right)\left(\left[(k\sin\theta)_{i+1,j} - (k\sin\theta)_{i-1,j}\right] + \right. \\ &\left. \left[(k\sin\theta)_{i+1,j+1} - (k\sin\theta)_{i-1,j+1}\right]\right)\end{aligned} \tag{4.40}$$

A smoothing parameter,τ, is now introduced. The $(k\cos\theta)$ terms for i, $i+1$, and $i-1$ for the offshore grid one step seaward are smoothed to yield.

$$(k\cos\theta)_{i,j+1} = \tau\,(k\cos\theta)_{i+1,j+1} + \tau\,(k\cos\theta)_{i-1,j+1} + (1-2\tau)\,(k\cos\theta)_{i,j+1} \tag{4.41}$$

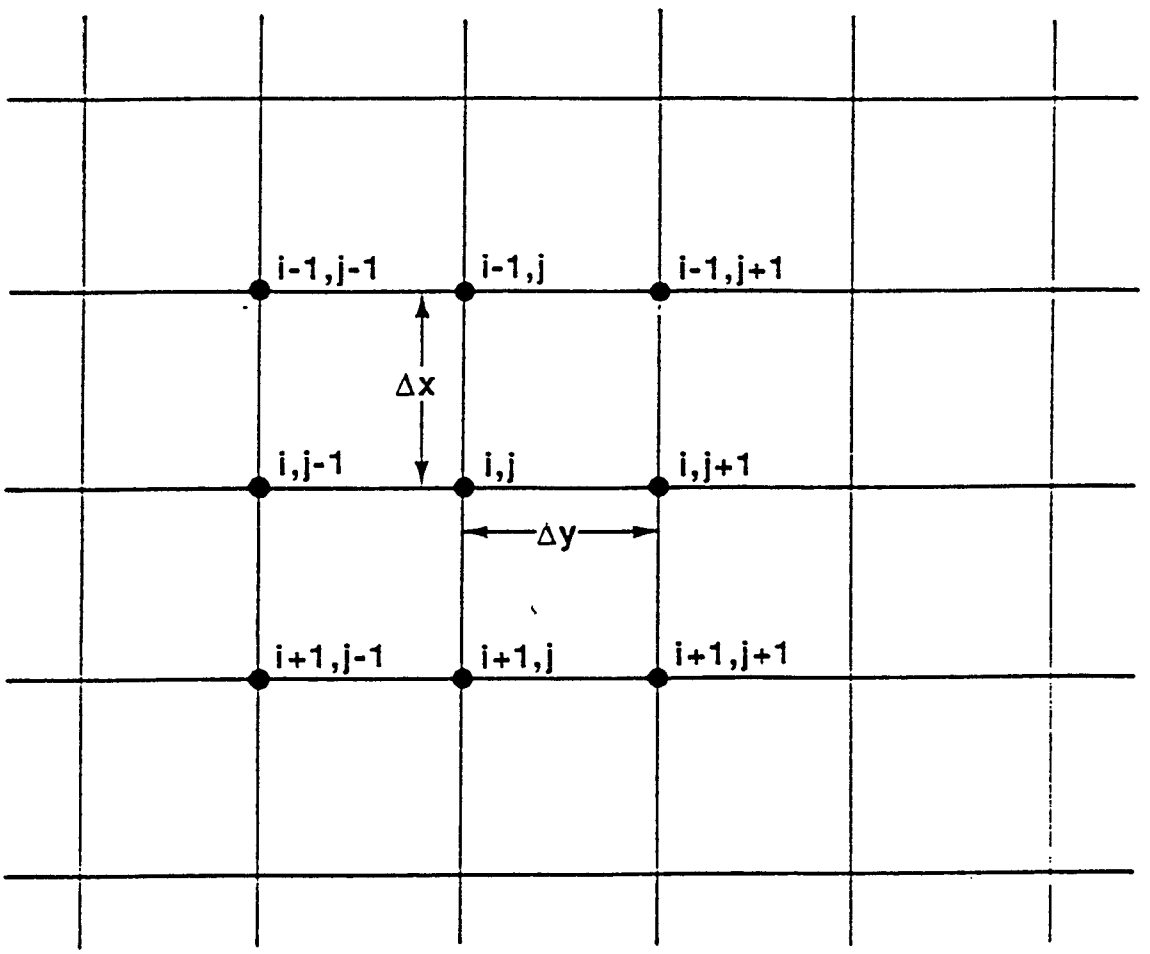

Figure 4.1: Refraction Grid System

Substituting equation 4.41 in equation 4.40 results in the finite differenced solution for $(k\cos\theta)$.

$$\begin{aligned}(k\cos\theta)_{i,j} &= r\left[(k\cos\theta)_{i+1,j+1} + (k\cos\theta)_{i-1,j+1}\right] + \\ &\quad (1-2r)\left[(k\cos\theta)_{i,j+1}\right] - \\ &\quad \frac{1}{2}\left(\frac{\Delta y}{2\,\Delta x}\right)\left(\left[(k\sin\theta)_{i+1,j} - (k\sin\theta)_{i-1,j}\right] + \right. \\ &\quad \left.\left[(k\sin\theta)_{i+1,j+1} - (k\sin\theta)_{i-1,j+1}\right]\right) \qquad (4.42)\end{aligned}$$

The field is originally initialized using wave angles from Snell's law, which relates the grid points with the wave angle at the most seaward grid. Then an iterative procedure was used that swept from the outermost grid at $j = jmax$ towards the most shoreward grid at $j = 1$. This iterative procedure was repeated a number of times until the wave angle for each grid point converged to a steady value.

Equation 4.38 was solved in similar fashion to determine the wave heights. From linear wave theory; wave energy was expressed as the wave height squared. The wave height field is initialized with values determined from conservation of wave energy flux with the wave height at the most seaward grid offshore.

$$\begin{aligned}\left(H^2C_g\sin\theta\right)_{i,j} &= r\left[\left(H^2C_g\sin\theta\right)_{i+1,j+1} + \left(H^2C_g\sin\theta\right)_{i-1,j+1}\right] + \\ &\quad (1-2r)\left[\left(H^2C_g\sin\theta\right)_{i,j+1}\right] + \\ &\quad \frac{1}{2}\left(\frac{\Delta y}{2\,\Delta x}\right)\left(\left[\left(H^2C_g\cos\theta\right)_{i+1,j} - \left(H^2C_g\cos\theta\right)_{i-1,j}\right] + \right. \\ &\quad \left.\left[\left(H^2C_g\cos\theta\right)_{i+1,j+1} - \left(H^2C_g\cos\theta\right)_{i-1,j+1}\right]\right) \qquad (4.43)\end{aligned}$$

It was found that for large bathymetric changes or incoming waves that differed from the shore normal by a large angle, the refraction routine would become unstable. The steady values of wave height and wave direction would need to be approached at a gradually increasing rate. To accomplish this, a damping factor was added to equations 4.42 and 4.43. To simplify the presentation of this damping procedure equation 4.42 is expressed in terms

of coefficients $B1$, $B2$, $B3$, and $B4$. The damping factor, Γ, was determined as a function of the hyperbolic tangent, tanh.

$$\Gamma = \tanh(m * 0.05) \tag{4.44}$$

Where m is the step of the iteration loop which is run until all values of height or direction converge to steady values.

$$B1 = r\left[(k\cos\theta)_{i+1,j+1} + (k\cos\theta)_{i-1,j+1}\right] \tag{4.45}$$

$$B2 = (1-2r)\left[(k\cos\theta)_{i,j+1}\right] \tag{4.46}$$

$$B3 = -\frac{\Delta y}{2\,\Delta x}\left[(k\sin\theta)_{i+1,j} - (k\sin\theta)_{i-1,j}\right] \tag{4.47}$$

$$B4 = -\frac{\Delta y}{2\,\Delta x}\left[(k\sin\theta)_{i+1,j+1} - (k\sin\theta)_{i-1,j+1}\right] \tag{4.48}$$

The solution then becomes

$$(k\cos\theta)_{i,j} = B1 + B2 + \Gamma\left[0.5\,(B3 + B4)\right] \tag{4.49}$$

4.4 Refraction Due to Currents

In the same manner as changes in depth refract waves, currents interacting with incoming waves also will cause refraction to occur. This wave and current interaction will cause wave crests to bend and wave height will also be altered. For example an ebb tidal jet will oppose incoming wave crests, causing waves to steepen and bend towards the inlet. The flood tide will generate a current which will reinforce the incoming wave crests, tending to decrease wave heights and cause the waves to bend away from the inlet. The wave refraction routine discussed in the previous section was modified to incorporate the effects of currents.

An intrinsic wave frequency (σ) is used which is the frequency apparent to an observer riding with the current.

$$\sigma = \omega - \vec{k}\cdot\vec{u} \tag{4.50}$$

where ω is the absolute frequency and $\vec{u}$ is the current vector.

Irrotionality of wave number and conservation of wave energy flux are still used as the governing equations, but are expressed to take into account the current. The wave number is now expressed in terms of the intrinsic frequency.

$$\sigma^2 = gk \tanh(kh) \tag{4.51}$$

$$\vec{\nabla} \times \vec{k} = 0 \tag{4.52}$$

$$\vec{\nabla} \cdot \left[\frac{E}{\sigma}\left(\vec{u} + \vec{C_g}\right)\right] = 0 \tag{4.53}$$

The group velocity, C_g, is now expressed in terms of the intrinsic frequency (Mei, 1983).

$$C_g = \frac{1}{2}\frac{\sigma}{k}\left(1 + \frac{2\,kh}{\sinh 2\,kh}\right) \tag{4.54}$$

The solution of the wave angle remained the same, except the wave number was now solved using equation 4.51. For the case of no current and only depth changes, the wave number is a function of depth and period only. The wave number for each grid point is then a constant and does not change. For the case of refraction due to currents, the wave number is related to the intrinsic frequency. The intrinsic frequency is a function of depth, period, and the current angle relative to the wave angle. When the refraction routine was modified for currents, the wave number had to be recalculated inside the loop which ran until steady values of wave direction were converged upon.

The wave heights were solved in a similar fashion as in the last section but with the modified conservation of wave energy equation. The intrinsic frequency (eqn. 4.50) cam be simplified to

$$\sigma = \frac{2\,\pi}{T} - \sqrt{u^2 + v^2}k\cos(\theta_c - \theta_w) \tag{4.55}$$

Where θ_c is the angle between the current and the shoreline and θ_w is the angle between the wave crests and the shoreline. The current component in the alongshore direction is u and v is the current component in the offshore direction. Coefficients $T1$ and $T2$ are introduced to simplify the presentation of the solution for wave height. For the case of refraction due

to currents and varying depth, the conservation of wave energy flux was expressed as

$$\frac{\partial\left[\frac{H^2}{\sigma}\left(u+C_g\cos\theta_w\right)\right]}{\partial x}+\frac{\partial\left[\frac{H^2}{\sigma}\left(v+C_g\sin\theta_w\right)\right]}{\partial y}=0 \tag{4.56}$$

$$T1=\frac{H^2}{\sigma}\left(u+C_g\cos\theta_w\right) \tag{4.57}$$

$$T2=\frac{H^2}{\sigma}\left(v+C_g\sin\theta_w\right) \tag{4.58}$$

The coefficients $B1$, $B2$, $B3$, and $B4$ are now expressed in terms of $T1$ and $T2$.

$$B1=r\left[T2_{i-1,j+1}+T2_{i+1,j+1}\right] \tag{4.59}$$

$$B2=(1-2r)\left[T2_{i,j+1}\right] \tag{4.60}$$

$$B3=\frac{\Delta y}{2\,\Delta x}\left[T1_{i+1,j}-T1_{i-1,j}\right] \tag{4.61}$$

$$B4=\frac{\Delta y}{2\,\Delta x}\left[T1_{i+1,j+1}-T1_{i-1,j+1}\right] \tag{4.62}$$

The solution for wave heights with shoaling due to varying depth and the presence of current then became.

$$\left[\frac{H^2}{\sigma}\left(v+\sin\theta_w\right)\right]_{i,j}\doteq B1+B2+\Gamma\left[0.5\left(B3+B4\right)\right] \tag{4.63}$$

4.5 Wave Diffraction

When wave crests pass a barrier a lateral transfer of energy occurs. In this model a diffraction routine was included to model the effects of wave diffraction due to the presence of a jetty. A shadow zone would be created in the lee of the jetty which would have lower wave energy than the shoreline farther away from the jetty. The diffraction routine used in this study is based on a solution by Perlin (1978) which used the previous work of Penny and Price (1952). The solution determines a diffraction coefficient K_D, which will alter the incoming wave heights in the shadow zone of a jetty. A definition sketch of the variables involved is shown in figure 4.2. The angle θ_O is the angle between incoming waves and the jetty axis. The angle θ_D is the angle between the jetty and the location where the diffraction coefficient will be calculated. The wave height at the tip of the jetty is H_O. The other variable needed is r, which is the radial distance from the tip of the

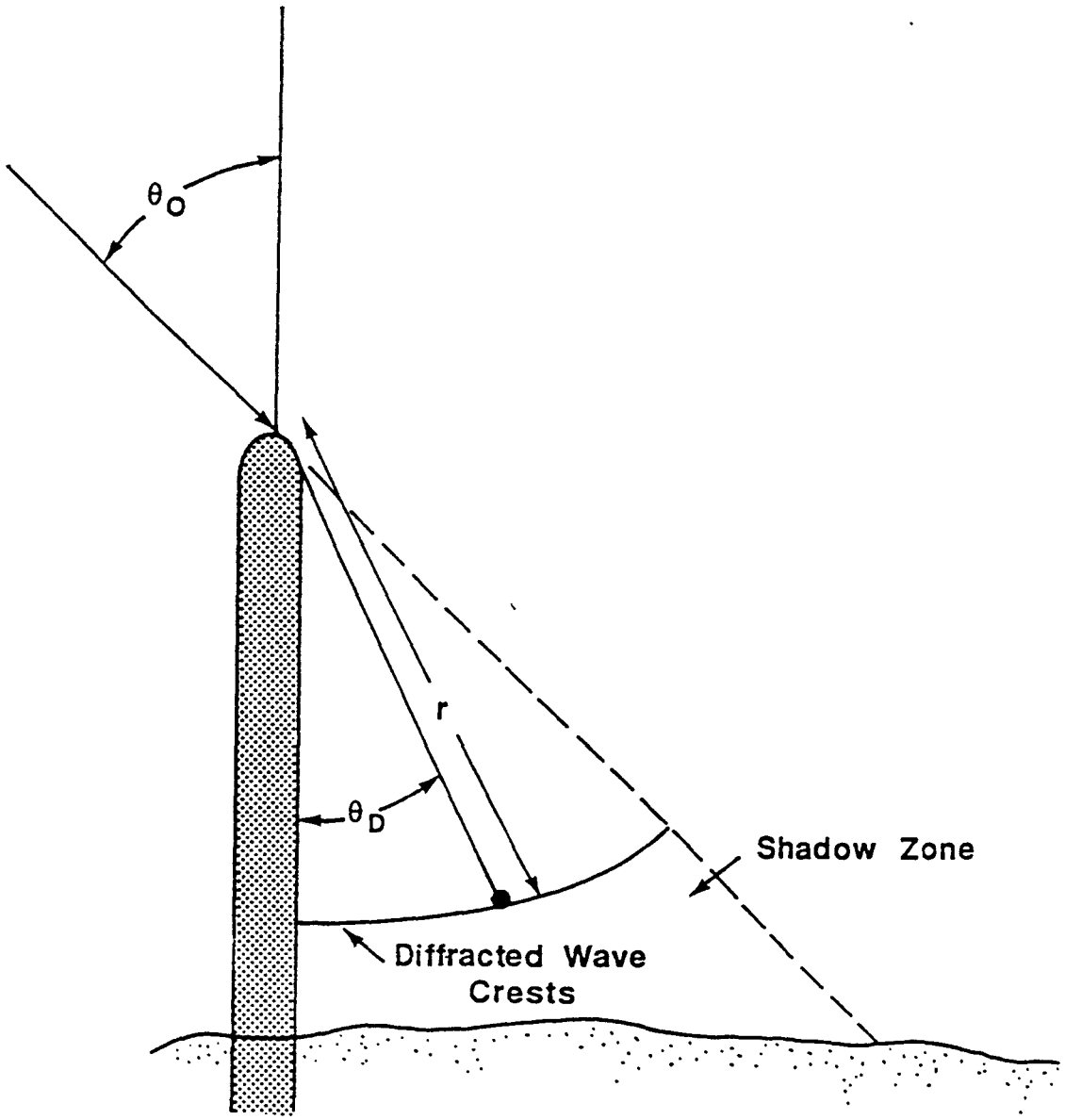

Figure 4.2: Definition Sketch for Wave Diffraction

jetty to the location where the diffraction coefficient will be calculated. The solution uses a dimensionless parameter, ρ', which is the product of the radial distance and the wave number. The quantity L to calculate this parameter is the wave length. The solution also uses Fresnel integrals C_F, and S, which were approximated by a numerical expansion (Abramowitz and Stegun, 1965).

$$\rho' = \left(\frac{2\,\pi}{L}\right) r \tag{4.64}$$

$$\begin{aligned} \text{Sum1} \;=\; & \cos\left[\rho' \cos\left(\theta_D - \theta_O\right)\right] \left[\frac{1}{2}\left(1 + C_F + S\right)\right] + \\ & \sin\left[\rho' \cos\left(\theta_D - \theta_O\right)\right] \left[-\frac{1}{2}\left(S - C_F\right)\right] + \\ & \cos\left[\rho' \cos\left(\theta_D + \theta_O\right)\right] \left[\frac{1}{2}\left(1 + C_F + S\right)\right] + \\ & \sin\left[\rho' \cos\left(\theta_D + \theta_O\right)\right] \left[-\frac{1}{2}\left(S - C_F\right)\right] \end{aligned} \tag{4.65}$$

$$\begin{aligned} \text{Sum2} \;=\; & cos\left[\rho' \cos\left(\theta_D - \theta_O\right)\right] \left[-\frac{1}{2}\left(S - C_F\right)\right] - \\ & \sin\left[\rho' \cos\left(\theta_D - \theta_O\right)\right] \left[\frac{1}{2}\left(1 + C_F + S\right)\right] + \\ & \cos\left[\rho' \cos\left(\theta_D + \theta_O\right)\right] \left[-\frac{1}{2}\left(S - C_F\right)\right] + \\ & \sin\left[\rho' \cos\left(\theta_D + \theta_O\right)\right] \left[\frac{1}{2}\left(1 + C_F + S\right)\right] \end{aligned} \tag{4.66}$$

The diffraction coefficient is the modulus of Sum1 and Sum2.

$$K_D = \sqrt{(\text{Sum1})^2 + (\text{Sum2})^2} \tag{4.67}$$

The diffracted wave height is the product of the diffraction coefficient and the wave height at the tip of the jetty.

$$H = K_D\, H_O \tag{4.68}$$

The wave direction is determined assuming a circular wave crest pattern along any radial.

The diffraction solution was modified to calculate a diffracted wave height which would be the breaking wave height. For grid points within the shadow zone, diffracted wave heights were computed for different offshore distances until the diffracted wave heights were equal

to the product of the depth and a constant, $\kappa = 0.78$.

$$H_b = \kappa\,(\mathrm{Depth}_b) \tag{4.69}$$

A simple bisection procedure was introduced to ensure that the diffraction routine converged to the offshore location where the diffracted wave height would be the breaking wave height. The bisection routine used a lower bound and an upper bound, and would determine a wave height at a location at half the distance between the bounds. For each iteration either the upper or the lower bound would change until the breaking wave height is converged upon. If the initial bounds represented locations shoreward and seaward of the breaking location, the bisection routine would absolutely converge to the breaking location. The initial lower bound was the shoreline with a depth of zero, and the initial upper bound was the outer edge of the shadow zone at that alongshore grid point. If the computed diffracted wave height was greater than the quantity, $\kappa \cdot (\mathrm{Depth}_b)$, the present guess became the next lower bound. If the computed wave height was less than the quantity, $\kappa \cdot (\mathrm{Depth}_b)$, the present guess became the next upper bound. This procedure was repeated until the guesses converged to the breaking height. A limitation to this method was that the combined processes of refraction and diffraction could not be modelled. In nature the diffracted waves in the lee of the structure would also be refracted due to changes in water depth, as the wave crests approached the shoreline.

CHAPTER 5
WAVE CHARACTERISTICS

5.1 Introduction

The model requires as inputs an original shoreline and wave characteristics. The wave characteristics needed are the breaking wave height and the breaking wave direction, these are used to compute transport. The model uses a deep water wave height and deep water wave direction and transforms these to shore over a specified offshore bathymetry. Diffraction around the jetty tip and refraction over an offshore ebb shoal will alter these deep water wave characteristics. This chapter will discuss the wave heights and wave angles used for the model and the effects of diffraction and refraction.

5.2 Wave Heights

The wave heights used in this study were obtained from the Coastal and Oceanographic engineering Department's Coastal Data Network (CDN). The CDN consists of eight stations that have been installed around the coast of Florida. These stations collect data at approximately six hour intervals. The breaking wave heights used were obtained by an analysis discussed in Phlegar (1989). This analysis assumed that the breaking wave heights can be represented by a Rayleigh Probability Distribution. Using this distribution a breaking wave height could be determined from a root mean square wave height from the CDN stations. The resulting wave parameter was a $\overline{H_b^{5/2}}$ for each month, using three years of data. This is an appropriate wave parameter because the wave height used to compute transport is raised to the 2.5 power.

5.3 Wave Direction

The wave directions used in this study were obtained from littoral drift roses (Walton, 1973). The drift roses use a large source of ship wave observations to compute littoral drift along Florida's coast. The wave data were from the U.S. Naval Weather Command, Summary of Synoptic Meteorological Observations (SSMO). These wave data were used to produce plots of transport as a function of shoreline orientations (see figure 5.1). Knowing the shoreline orientation, transport in directions to the right and left when looking offshore could be obtained. Q_+ is directed to the right when looking offshore, and Q_- is directed to the left. For a specified shoreline orientation, a net transport was calculated as

$$Q_{(net)} = Q_{(+)} - Q(-) \tag{5.1}$$

These values are estimates of transport and often do not agree with reported Corps of Engineer transport values. It is also stated in Walton (1973) that transport values south of Ft. Pierce may be in error due to wave sheltering by the Bahamian Bank, and the effects of the Gulf Stream.

The main advantage of using the littoral drift roses (LDR) was that a net transport could be obtained on a monthly basis for each site. Using these data and monthly wave heights from the CDN data transport reversals could be modeled. The shore normal for each site was determined, and a net drift for each month was obtained from the LDR. A breaking wave angle was calculated using the LDR transport and the CDN wave height. The transport equation developed earlier was

$$Q = K^* H_b^{5/2} \sin 2(\beta - \alpha_b) \tag{5.2}$$

$$K^* = \frac{K\sqrt{g/\kappa}}{16(s-1)(1-p)} \tag{5.3}$$

Solving 5.2 for the breaking wave angle results in the following expression.

$$\alpha_b = \beta - \sin^{-1}\left(\frac{Q}{K^* H_b^{5/2}}\right) \tag{5.4}$$

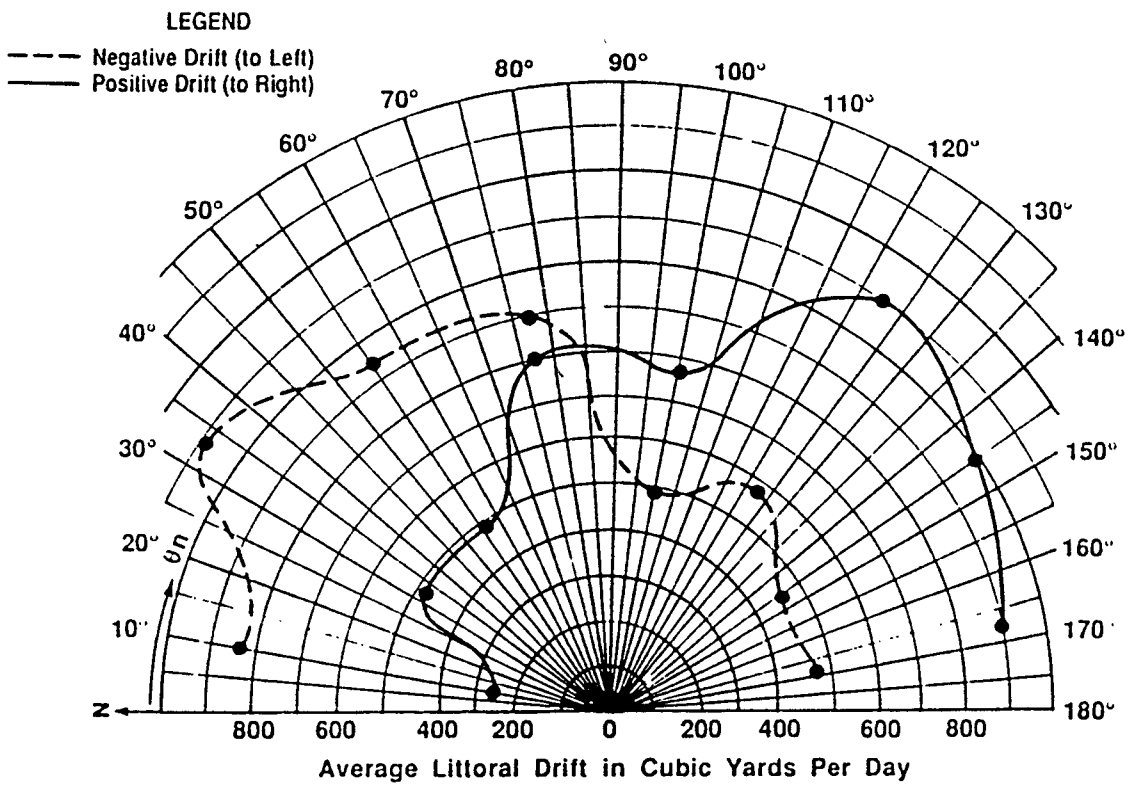

Figure 5.1: Example Littoral Drift Rose

These breaking angles were then brought out to deep water using Snell's Law (eqn. 5.5).

$$\frac{\sin(\beta - \alpha_b)}{C_b} = \frac{\sin(\beta - \alpha_o)}{C_o} \tag{5.5}$$

$$\alpha_o = \beta - \sin^{-1}(\beta - \alpha_b)\frac{C_o}{C_b} \tag{5.6}$$

The wave heights were also brought out to deep water. Conservation of wave energy flux (Dean and Dalrymple, 1983) can be expressed as

$$[EC_g \cos(\beta - \alpha)]_b = [EC_g \cos(\beta - \alpha)]_0 \tag{5.7}$$

E is the wave energy and is a function of the wave height squared. C_g is the wave group velocity. The conservation of flux (eqn. 5.7) can be rewritten as:

$$H_b^2 C_{g_b} \cos(\beta - \alpha_b) = H_o^2 C_{g_o} \cos(\beta - \alpha_o) \tag{5.8}$$

Equation 5.8 is solved for H_o.

$$H_o = \left[\frac{H_b^2 C_{g_b} \cos(\beta - \alpha_b)}{C_{g_o} \cos(\beta - \alpha_o)}\right]^{1/2} \tag{5.9}$$

$$C_{g_b} = C_b = \sqrt{g\,h} \tag{5.10}$$

$$C_{g_o} = \frac{1}{2}C_o = \frac{1}{2}\left(\frac{g}{2\pi}T\right) \tag{5.11}$$

The variable h is the breaking depth, and T is the wave period.

Values are now known for the deep water wave height and deep water wave angle for each month. These values were then used as inputs to a refraction routine which calculated a breaking height and direction for each grid point.

5.4 Modified Wave Angles

A net transport value, $\overline{Q}_m$, was calculated for each site from the measured shoreline change data, by considering the inlet jetty system to be a complete barrier. This measured transport value was an average net transport value. The monthly LDR transport values were averaged to determine a predicted average net transport value, $\overline{Q}_p$. In particular, the predicted values did not agree with the measured values. It was also found that the deep

water wave angles determined from the LDR transport data could vary greatly from the shore normal. The refraction routine used in the numerical model could operate only with gradually changing bathymetry and wave characteristics. If the wave approach was too large relative to the shore normal the refraction routine would become unstable and not function properly.

The wave angles determined from the LDR transport were modified to yield the calculated transport and to represent a more natural wave climate with a wave approach that approximated the shore normal. A procedure was developed that modified the mean breaking angle to generate the measured transport, and modified the deviation from the mean to make angles closer to shore normal.

The following discussion will describe this modification procedure; all angles mentioned refer to breaking angles. The breaking angles determined from the roses were assumed to be a mean value plus a fluctuation from this mean.

$$\theta_{p_i} = \overline{\theta}_{p_i} + \theta' \tag{5.12}$$

θ' is the fluctuation for each month from the mean value. The objective was to determine a new angle , θ_{mod}, which consisted of a modified mean, $\overline{\theta}_{mod}$ which would generate the calculated transport plus the fluctuation θ' determined form the LDR's multiplied by a factor from zero to one.

$$\theta_{mod_i} = \overline{\theta}_{mod} + K'(\theta_i^c) \tag{5.13}$$

$$\theta_i' = \theta_{p_i} - \overline{\theta}_{p_i} \tag{5.14}$$

The transport could now be expressed as

$$T\,Q = \sum K^* H_{b_i}^{5/2} \sin 2\left[\beta - \left(\overline{\theta}_{mod} + K'\theta_i'\right)\right]\Delta t \tag{5.15}$$

where T is equal to one year and Δt is equal to one month. Equation 5.15 can also be expressed as equation 5.16 when the sine term is expanded, and coefficients A and B are introduced.

$$\left[\frac{T\,Q}{\Delta t}\right] = A\cos 2\overline{\theta}_{mod} + B\sin 2\overline{\theta}_{mod} \tag{5.16}$$

$$A = \sum H_{b_1}^{5/2} K^* \sin 2\left(\beta - K' \theta_i'\right) \tag{5.17}$$

$$B = -\sum H_{b_i}^{5/2} K^* \cos 2\left(\beta - K' \theta_i'\right) \tag{5.18}$$

This simplified form of the transport (eqn. 5.16) can also be expressed as

$$\left[\frac{TQ}{\Delta t}\right] = C \cos\left(2\bar{\theta}_{mod} - \varepsilon\right) \tag{5.19}$$

Solving for $\bar{\theta}_{mod}$ yields

$$\bar{\theta}_{mod} = \frac{1}{2}\left[\varepsilon + \cos^{-1}\left(\frac{TQ}{\Delta t C}\right)\right] \tag{5.20}$$

Equation 5.19 can also be expressed as

$$\left[\frac{TQ}{\Delta t}\right] = C \cos 2\bar{\theta}_{mod} \cos\varepsilon + C \sin 2\bar{\theta}_{mod} \sin\varepsilon \tag{5.21}$$

Equating equation 5.21 with equation 5.16, C and ε can be expressed in terms of A and B which are known quantities.

$$A = C \cos\varepsilon \tag{5.22}$$

$$B = C \cos\varepsilon \tag{5.23}$$

$$C = \sqrt{A^2 + B^2} \tag{5.24}$$

$$\varepsilon = \tan^{-1}\left(\frac{B}{A}\right) \tag{5.25}$$

The procedure was now to set Q in equation 5.20 equal to the measured transport $\bar{Q}_m$, then specify a value of K'. A and B were determined using equations 5.17 , 5.18, once these values were known a $\bar{\theta}_{mod}$ could be calculated. It should be noted that each value of K' would result in a different $\bar{\theta}_{mod}$ value. But every combination of K' and $\bar{\theta}_{mod}$ would generate an average net transport equal to the calculated transport. If K' equals zero, the breaking angle for each month would be the same, and if K' equals one then the fluctuation value θ' would equal the deviation from the unmodified LDR angle values.

Figure 5.2 shows the modified monthly breaking angles for Ft. Pierce for K' values of one, zero, and one half. Figure 5.3 shows the resulting transport generated by these wave angles. It was found that even though it appears that different K' values change the

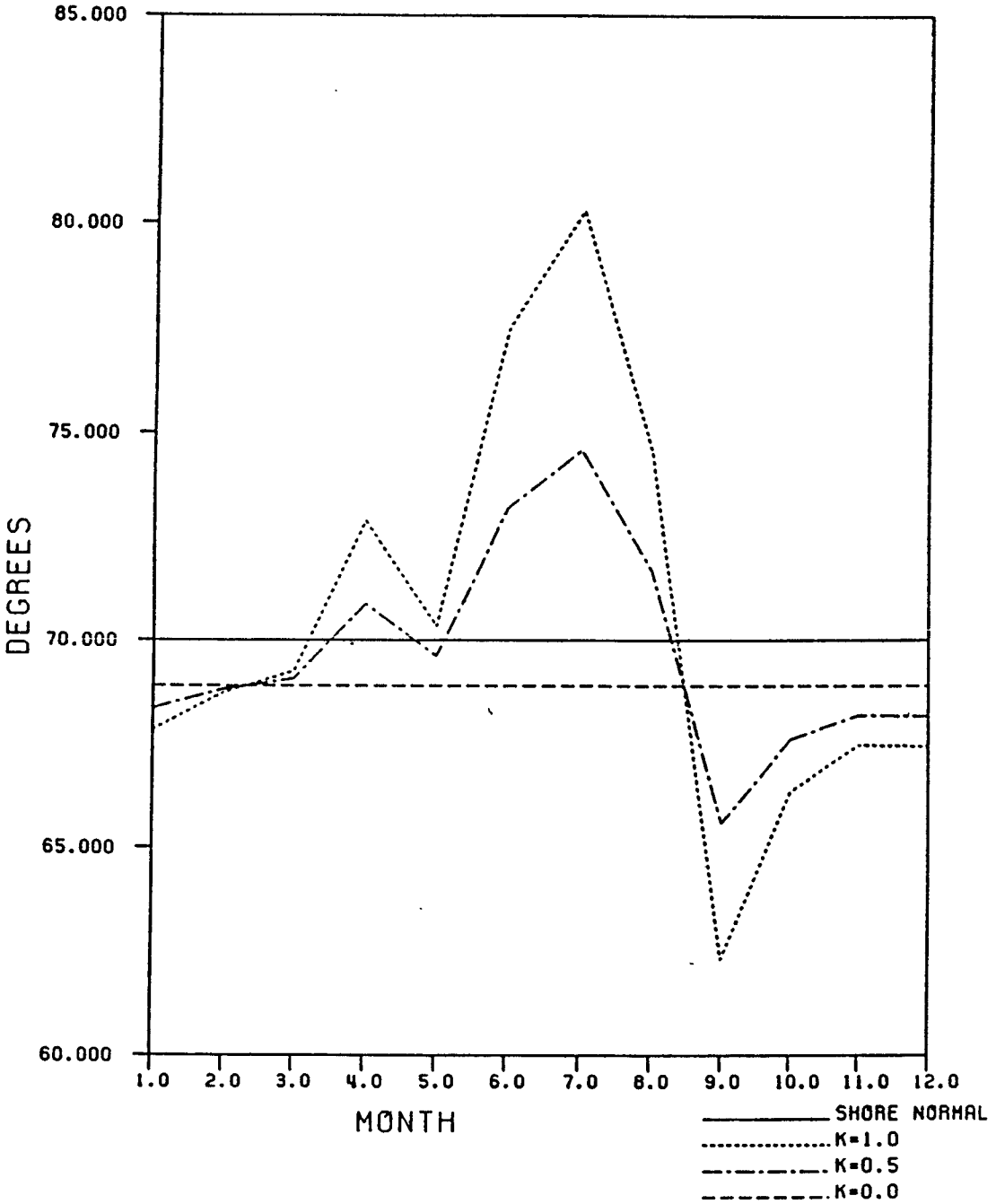

Figure 5.2: Modified Monthly Breaking Wave Angles for Ft. Pierce

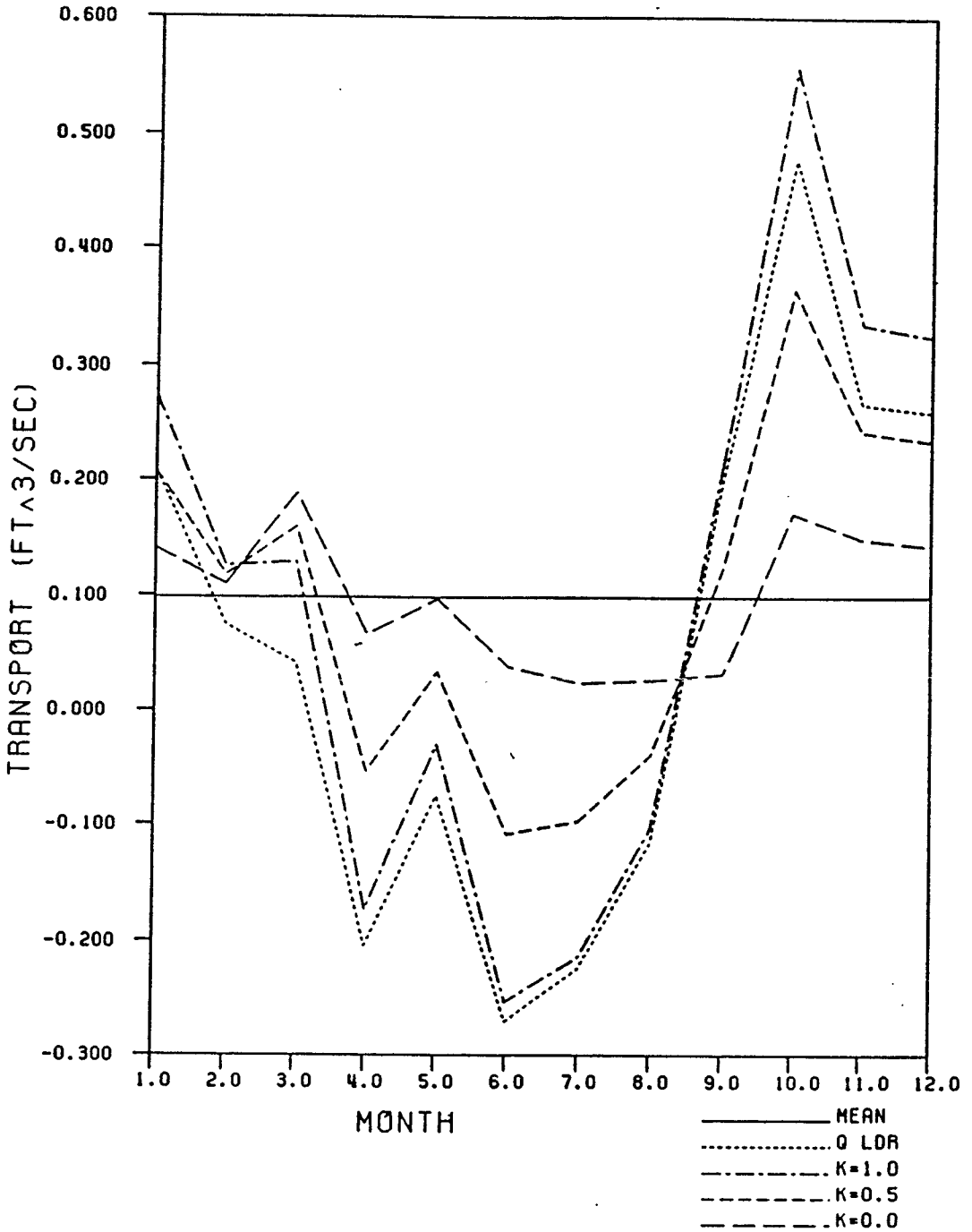

Figure 5.3: Modified Transport for Ft. Pierce

breaking angles and transport considerably the effect on the final predicted shorelines run for several years was negligible. This was because regardless of the value of K, the net transport generated would always equal the measured net transport.

CHAPTER 6
ANALYTICAL RESULTS

6.1 Introduction

This chapter will present the measured shoreline changes for several inlets on Florida's East and West coasts. A wide range of physical processes are represented by these data. The inlets studied differed in wave climate, transport, number of jetties present, and shoaling. The comparison of these inlets results in a better understanding of the processes occurring at tidal inlets. A brief history of each inlet and plots of the shoreline changes are included. An attempt was made to show shoreline changes for updrift and downdrift shorelines, but for some inlets complete data sets were not available. For inlets with complete data sets, the shoreline change plots present the net change, and the even and odd components of the net change. Unless otherwise stated negative distances from the inlet are to the north, and positive distances are to the south. When applicable the analytical solution developed in this study was fitted to the downdrift net shoreline change.

6.2 Sebastian Inlet

Sebastian Inlet is a man made inlet located at the Brevard and Indian River County line on Florida's East Coast. The inlet is approximately 45 miles south of Cape Canaveral and 23 miles north of Fort Pierce Inlet. Sebastian Inlet connects the Indian River lagoon to the Atlantic Ocean. Several attempts were made to make a cut through the barrier island in this area from 1886 to 1924, but these efforts failed to create a minimum flow cross section required to maintain a stable inlet (Mehta, et al., 1976). In 1886, using shovels a cut known as Gibson's Cut was started. This work stopped before the cut was completed. In 1895 a cut was completed, but was closed by a storm. The first attempt to make a cut with a

dredge was undertaken in 1918, a channel was completed and two jetties were constructed out of local rock. Four hours after the cut was completed a northeaster closed the channel (Mehta, et al., 1976). Construction was again started in 1924, this time as the work drew near to completion a storm entered the area and opened the cut. The channel shoaled quickly and a 1,500 feet bulkhead was constructed on the south channel bank in 1931, to direct tidal flows to erode the inner channel shoals. Efforts to maintain the shoaling failed and the cut closed in 1941-1942.

In 1948, the present inlet was dredged, this channel was orientated 43 degrees to the south of the old 1924 channel, with the former shoals now forming islands along the new northern bank. A new northern jetty was constructed in 1952, and this jetty received major extensions in 1955 and 1970. A sand trap was dredged in the inner channel in 1962, this trap was re-dredged and enlarged in 1972. During both of these sand trap dredgings, spoil was placed on the downdrift beaches.

The inlet channel has various sizes of rocks in it, and Sabellariid worm reefs are also present. This hard rock underlayer has created a throat cross section which is approximately one half the size of the cross section associated with a similar inlet with a sandy bottom (Mehta, et al., 1976). This smaller cross section has resulted in unusually high tidal currents through the inlet, these currents probably have contributed to the very high shoaling rates and the associated dredging. The almost constant dredging at this inlet indicates that large amounts of material are passing into the inlet.

Figure 6.1 shows the shoreline changes for Sebastian Inlet from 1946 to 1970, these data would indicate the shoreline changes associated with the present inlet location. The net shoreline change shows the extensive downdrift erosion and the updrift accumulation of sediment. It appears that Sebastian Inlet is affecting shorelines for approximately 5 miles updrift and downdrift of the inlet. The most severe erosion has occurred 2 to 3 miles south of the inlet. The downdrift shorelines have eroded an average of 72 feet for this time span; or an erosion rate of approximately 3 feet per year. The updrift shorelines have accreted

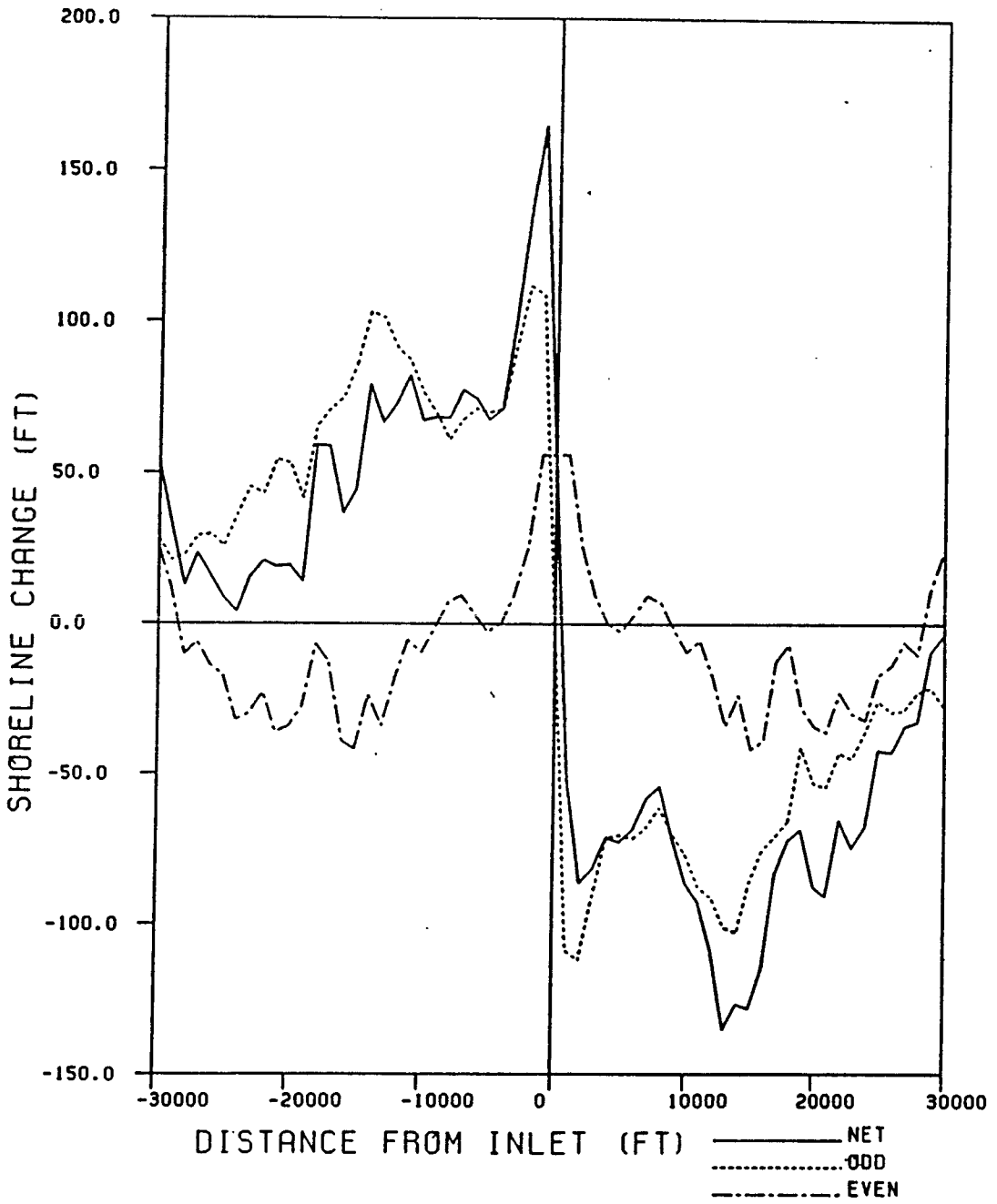

Figure 6.1: Shoreline Changes for Sebastian Inlet 1946 to 1970

an average of approximately 55 feet; resulting in an accretion rate of 2.3 feet per year. The even component indicates a loss of sediment over this region for the time span considered.

Figure 6.2 shows the shoreline changes for Sebastian Inlet for 1928 to 1946, a time period which includes the shoaling and closure of the 1924 cut. The 1928 shoreline would still be experiencing the effects of the 1924 cut, and the 1946 shoreline would be experiencing recovery from the inlet closure in 1941-1942. The shoreline change from 1928 to 1946 shows accretion for 3 miles updrift and downdrift of the inlet. the average accretion was approximately 52 feet. The even component of shoreline change is positive over the entire region indicating a very large net gain of sediment over this region for the time span considered. The odd component of shoreline change is difficult to interpret in that it does not have any noticeable maximum or minimum values, but rather a general trend of decreasing in magnitude from north to south. The lack of an offset between the updrift and downdrift shorelines is most likely the cause of the behavior of the odd component. The odd component indicates that the updrift shorelines are gaining more sediment then the downdrift shorelines, but there is no discontinuity at the inlet.

6.3 Fort Pierce Inlet

Ft. Pierce Inlet is located in St. Lucie County, and connects the Indian river to the Atlantic Ocean. Ft. Pierce Inlet is located between Sebastian and St. Lucie Inlets, Hutchinson Island is directly to the south of the inlet. Prior to the cutting of this inlet, Indian River Inlet existed 2.7 miles to the north of the present location of Ft. Pierce Inlet. This inlet shoaled and eventually closed in the early 1900's, most likely due to the opening of St. Lucie Inlet in 1892 which took much of the tidal flow from Indian River to the ocean (Walton, 1974). Ft. Pierce Inlet was cut in 1920, the original cut was 350 feet wide and the design depth was 25 feet. The original construction also included a pair of 400 feet long jetties, these jetties were too short and were lengthened in 1926. The north jetty was lengthened to 1800 feet and the south jetty was lengthened to 1200 feet. Rapid shoaling occurred in the inlet channel after construction and the channel was dredged often.

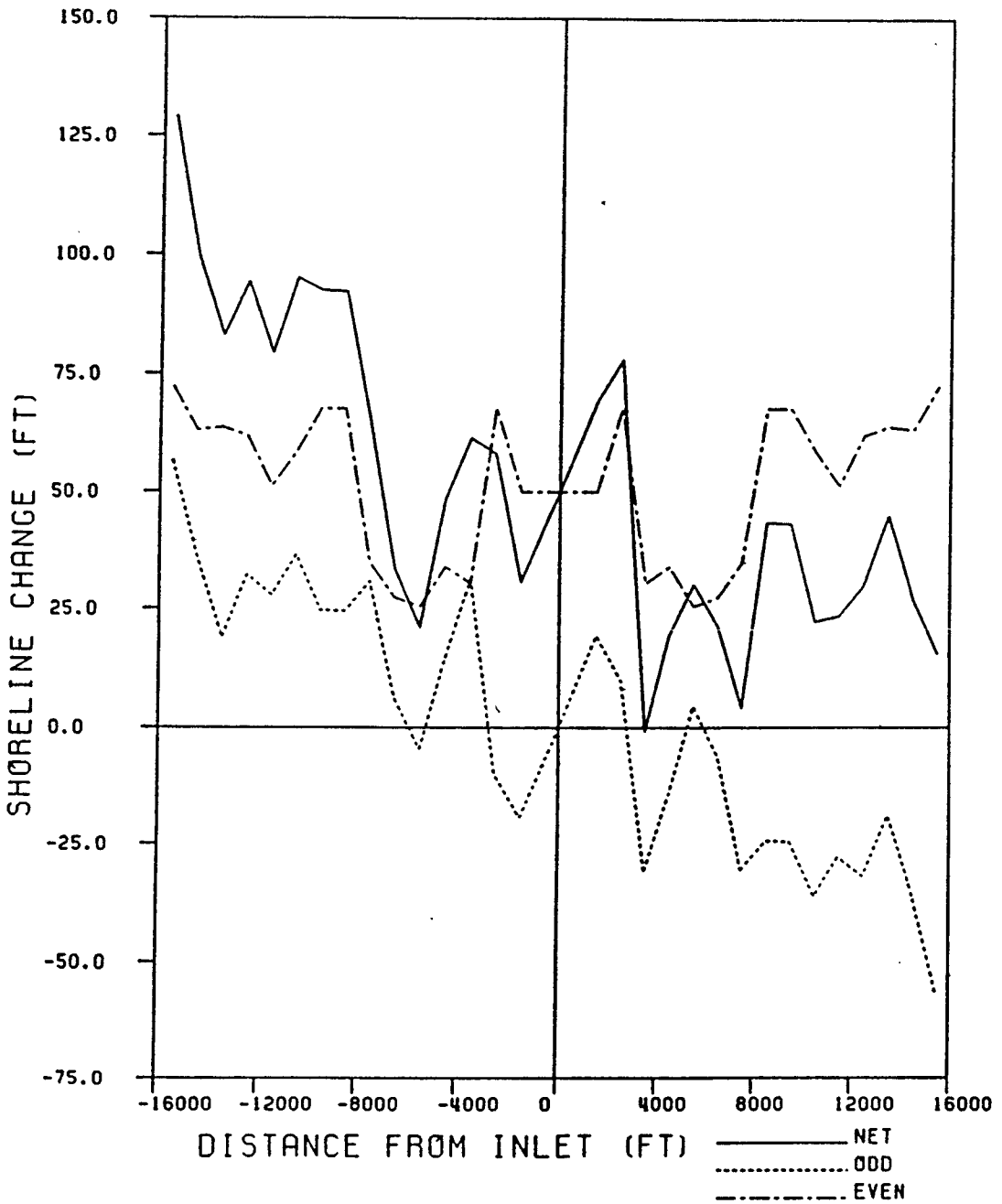

Figure 6.2: Shoreline Changes for Sebastian Inlet 1928 to 1946

Ft. Pierce Inlet is affected by an offshore reef and porous jetties. A reef is located approximately 1250 feet offshore in 10 to 14 feet of water. This reef forms an almost horizontal platform. Both the north and south jetties are permeable and allow sediment to pass through and over them into the inlet. A study of this inlet by the Coastal Engineering Laboratory at the University of Florida in 1957 presented evidence of these jetties acting to drain sediment into the inlet. Profiles near the jetties were found to have a gentler slope compared to profiles farther away form the inlet, and the shoreline for 1500 feet north of the inlet was very stable. It was determined that sand would accumulate at the north jetty and also flow through the jetty to the inlet, causing the inlet to act as a drain. Sediment was found to also pass through the southern jetty, but at a lesser rate than the north jetty. This same study also hypothesized that a natural sand bypassing system existed at the inlet. The ebb tidal currents would bring sediment out of the channel and deposit a large portion of this material on the offshore reef, this material would then migrate along the reef by longshore transport. Wave action on the reef would push some of this sediment back towards the shoreline near the south jetty. If the jetty had been longer this material most likely would have been transported offshore and lost to the longshore transport system.

Figure 6.3 shows the measured shoreline change for Ft. Pierce Inlet from 1883 to 1928, this time period includes pre-cut up to 8 years after the initial cut. Shoreline recovery from the closing of Indian River Inlet can be seen at 8000 to 16,000 feet to the north of the inlet. Updrift accretion and downdrift erosion at the inlet can also be seen. Additionally evident is that the shorelines to the south of the location of the cut were generally accreting during this time period. The even component shows a net increase of sediment over this region during this time span.

Figure 6.4 shows the measured shoreline changes for Ft. Pierce Inlet from 1928 to 1967, this time span is post-cut and includes no beach nourishments. The effects of the inlet are clearly present in this figure, the downdrift shorelines are experiencing erosion for approximately 6 miles and the updrift shoreline is accreting sediment north of the inlet. The

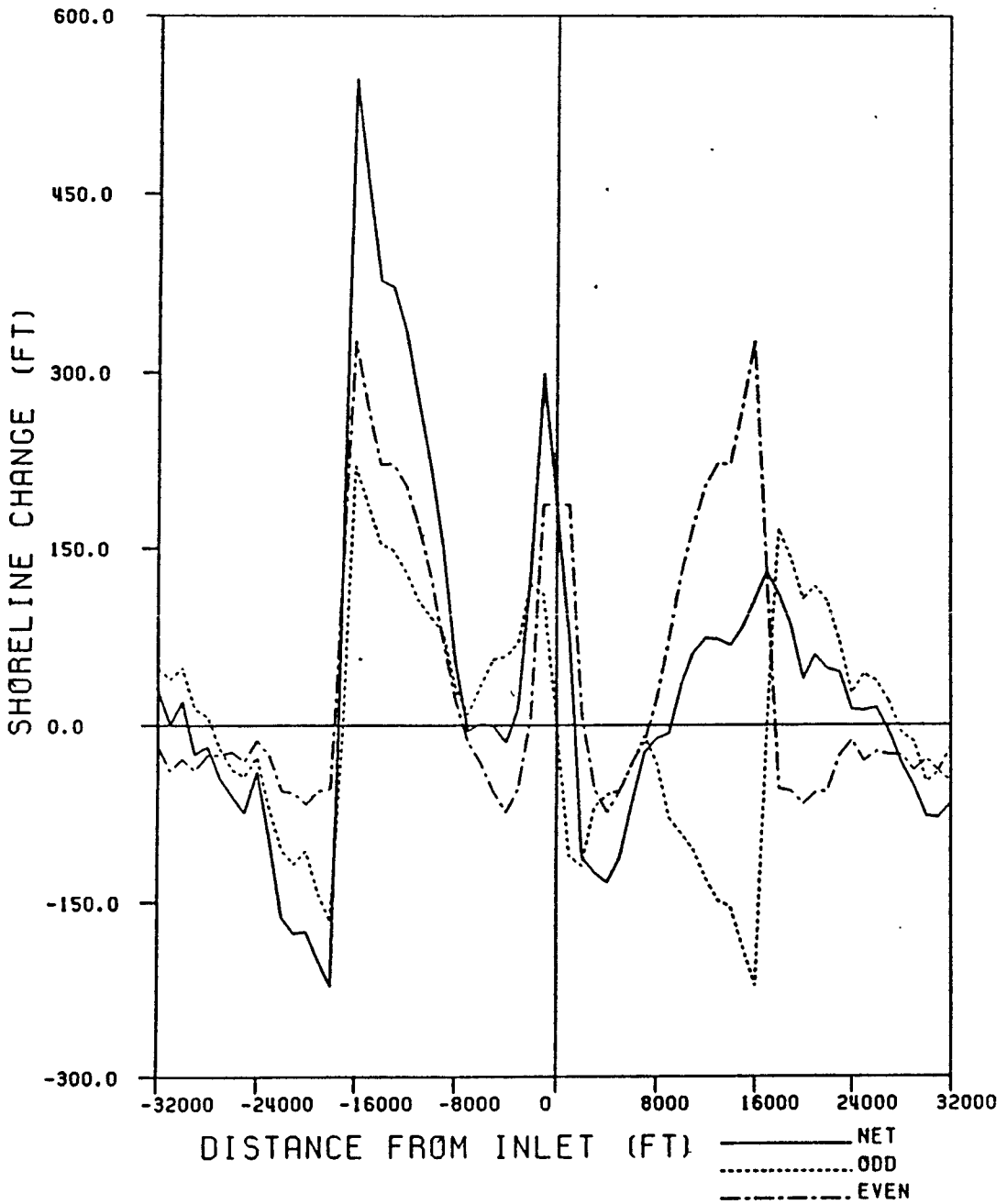

Figure 6.3: Shoreline Changes for Ft. Pierce Inlet 1883 to 1928

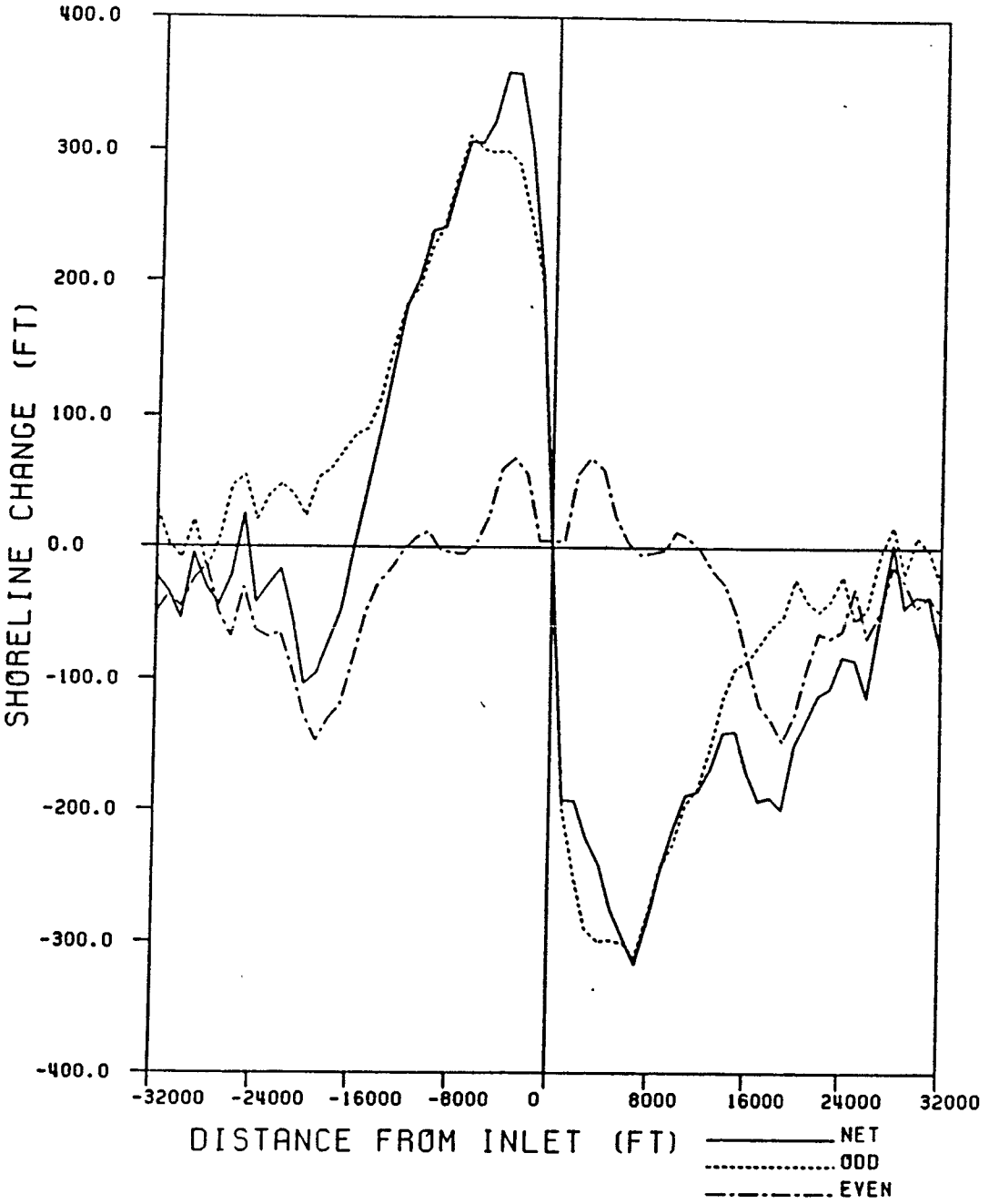

Figure 6.4: Shoreline Changes for Ft. Pierce Inlet 1928 to 1967

maximum erosion was located approximately 1.5 miles downdrift. For a time span from 1928 to 1945 this maximum erosion was one mile downdrift, showing that this point is migrating to the south with time. The effects of the inlet can also be seen by noticing that the odd component of shoreline change is almost identical to the net change for approximately 3 miles north and south of the inlet. The even component of shoreline change indicates a net loss of sediment over this region during this time span, it has been reported that 80,000 cubic yards of sediment per year are lost to the inlet (Coastal Engineering Laboratory Staff, 1957).

The analytical solution was fitted to the net shoreline change for 1928 to 1967, these results are shown in figure 6.5. In both of these figures a sheltered zone next to the inlet is present, a more thorough discussion of this zone is presented in the numerical results chapter of this report. Two predicted shoreline changes are presented in figure 6.5, one uses the entire data set, and the other only uses the portion of the data south of the sheltered zone. For the net shoreline changes the analytical solution yielded a wave height of 2.29 feet and a breaker angle of 1.62 degrees, for the odd shoreline changes the solution yielded a breaking wave height of 1.72 feet and a breaker angle of 2.41 degrees. The CDN data for Ft. Pierce indicate an average yearly $\overline{(H_b^{5/2})}^{0.4}$ of 2.26 feet.

6.4 St. Lucie Inlet

St. Lucie Inlet is an opening from the Indian and St. Lucie Rivers to the Atlantic Ocean. The inlet is located between Hutchinson Island to the north and Jupiter Island to the south. The inlet was opened by local interests in 1892, the original inlet dimensions were a width of 30 feet and a depth of 5 feet. The inlet widened quickly and by 1898 the dimensions of the cut were 1700 feet by 7 feet. In 1926 to 1929 a 3,325 feet long jetty was constructed on the north side of the inlet. After the initial cut and up to the time of construction of this jetty the northern shoreline retreated. After jetty construction the updrift shoreline stabilized and accretion began to take place. The southern shoreline has experienced continual erosion since the cutting of the inlet. Before jetty construction there

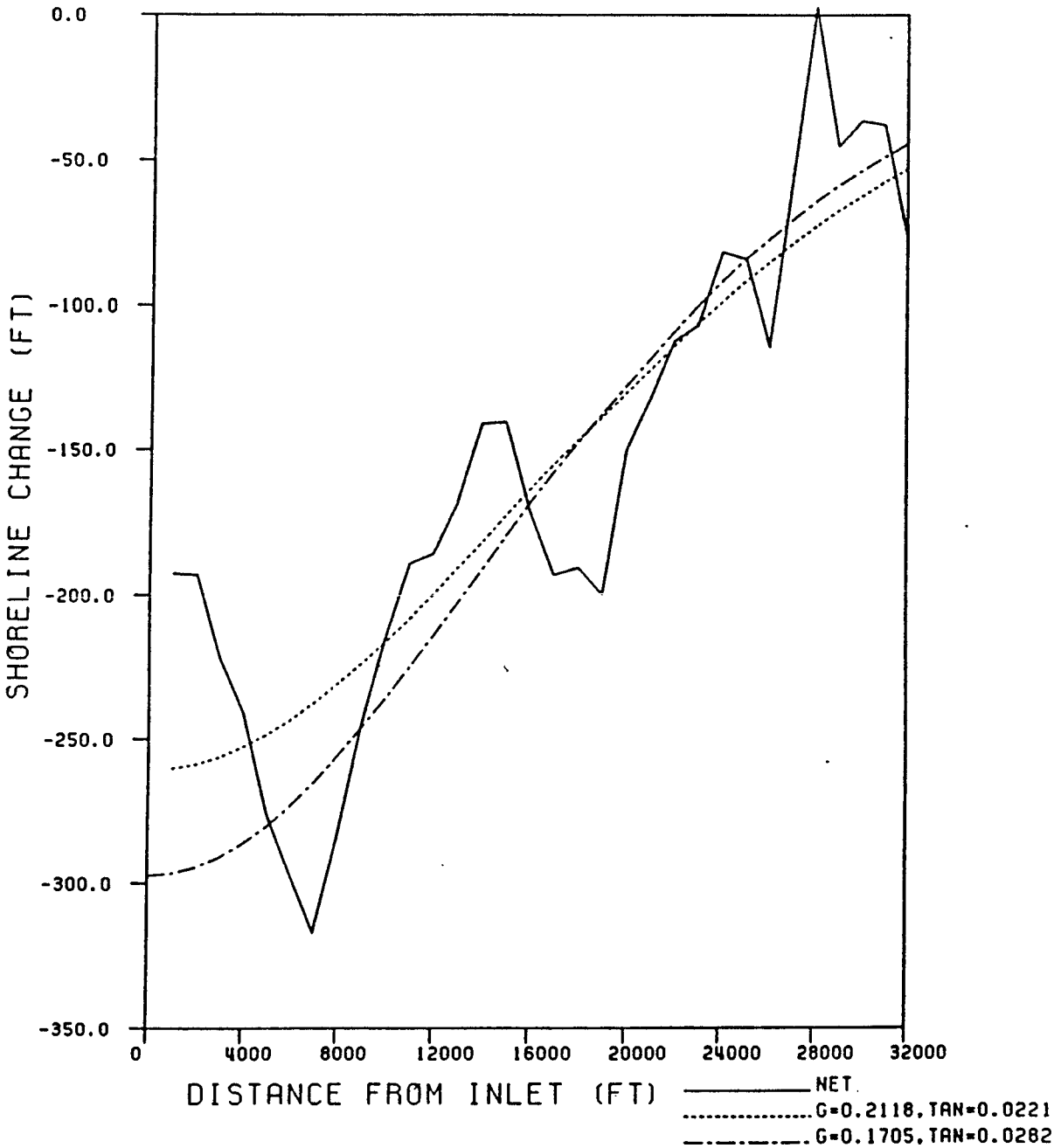

Figure 6.5: Predicted Net Shoreline Change for Ft. Pierce Inlet 1928 to 1967

was transport across an offshore bar , but this transfer of sediment was irregular (U.S. Army Corps of Engineers, 1971). The shoreline south of the inlet along Jupiter Island has experienced one of the most severe erosion problems in the state, with erosion rates of up to 40 feet per year (U.S. Army Corps of Engineers, 1968). The measured shoreline change data indicate an average erosion rate of 14 feet per year for a time period from 1928 to 1970 for 1.5 miles south of the inlet to 6.5 miles south of the inlet.

Figure 6.6 shows the net shoreline change from 1883 to 1948, and figure 6.7 shows the net shoreline change from 1948 to 1970. The odd and even components of the net change are also presented in these figures. The net change from 1883 to 1948 shows the massive erosive power associated with the cutting of this inlet. The updrift region shows signs of accretion after the jetty construction in 1928, by 1948 this shoreline has almost returned to the 1883 position. Unfortunately the 1928 survey does not include any data north of the inlet. The accretion north of the inlet is more clearly seen in the data from 1948 to 1970. The maximum erosion is located 8,000 to 16,000 feet south of the inlet. This maximum erosion region is spread over a region approximately one mile long. This one mile region has a erosion rate of 27 feet per year. For both time spans the even component denotes a loss of sand over the region considered, this loss could either be to the inlet or offshore shoals. At the inlet the even component changes sign, in figure 6.6 the even component is negative,in figure 6.7 the even component has become positive. The negative even component is associated with the widening of the channel and the westward migration of the northern end of Jupiter Island. By 1948 the inlet region has started to stabilize its orientation and the positive even component is indicating some build up of material in this region. It should also be noted that the odd component in figure 6.6 is almost identical to the shoreline change signature of the analytical solution.

Figure 6.8 shows the predicted shoreline change and the measured data for surveys of 1928 and 1970. This time period encompasses the jetty construction up to the first major beach nourishment project. There were no survey data directly south of the inlet, causing

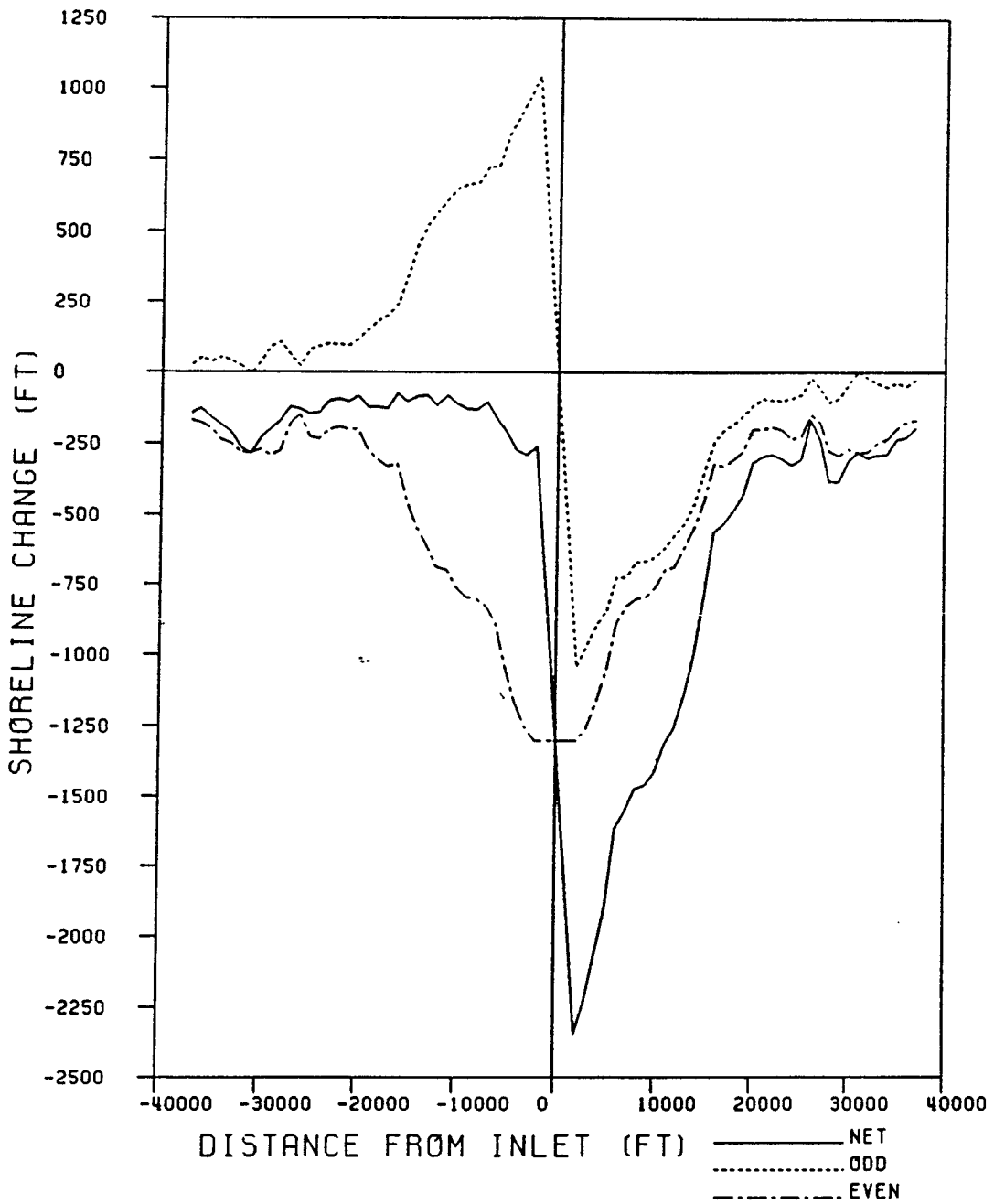

Figure 6.6: Shoreline Change for St. Lucie Inlet 1883 to 1948

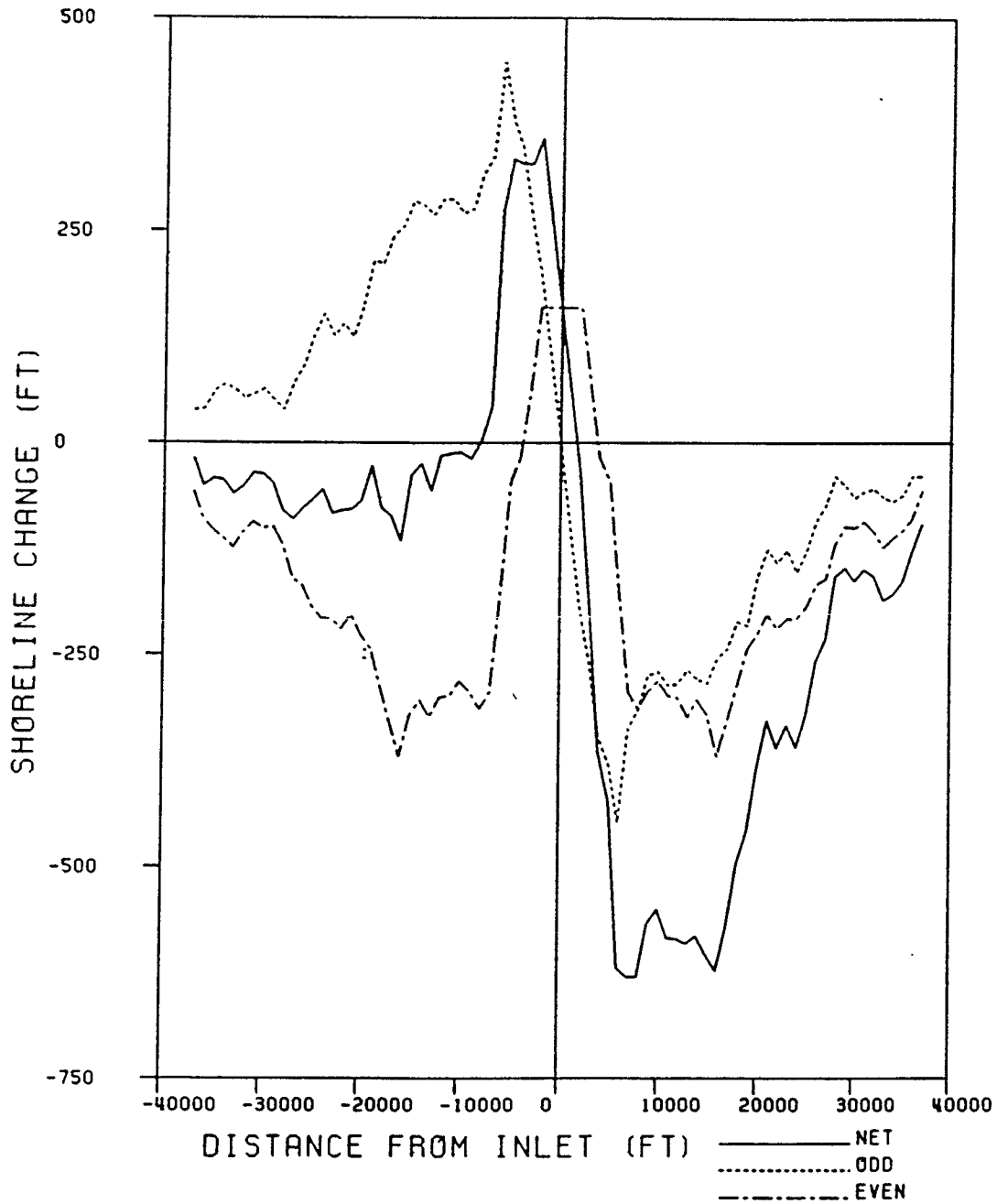

Figure 6.7: Shoreline Change for St. Lucie Inlet 1948 to 1970

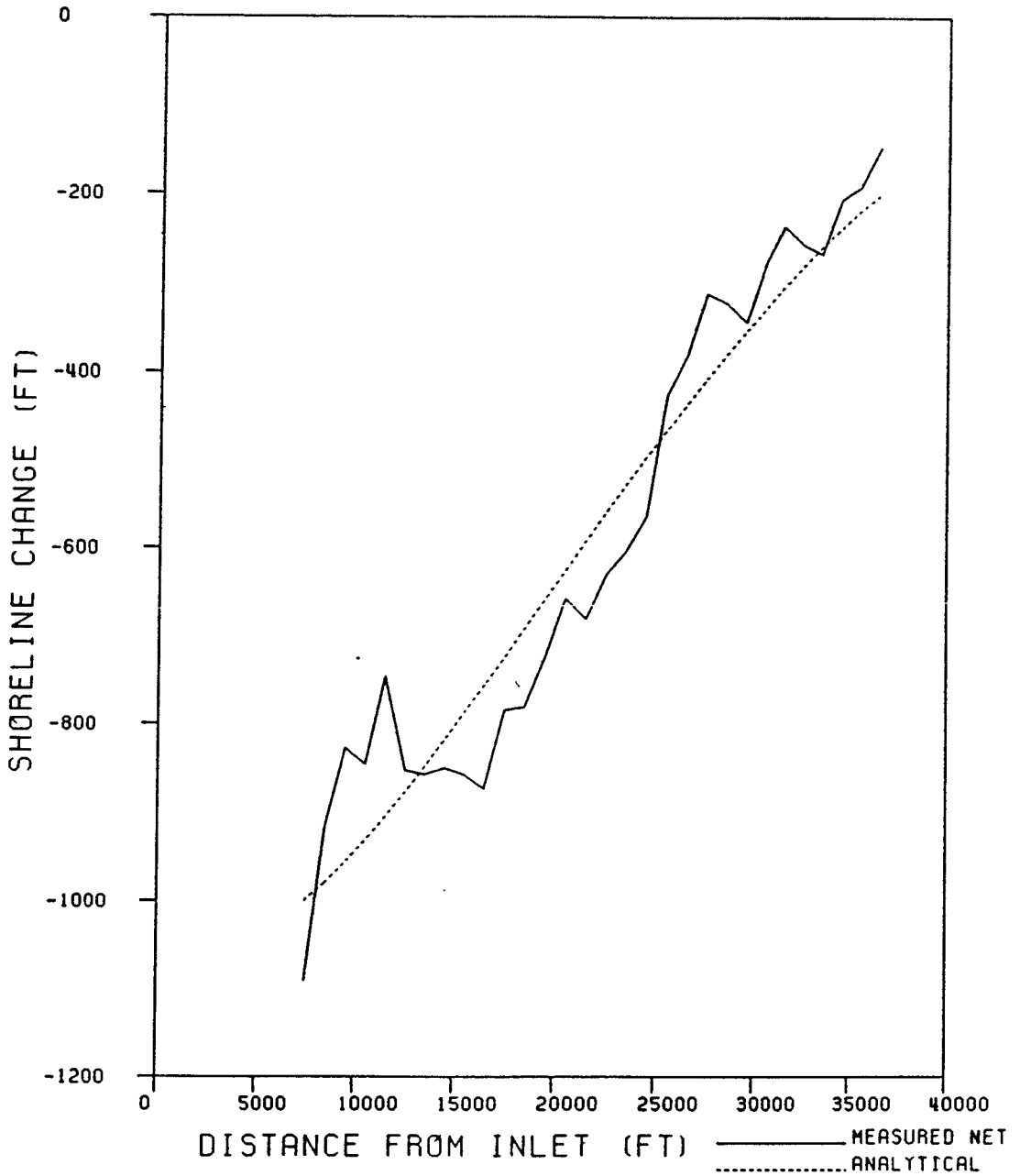

Figure 6.8: Predicted Shoreline Change for St. Lucie Inlet 1928 to 1970

a gap of approximately a mile and a half to occur. The maximum erosion was at the first survey data point south of the inlet, and the erosion decreased as distance from the inlet increased. The analytical solution yields an average breaking wave height of 1.95 feet and a breaker angle of 10 degrees. These wave parameters would produce a longshore transport of approximately 617,000 cubic yards per year, a reported gross transport rate for St. Lucie is 523,000 cubic yards per year (Walton, 1973). The measured data show a loss of sediment of 512,000 cubic yards per year. The CDN wave data indicate a $\overline{(H_b^{5/2})}^{0.4}$ wave height of 2.18 feet.

Figure 6.9 shows the predicted shoreline and measured data for 1948 to 1970. Two predicted shoreline change results are shown, one using all the data and one excluding the sheltered zone immediately south of the inlet. Excluding the sheltered zone, the analytical solution yields an average breaking wave height of 1.73 feet and a breaker angle of 16 degrees. The transport produced by these values is 711,000 cubic yards per year. This was a complete data set and extended up to the inlet.

6.5 South Lake Worth Inlet

South Lake Worth Inlet is located in Palm Beach County on Florida's east coast. Lake Worth Inlet is to the north and Boca Raton Inlet is to the south. Lake Worth Inlet was cut in 1918 to form a connection from Lake Worth, a salt-water sound, to the Atlantic Ocean. The southern end of Lake Worth was becoming stagnant, and South Lake Worth Inlet was cut in 1927 to increase flushing. South Lake Worth Inlet has also been referred to as Boynton Inlet. A pair of 300 feet long jetties was also constructed at this time. Sediment quickly built up next to the northern jetty, and shoals formed in the inlet. This shoaling threatened to close the inlet, and a sand transfer plant was constructed on the north jetty in 1937. This sand transfer plant has operated continually except from 1942 to 1945 because of fuel shortages during World War II. The sand transfer plant is estimated to transfer approximately 75 cubic yards per hour (U.S. Army Corps of Engineers, 1953), it has also been estimated that prior to 1958 one million cubic yards of material had been transferred

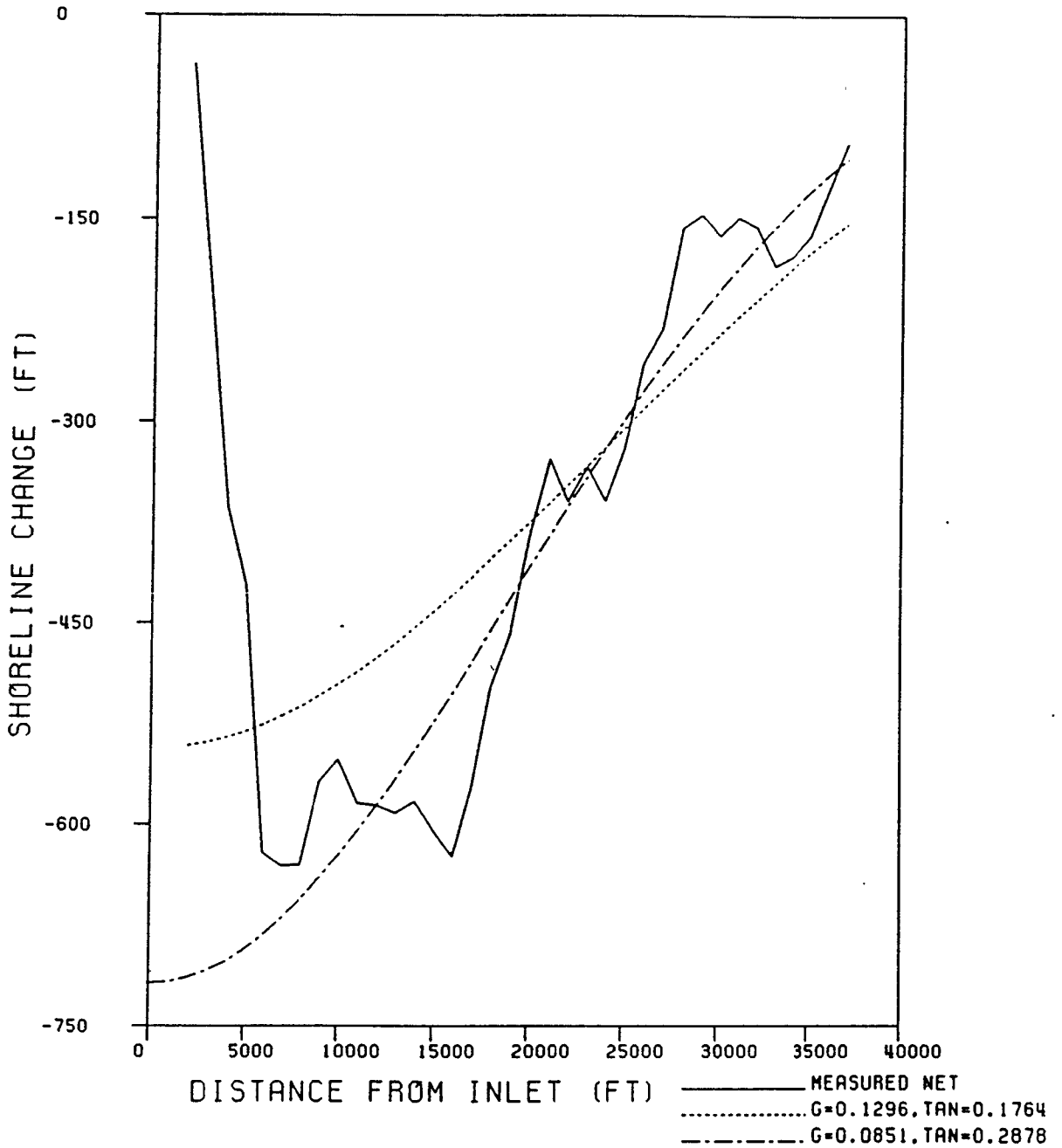

Figure 6.9: Predicted Shoreline Change for St. Lucie Inlet 1948 to 1970

(U.S. Army Corps of Engineers, 1971). The transfer plant consists of a suction line on a swinging boom and is operated for two to three hours a day. The sand transfer plant was relocated in 1967, when jetty additions were made. Shorelines on both sides of the inlet have been heavily armored with groins and seawalls.

Figure 6.10 shows the shoreline changes for South Lake Worth Inlet from 1883 to 1927. The shoreline near the inlet has accreted a considerable distance, with adjacent shorelines generally eroding at differing rates. Notice that the shorelines south of the inlet have built out more than the shorelines to the north of the inlet. The odd component of shoreline change has a very unusual feature; the odd component directly south of the inlet is much greater than the odd component directly north of the inlet. The usual odd shoreline component has a maximum value updrift of an inlet and a minimum value downdrift of an inlet. The odd component indicates that adjacent to the present location of the inlet the shoreline to south was accreting and the shoreline to the north was eroding sediment from 1883 to 1927.

Figure 6.11 shows the shoreline changes for South Lake Worth Inlet for 1927 to 1942. The effects of the inlet cutting can be seen as updrift accretion and downdrift erosion. For 1883 to 1927 the updrift shoreline was experiencing more erosion than the downdrift shorelines, from 1927 to 1942 almost the entire updrift shoreline is accreting. The decreased erosion located approximately 10,000 feet south of the inlet, coincides with the location of a groin field which fronts a seawall that was constructed during this time. The effects of the sand transfer plant are not easily seen from these data. The odd component now exhibits the usual pattern of a maximum value updrift of the inlet, and a minimum downdrift of the inlet. It should also be noted that the odd component of shoreline change almost exactly matches the net shoreline change for 10,000 feet north and south of the inlet. This matching of the net change and the odd change is an indication of the overwhelming influence the inlet cutting has had on the longshore transport in this region. The accretion starting approximately 20,000 feet south of the inlet may be due to influences of Boca Raton Inlet.

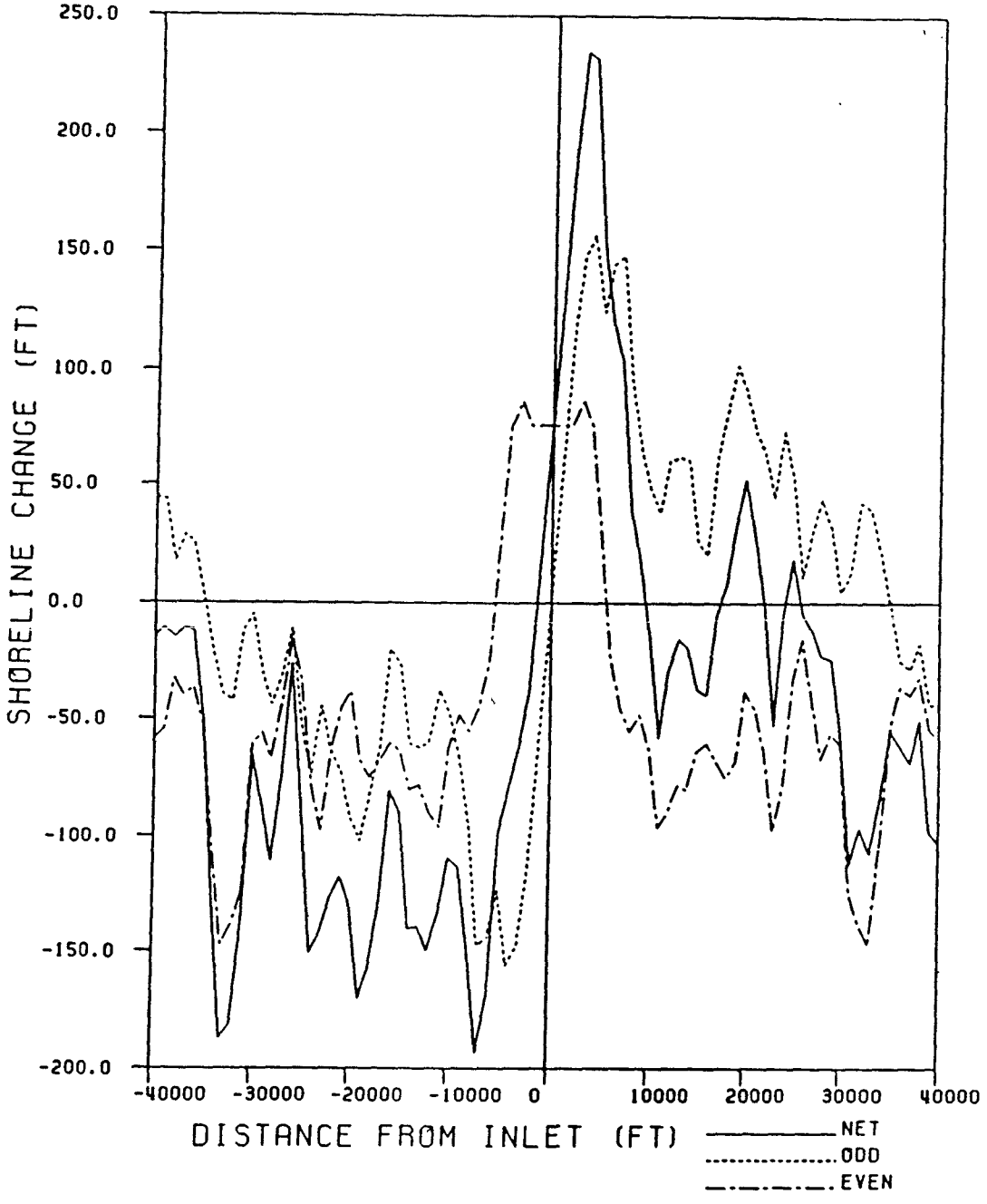

Figure 6.10: Shoreline Changes for South Lake Worth Inlet 1883 to 1927

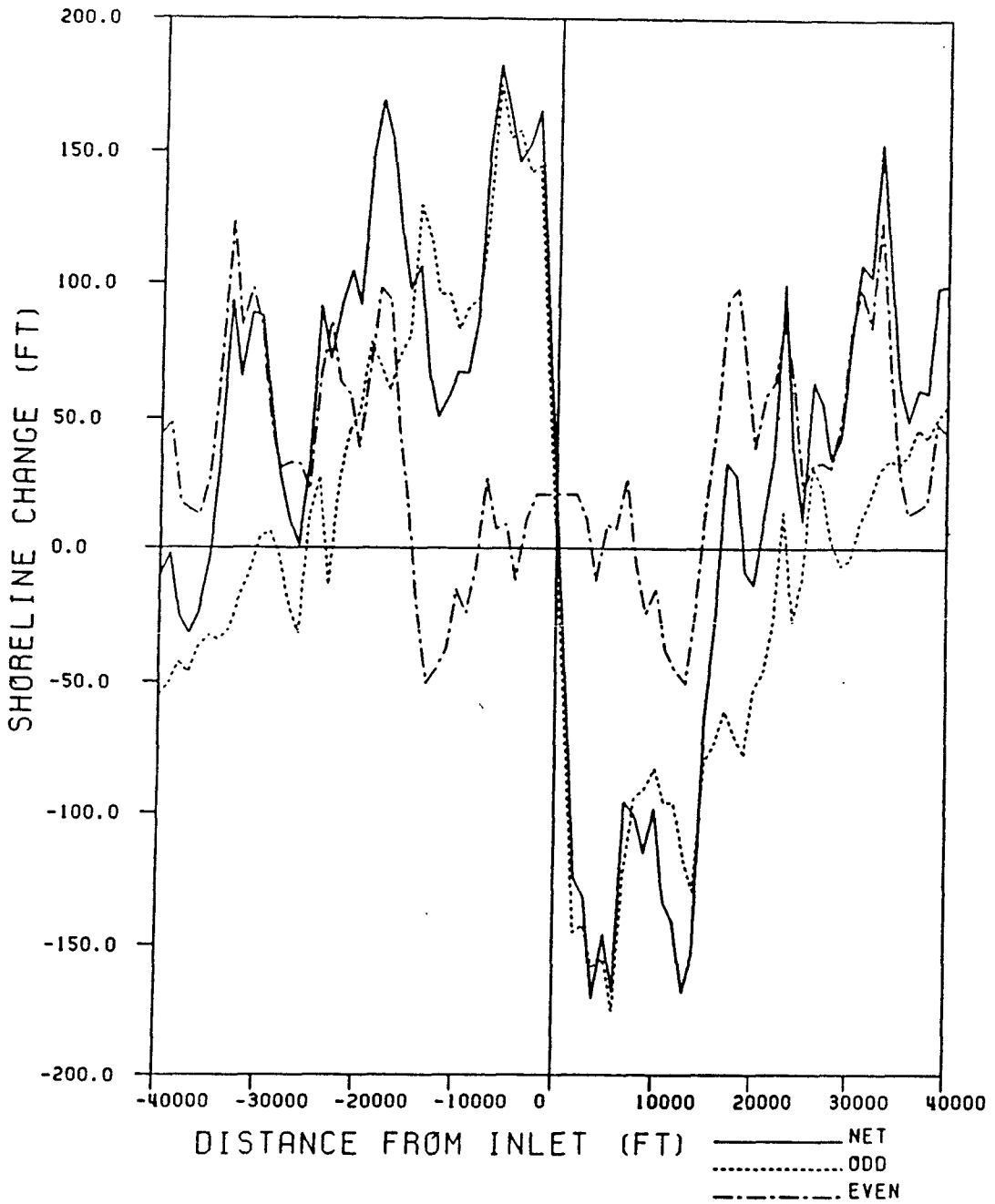

Figure 6.11: Shoreline Changes for South Lake Worth Inlet 1927 to 1942

The effects of the sand transfer plant can be seen in figure 6.12, which shows the shoreline changes for South Lake Worth Inlet from 1942 to 1970. Shorelines for approximately 15,000 feet north and south of the inlet are accreting during this time span. The even component of shoreline change indicates a net gain of sediment for this region of plus or minus 15,000 feet. For the entire region the even component of shoreline change indicates a net loss of sediment for the time span considered.The maximum erosion has moved to approximately 20,000 feet south of the inlet. The region from 10,000 feet to 20,000 feet north of the inlet is also experiencing erosion.

6.6 Boca Raton Inlet

Boca Raton Inlet is at the southern end of Palm Beach County near the boundary with Broward County on Florida's east coast. South Lake worth Inlet is to the north and Hillsboro Inlet is to the south. Before the original cut was made in 1925, an occasional outlet from Lake Boca Raton would open during heavy rainy seasons (Fluet, 1973). This opening would then soon close because of wave action and shoaling. In 1925 a private corporation purchased the rights to the waterway in the vicinity of this opening and improved the inlet by dredging. This improved cut experienced shoaling and jetties were constructed in 1930 to 1931, after this construction an ebb shoal soon formed (Strock, 1979). This inlet frequently closed due to shoaling, and in 1957 improvements by dredging were carried out again. Once again the inlet was plagued by a severe shoaling problem. Boca Raton Inlet also had the unique problem of whom had legal responsibility to maintain the inlet and jetties. These legal problems often hindered efficient inlet maintenance. In 1972 the privately owned jetties and the inlet waterway were deeded to the City of Boca Raton.

Because of the frequent dredging needed to maintain the inlet, the northern jetty was extended in 1975. This extension was successful in maintaining a navigable waterway, but caused severe erosion to the south of the inlet. Since 1972, the City of Boca Raton has maintained a dedicated dredge at the inlet, and spoil has been placed on the downdrift shorelines. To help alleviate the erosion problems at the inlet a weir section was constructed

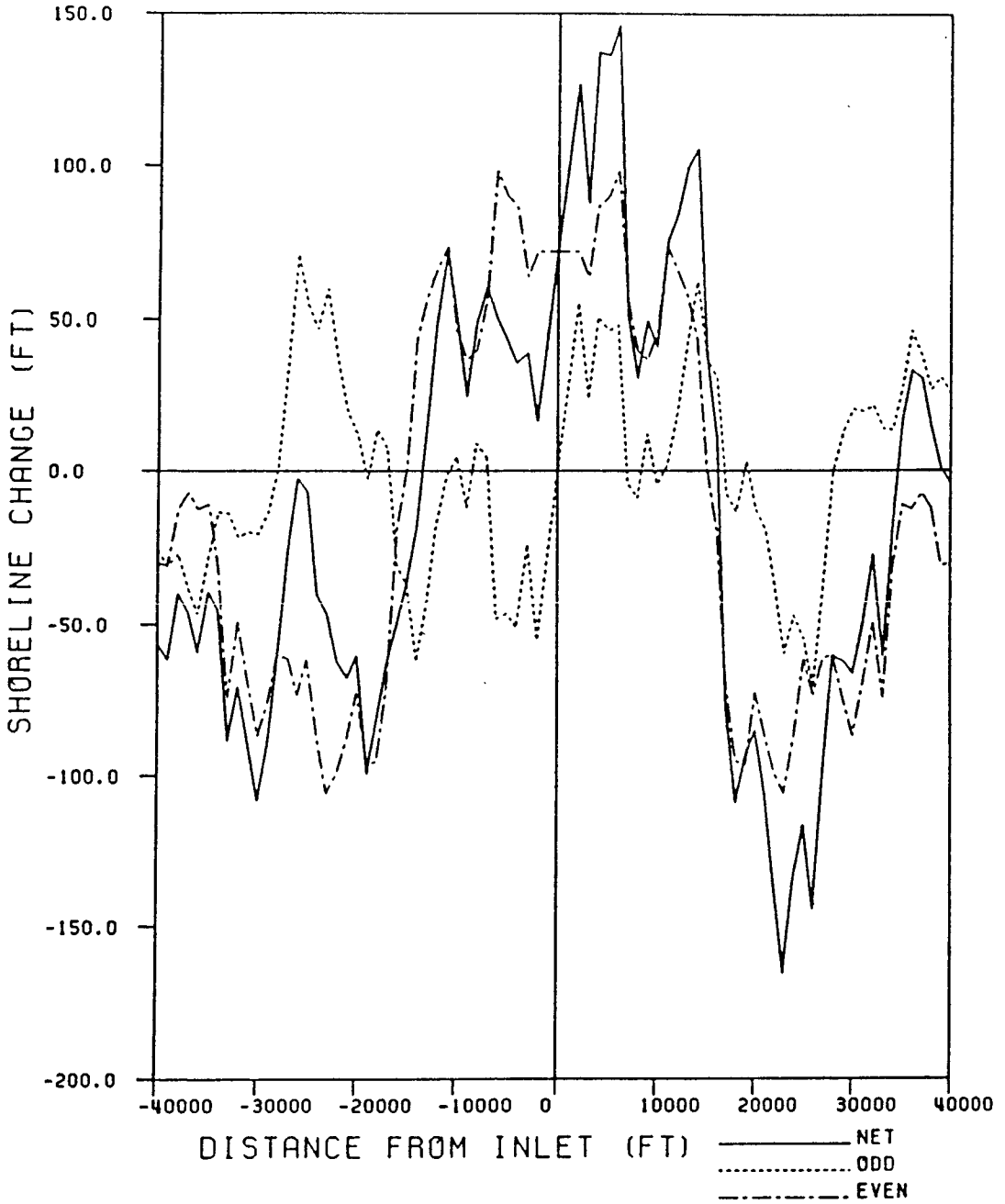

Figure 6.12: Shoreline Changes for South Lake Worth Inlet 1942 to 1970

in the north jetty in 1980. Sediment bypassing took place by dredging this sand trap at the weir and placing the material south of the inlet.

Figure 6.13 shows the measured shoreline changes for Boca Raton Inlet for 1927 to 1970. These surveys span a time period from shortly after the initial cut and up to just prior to the northern jetty extension. The shoreline changes are then representative of the shoreline history of Boca Raton Inlet up to the 1975 jetty extension, and will include effects of several openings, closings, and almost continuous series of channel dredgings. The downdrift shorelines experienced erosion with a maximum retreat at approximately 12,000 feet south of the inlet. A groin field is located half a mile south of the inlet, and may be the cause of the region of decreased erosion rate located about a mile south of the inlet. The effects of bypassing can be seen as accretion just south of the inlet. The entire updrift shoreline experienced accretion during this time span. The even component of shoreline change indicates a net gain of sediment over this region for the time period considered.

A beach nourishment project was completed in 1980, in response to erosion due to the northern jetty extension. The project length was approximately one mile, and approximately 44,000 cubic yards of material was placed over this project length (Stauble, 1986). Figure 6.14 shows the downdrift shoreline changes for Boca Raton Inlet for 1974 to 1985. The fill can be seen as the bulge in the shoreline changes centered at 10,000 feet south of the inlet. The shorelines south of this fill are experiencing an increased erosion rate compared to the 1927 to 1970 shoreline changes. The analytical solution was fitted for this erosion region. The solution yielded a wave height of 1.27 feet and a breaker angle of 1.1 degrees.

6.7 Baker's Haulover Inlet

Baker's Haulover is located in Dade county and connects the Atlantic Ocean to the northern end of Biscayne Bay. The inlet is nine miles north of Government Cut, and 14 miles south of Port Everglades Harbor. The original cut was made in 1925 to rid the northern end of Biscayne Bay from accumulating pollution. Due to the increased development of south Florida this inlet has become increasingly important for navigation purposes. In September

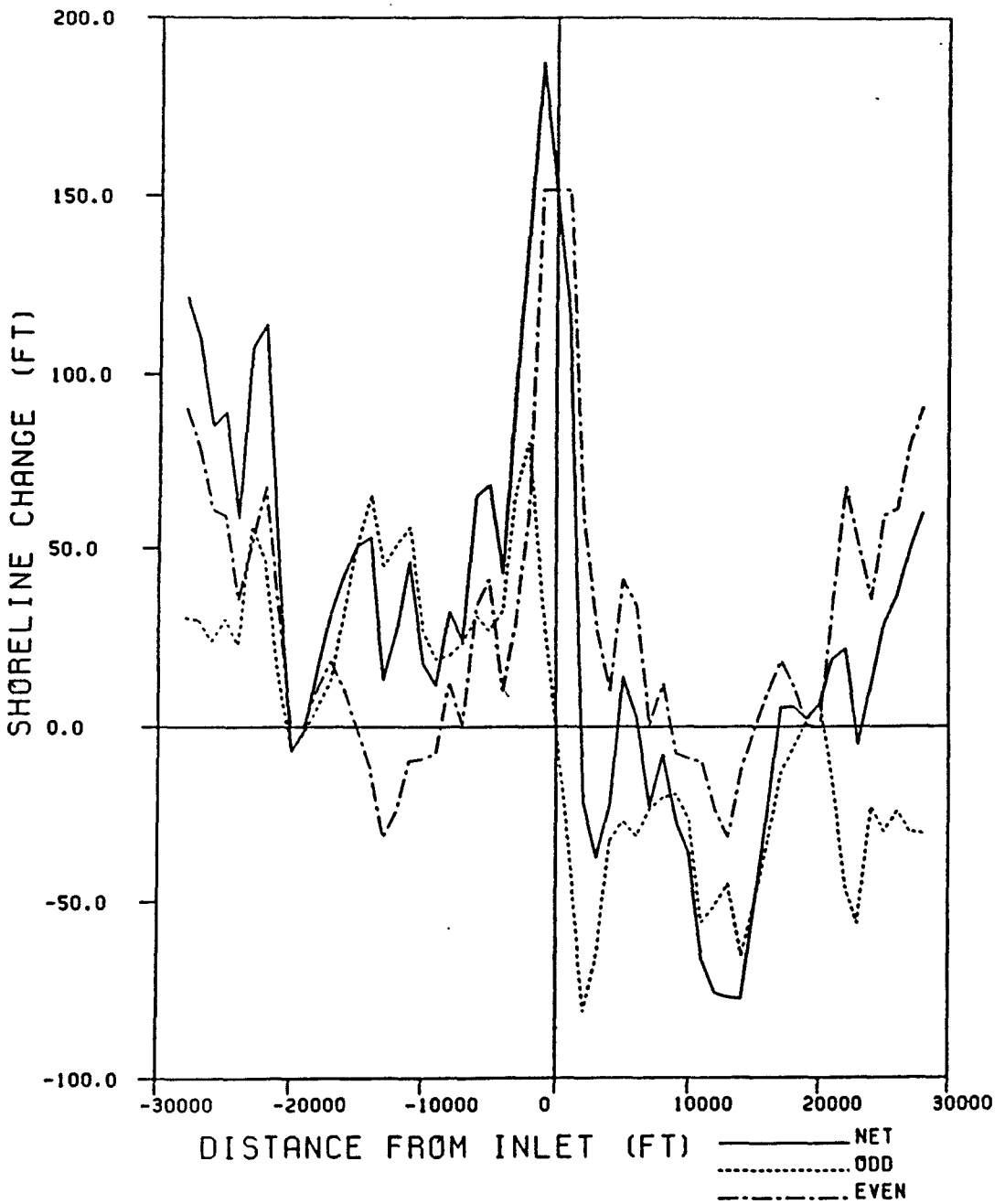

Figure 6.13: Shoreline Changes for Boca Raton Inlet 1927 to 1970

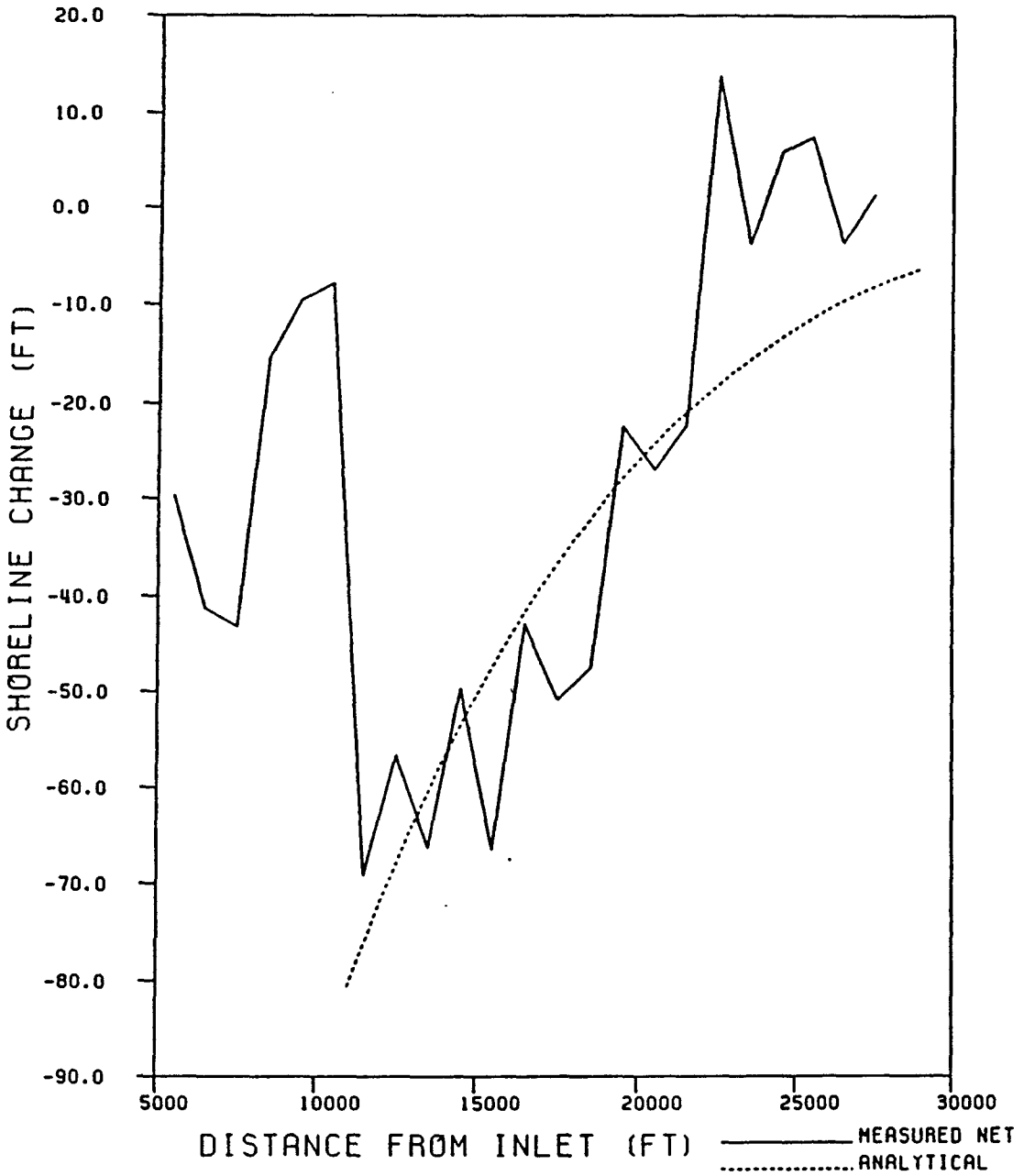

Figure 6.14: Shoreline Changes for Boca Raton Inlet 1974 to 1985

1926 a severe hurricane passed over this area destroying all of the construction associated with the inlet and causing massive erosion throughout the region. The hurricane had winds up to 120 m.p.h and gusts up to 130 m.p.h, and a storm surge of 10.6 feet above mean sea level (U.S.Army Corps of Engineers, 1946). By 1928 the inlet was repaired and two short steel cellar jetties were installed, the inlet width was 300 feet. Steel sheet-pile bulkheads were also constructed parallel to the shorelines for approximately 700 feet north and south of the inlet.

This inlet has experienced a varying shoreline history of erosion and accretion. Because of the influence of several inlets to the north the quantity of sand reaching this area is far below the transport capacity of incoming waves. Estimates of net longshore southerly transport are 50,000 cubic yard per year at the north county line and 20,000 cubic yards per year at Government Cut (Coastal and Oceanographic Engineering Department, 1958). The Little Bahama and Great Bahama Banks lay approximately 60 miles due east of the coast of Florida from this shoreline. These banks shelter the coast from waves and also prevent some long period swell that would arrive from the north east from affecting the area. These north east waves are generally associated with winter storms and tend to transport sediment back on shore (Coastal and Oceanographic Engineering Department, 1969). Another important fact for this region is that for 4,500 feet south of the inlet an almost continuous line of seawalls has been built by property owners. These structures were usually exposed to wave action at high tide (Coastal and Oceanographic Department, 1958).

Unlike most inlets studied in this investigation, both the north and south shorelines have experienced erosion. The jetties are very permeable and sediment leaks through them and bypasses around both the south and north jetties. This region also has a hard rock layer underlying the surface. This rock has prevented the inlet from scouring to a depth of natural stability of a similar sandy inlet. This has caused high tidal currents to occur, the flood tide draws sediment into the inlet causing large shoals. The Corps of Engineers reports that 17,000 cubic yards of sediment were dredged from the inlet channel yearly (U.S. Army

Corps of Engineers, 1946), before the south jetty was extended. The ebb tidal currents are strong enough to move most suspended sediment offshore. These tidal currents are also large because of the relatively small size of the inlet compared to the size of Biscayne Bay. The results are that both the north and south shorelines have experienced erosion due to the inlet being both a barrier and a drain for sediment.

From 1851 to 1919 the shorelines for the region were accreting throughout the county, the area where the inlet would be cut experienced some erosion (figure 6.15). From 1919 to 1927 the shorelines eroded due to the September 1926 hurricane. The shoreline change from 1919 to 1945 is shown in figure 6.16. It can be seen that no dominant trend is present, this is most likely due to the heavy armoring of the shorelines during this time period. The next period for which survey data were available was 1945 to 1962, this time span includes beach nourishments placed north and south of the inlet in 1960. The shoreline changes for 1945 to 1962 are presented in figure 6.17. A laboratory study in 1958 states that very little shoreline change occurred between 1943 and 1957 (Coastal and Oceanographic Department, 1958). The shoreline advance from the nourishment projects can be seen, but it also evident that the nourishment is spreading and erosion is starting to occur at the inlet.

A period of high erosion was found to occur from 1935 to 1945, for the region south of the seawalls for approximately 5 miles (figure 6.18). The analytical solution agreed well with the measured data for this time span, the solution yielded a breaking wave height of 2.22 feet and a breaker angle of 4.75 degrees.

6.8 Venice Inlet

Venice Inlet is located on Florida's West coast in Sarasota County, and separates Casey Key from Manosota Key. Venice Inlet connects Little Sarasota Bay and Roberts Bay with the Gulf of Mexico. This inlet has also been referred to as Casey Pass.

Venice Inlet is a natural inlet which migrated before a nine feet deep channel was dredged in 1937 to 1938. Accompanying the channel dredging was the construction of a pair of sheet-pile jetties. Because of severe erosion associated with the jetty construction,

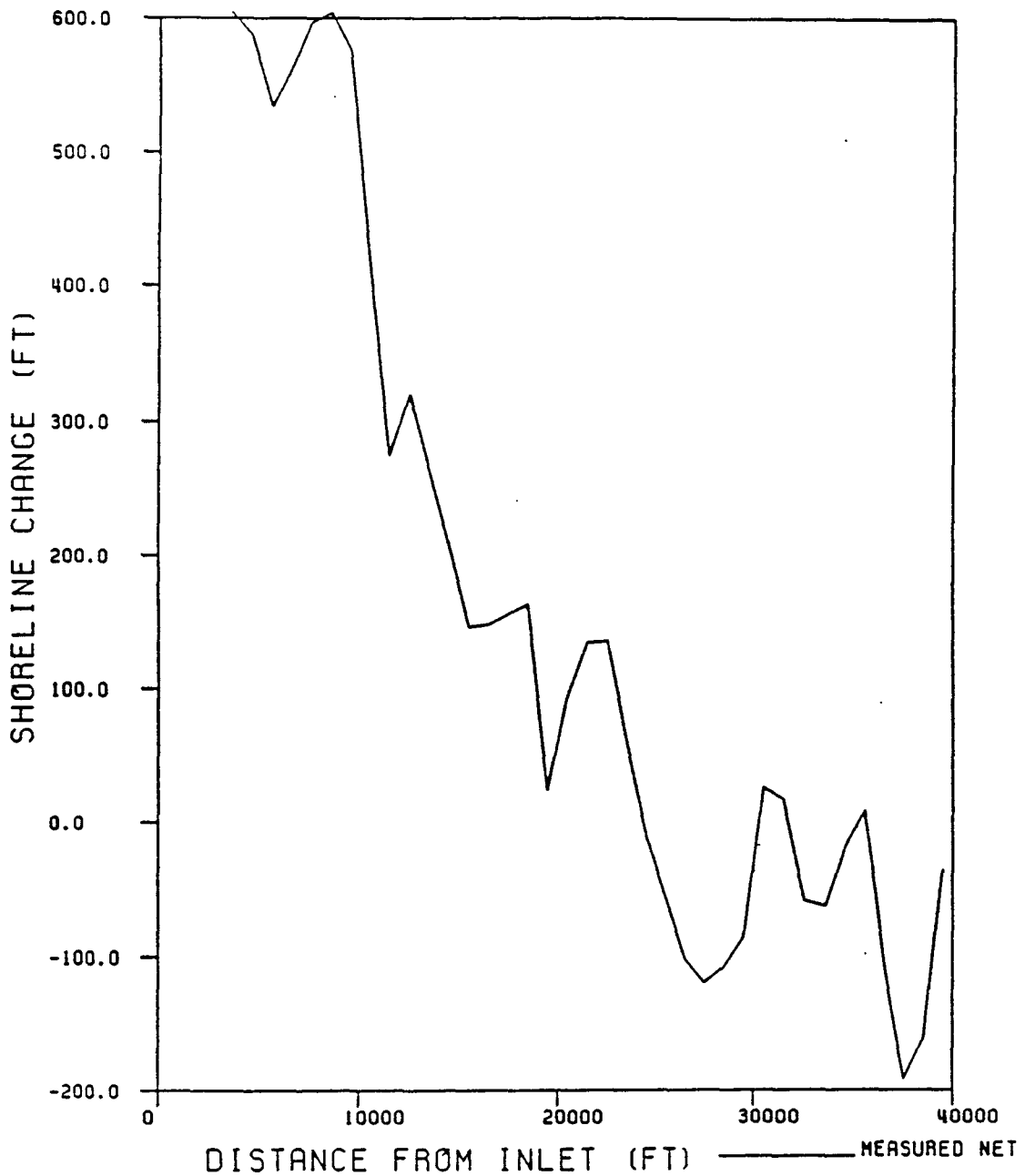

Figure 6.15: Shoreline Change for Baker's Haulover 1851 to 1919

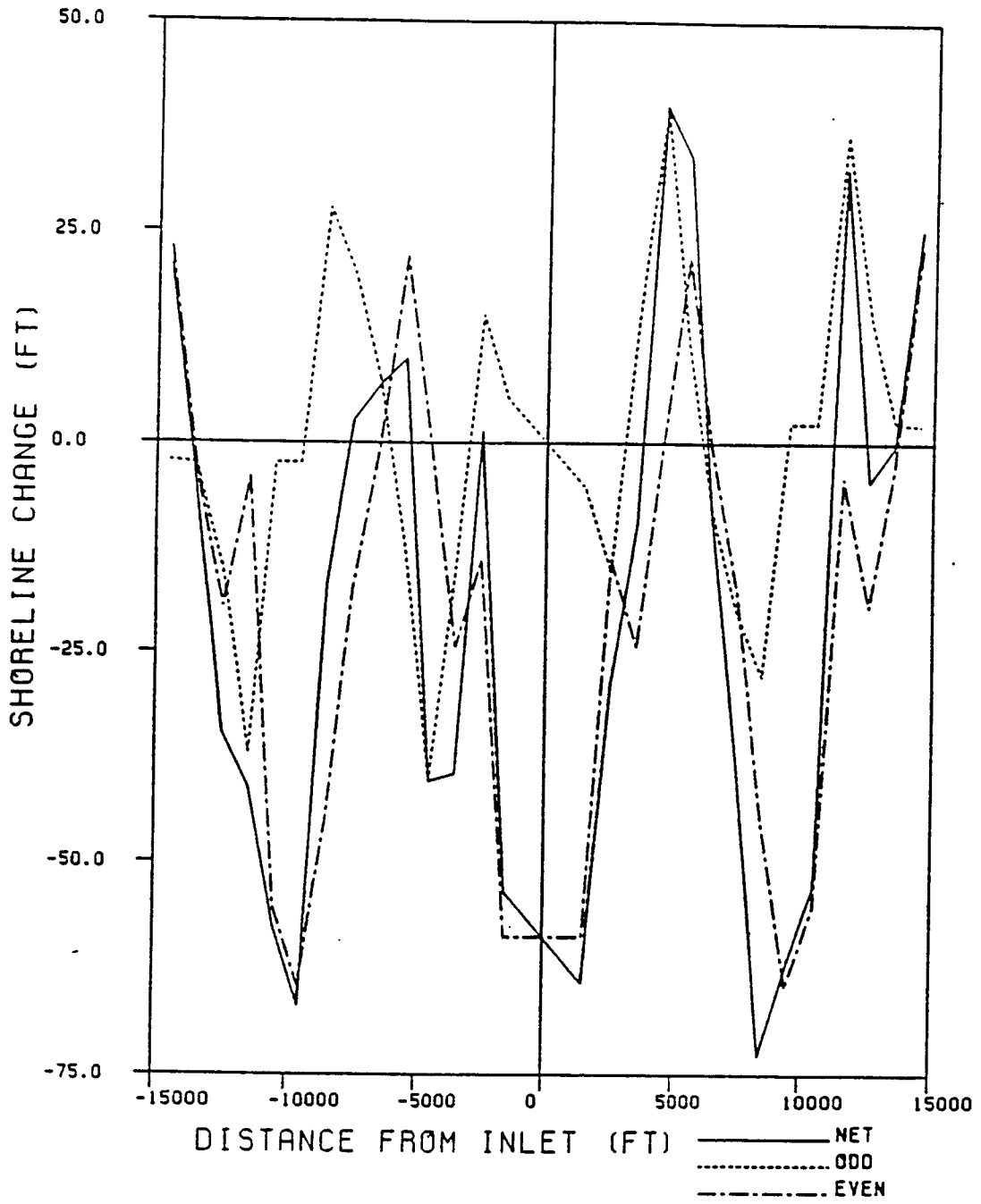

Figure 6.16: Shoreline Change for Baker's Haulover 1919 to 1945

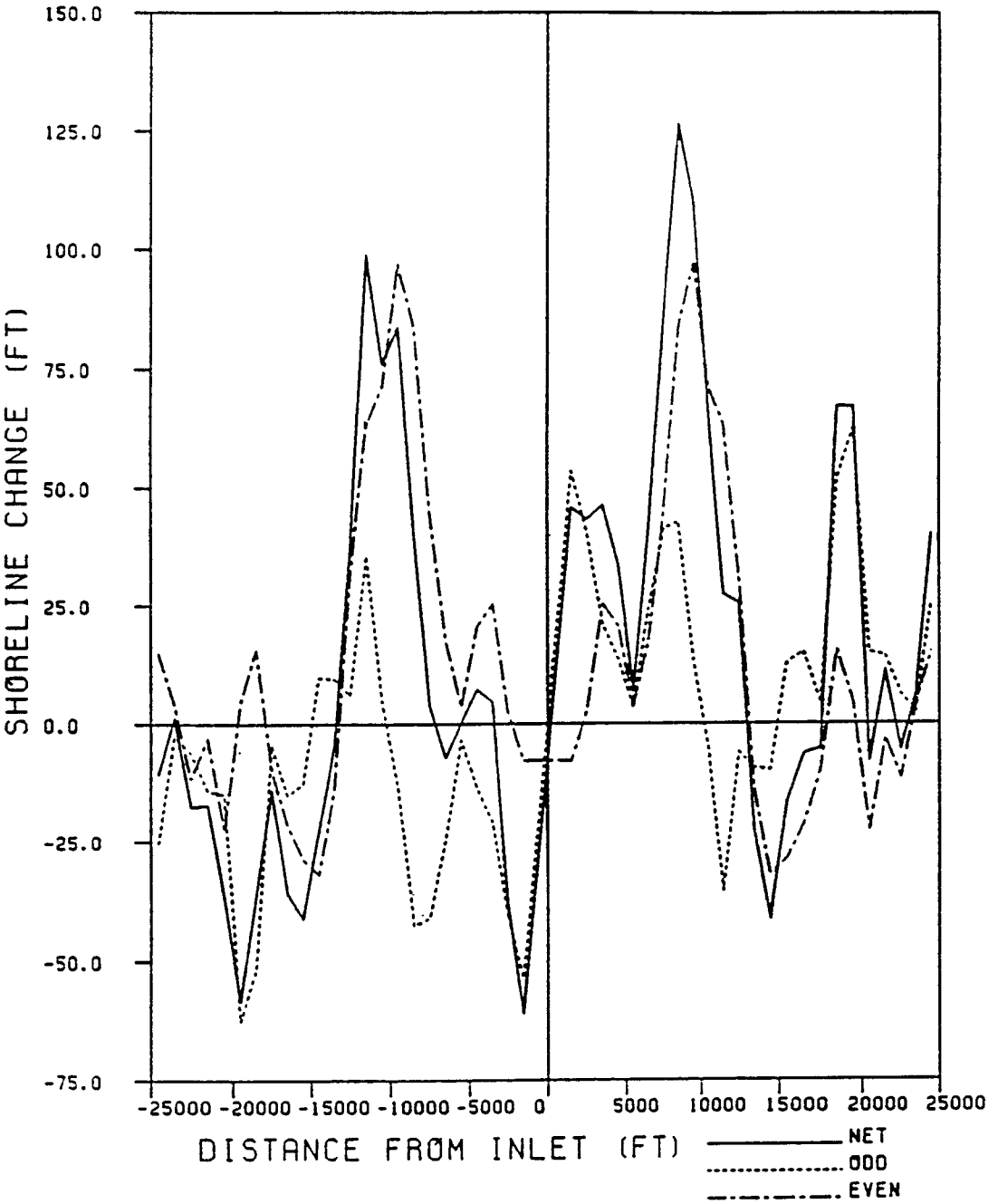

Figure 6.17: Shoreline Changes for Baker's Haulover 1945 to 1962

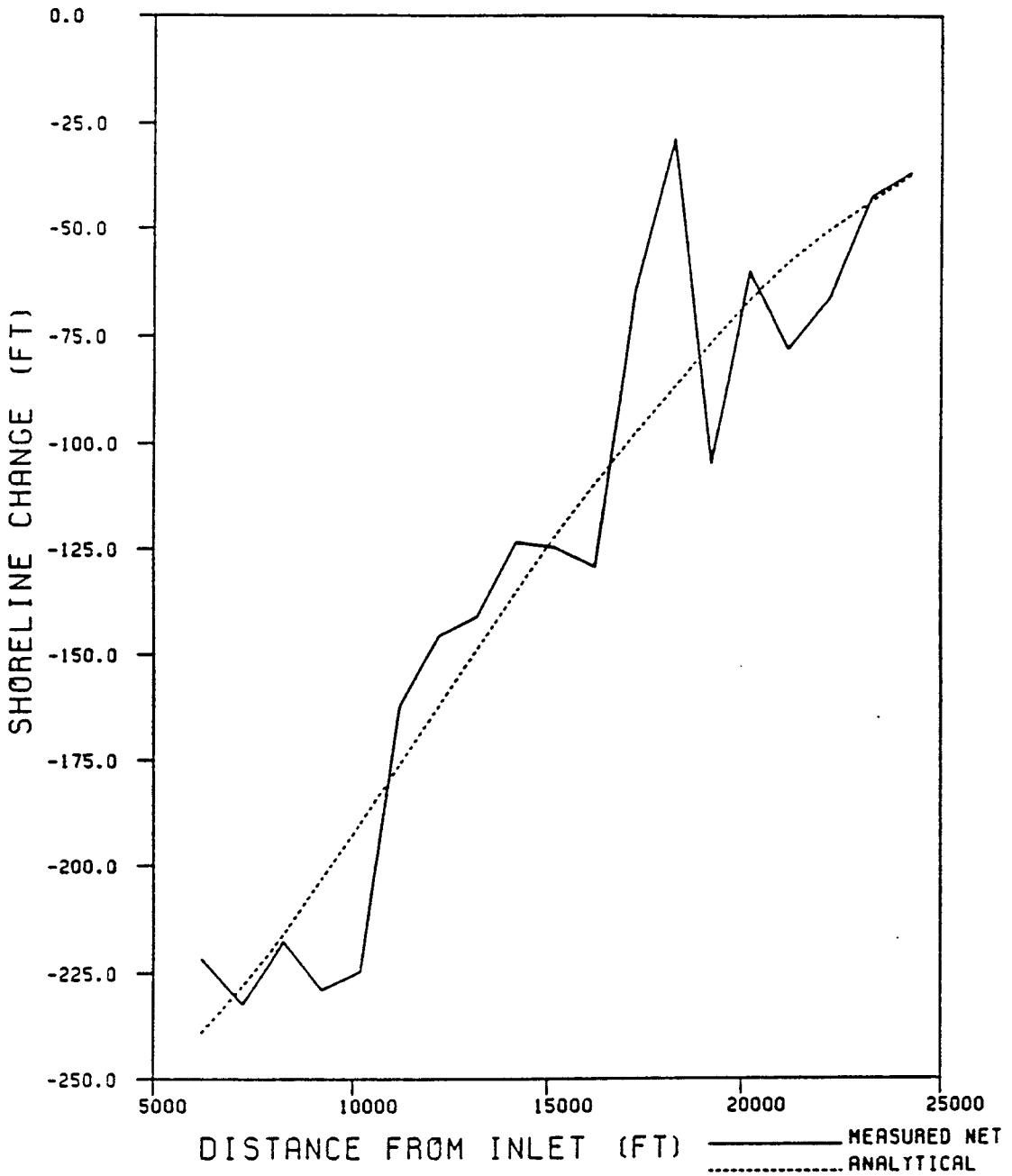

Figure 6.18: Shoreline Changes for Baker's Haulover 1935 to 1945

flanking revetments and bulkheads were added to the jetties in 1938 to 1940. The south jetty experienced severe erosion and the flanking revetment was constructed for approximately 1000 feet, this region south of the jetty has tended to remain stable and sometimes show accretion due to the presence of this structure.

The net transport at Venice Inlet is towards the south. This improved inlet has never had any maintenance dredging, indicating that the net transport across the inlet is very small (U.S. Army Corps of Engineers, 1984). This lack of maintenance dredging also indicates that the jetties are very sand tight and do not allow much sediment to pass through them into the inlet channel.

Several features along this shoreline besides the inlet itself influence the shoreline evolution. Approximately 10,000 feet south of the inlet at Horse and Chaise Point there is a rock outcropping; this region has been stable for several years compared to adjacent shorelines. Groin fields are present 5,000 feet south of the inlet at Venice Beach and at 22,000 feet south of the inlet at Caspersen Beach. These structures have stabilized the beach they front, but by their very presence these regions must be high erosion areas. Bluff line erosion along these shorelines has also added an unknown quantity of material to the longshore transport system (U.S. Army Corps of Engineers, 1984).

Figure 6.19 shows the measured shoreline change for Venice Inlet from 1883 to 1942, this time span includes a period before the inlet modifications and five years after the inlet modifications. The severe erosion downdrift and the build up of material at the north jetty is clearly evident; the maximum accretion and maximum erosion values both are approximately 300 feet. This may be another indicator of very small net transport across the inlet and sand tight jetties. The amount of background rates of shoreline change included in these shoreline changes is unknown, because only one pre 1937 survey was available. The maximum erosion was located south of the revetment flanking the southern jetty, the erosion rate then decreased south of this point due to the effects of the groin field at Venice Beach and the rock outcropping at Horse and Chaise Point. The even component of shoreline

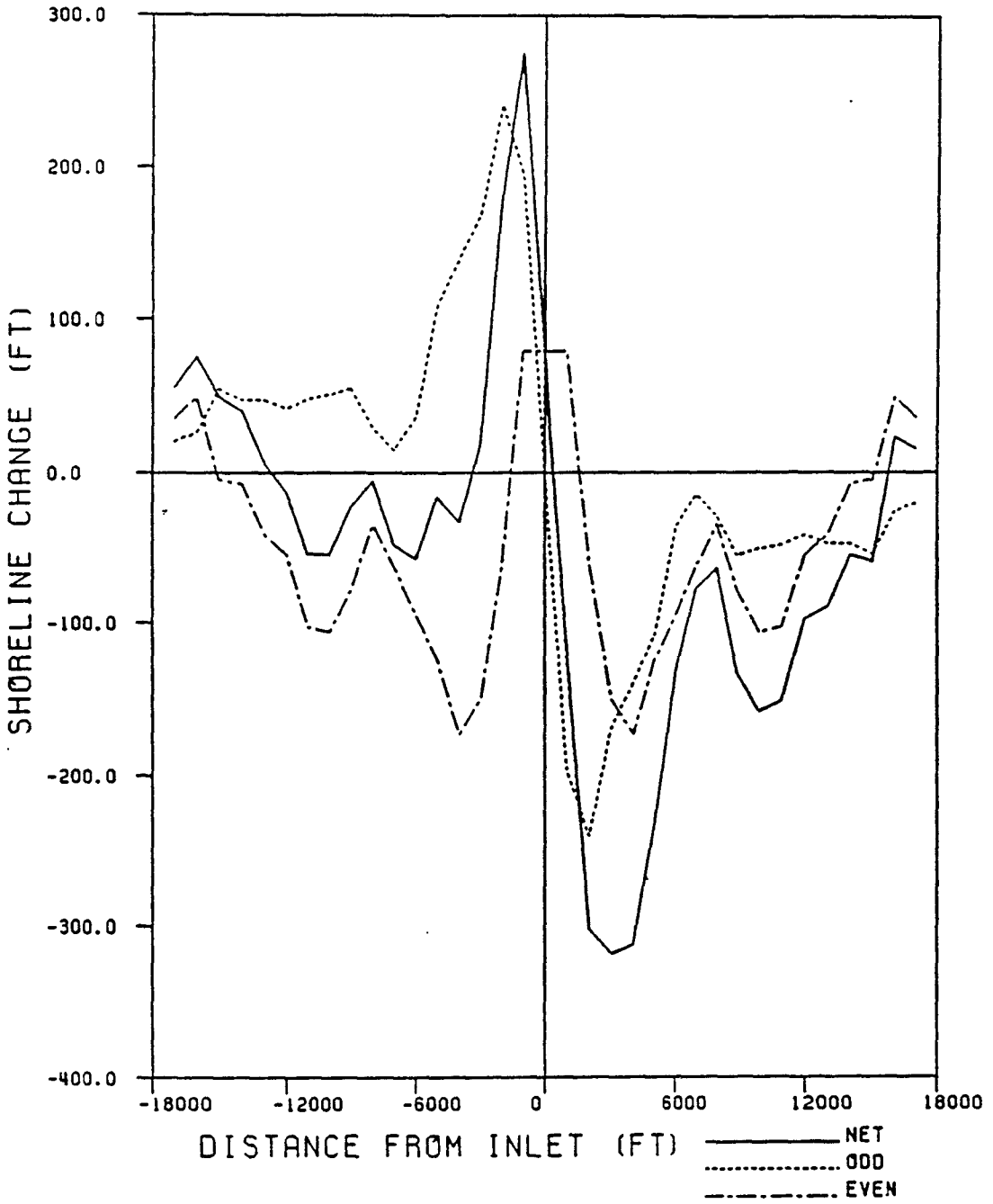

Figure 6.19: Shoreline Changes for Venice Inlet 1883 to 1942

change indicates a loss of sediment in this region over the time span considered. The net shoreline changes show that almost all of this loss is occurring downdrift of the inlet.

Figure 6.20 shows the shoreline changes for Venice Inlet from 1942 to 1978. The updrift beaches during this time span accumulated much more material than during the 1883 to 1942 time span. The average shoreline change updrift of the inlet is plus 60 feet, this results in a shoreline change rate of 1.67 feet per year. The downdrift beaches still experienced erosion, with the maximum erosion occurring approximately 15,000 feet south of the inlet. This location is between the rock out cropping at Horse and Chaise Point and the groin field at Caspersen Beach. The rock out cropping is acting as a littoral barrier and the updrift accretion effects of the groin field have not propagated quite this far north yet. The stabilizing effects of the revetment at the south jetty can be seen as a small region of accretion just south of the jetty.

The even component of shoreline change indicates approximately no net gain or loss of sediment over this region for the time span considered. But the even component does indicate that the region adjacent to the inlet was building up sediment, while the regions farther away from the inlet were losing sediment. The odd component of shoreline change has an unusual shape, in that this component has approximately the same slope for a distance of $\pm$12,000 feet centered at the inlet. The usual behavior for the odd component is to have maximum and minimum points which are very near the inlet. This indicates that the shoreline changes from 1942 to 1978 are of generally the same magnitude over the entire range of shorelines investigated. If the greatest changes are confined to an area centered at the inlet, the odd component will have a large offset at the inlet, then tend to approach zero as distance increases.

6.9 St. Andrews Bay Entrance

St. Andrews Bay Entrance is located in Bay County on Florida's West coast. The inlet connects Panama City Harbor to the Gulf of Mexico. St. Andrews was cut in 1934 across a peninsula, 4 miles to the west of an existing natural channel known as East Pass.

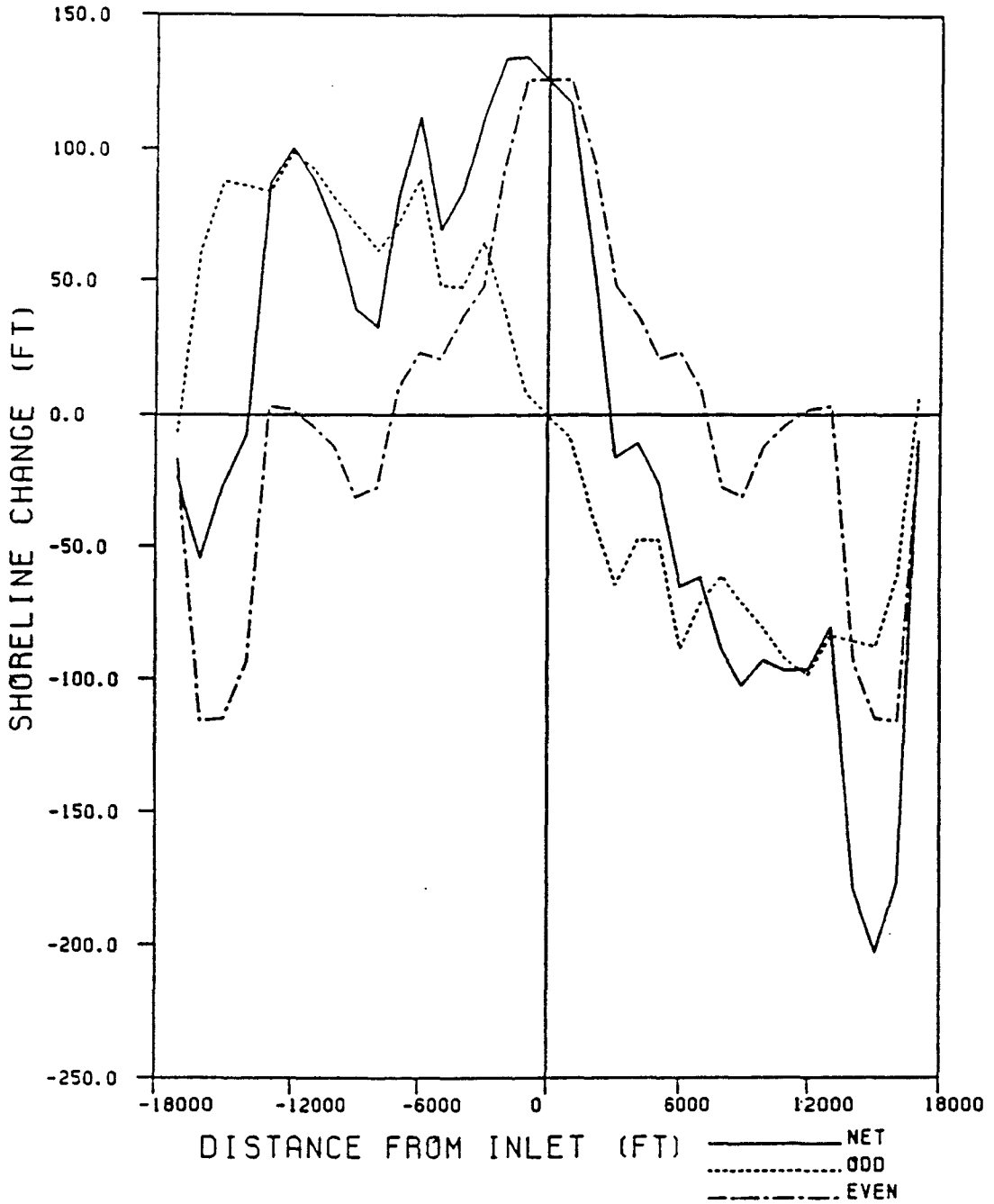

Figure 6.20: Shoreline Changes for Venice Inlet 1942 to 1978

This pass was abandoned after the new cut was made. St. Andrews Entrance created a barrier island to the east, now known as Shell Island. The initial cut was to a depth of 32 feet, two jetties spaced 1500 feet apart were also constructed. The west jetty was 550 feet long and the east jetty was 500 feet, wave action caused scour to the inner channel banks. To protect the channel against this erosion, bulkheads and revetments were built as jetty wings on both sides of the inlet, after the initial cut these jetty wings had to be repaired and lengthened frequently (U.S. Army Corps of Engineers, 1948). The shoreline behind these wings has continued to erode and the jetties have at different times had the potential to become totally detached from the adjacent channel banks.

The predominant net longshore drift is to the west. Bay County has two or three possible transport nodal points (U.S. Army Corps of Engineers, 1971). A nodal point may exist at the jettied entrance, with drift to the east along Shell Island and drift to the west along Panama City Beach. Another nodal point may exist between the eastern tip of Shell Island at Lands End and the western tip of Crooked Island. This nodal point would be in the middle of the abandoned East Pass.

Figure 6.21 shows the measured shoreline change for St. Andrews Bay Entrance from 1855 to 1934, this time period is pre-cut and should not include any effects of the inlet. The negative distances from the inlet are to the west, and the positive distances are to the east. The dominant feature of this region is the landward migration of the eastern end of the peninsula at Lands End. It can be seen that the peninsula rotated landward from a point located near the present location of the inlet. Shorelines east of the present cut eroded at an increased rate as distance to the east increased, while shorelines west of the present cut remained very stable. The even component of shoreline change indicates a net loss of sediment over the region considered from 1855 to 1934. The odd component has the unusual form of an almost straight line indicating accretion to the west with continuing erosion as distance is increased to the east.

Figure 6.22 shows the shoreline changes for St. Andrews Bay Entrance for 1934 to 1977,

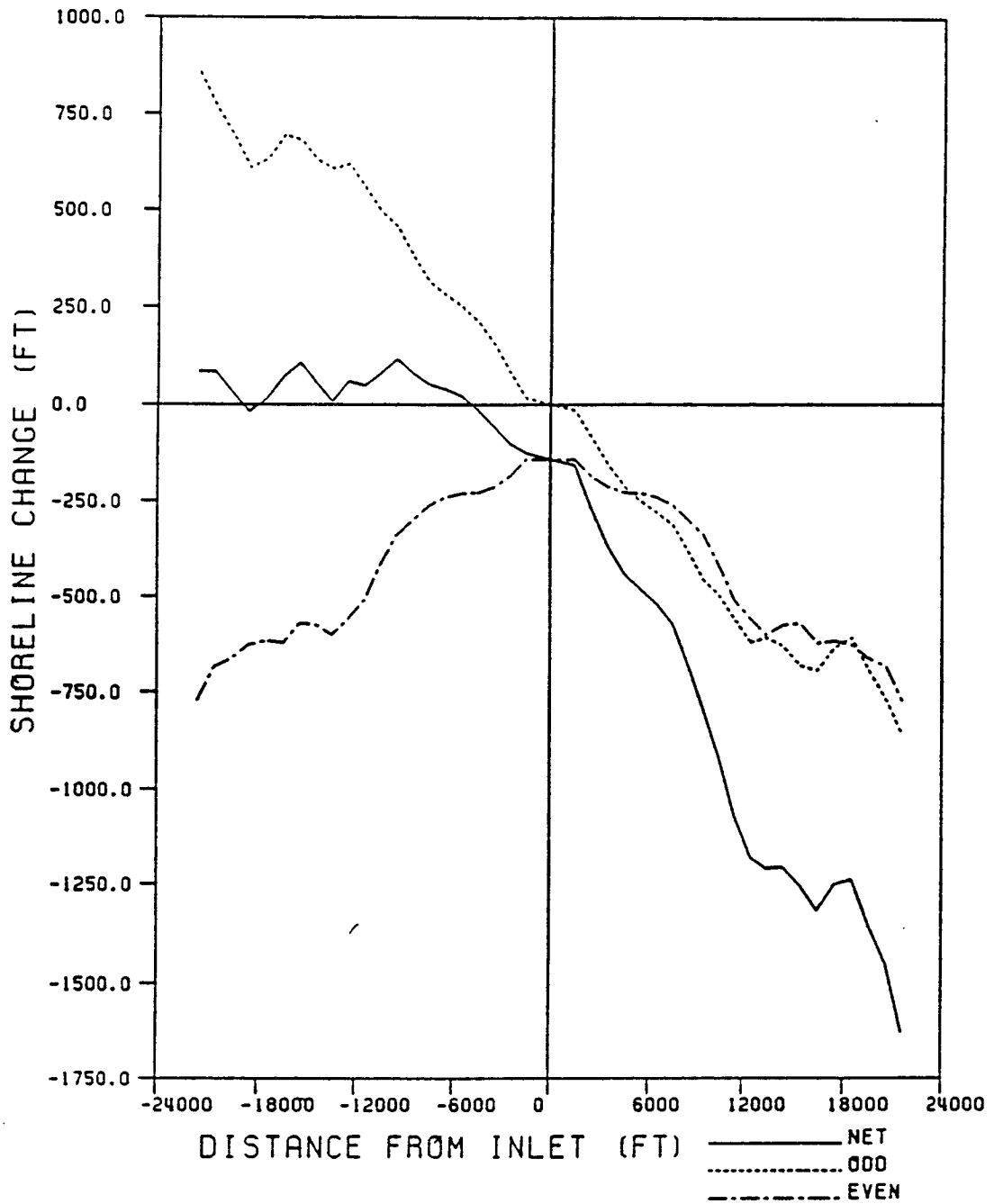

Figure 6.21: Shoreline Changes for St. Andrews Bay Entrance 1855 to 1934

this time span shows the effects of cutting the inlet. This figure indicates net transport to the west, with the western shoreline retreating and the eastern shoreline advancing. This shoreline behavior is completely reversed from the shoreline changes observed before the inlet was cut. The previously eroding shoreline east of the inlet is now advancing due to sediment accumulating at the inlet, and the stable shorelines that existed to the west are now experiencing severe erosion. The maximum erosion was located at the west jetty, with the erosion decreasing as distance increased away from the jetty. The volume of material eroded to the west almost equals the volume of material that accumulated to the east.

Figure 6.23 shows the predicted shoreline change for 1934 to 1977 compared to the measured shoreline change. The predicted shoreline change for this 43 year time span agrees very well with the measured changes. The analytical solution yields a breaking wave height of 1.71 feet and a breaker angle of 1.56 degrees. These wave parameters would indicate a net transport of 55,000 cubic yards per year.

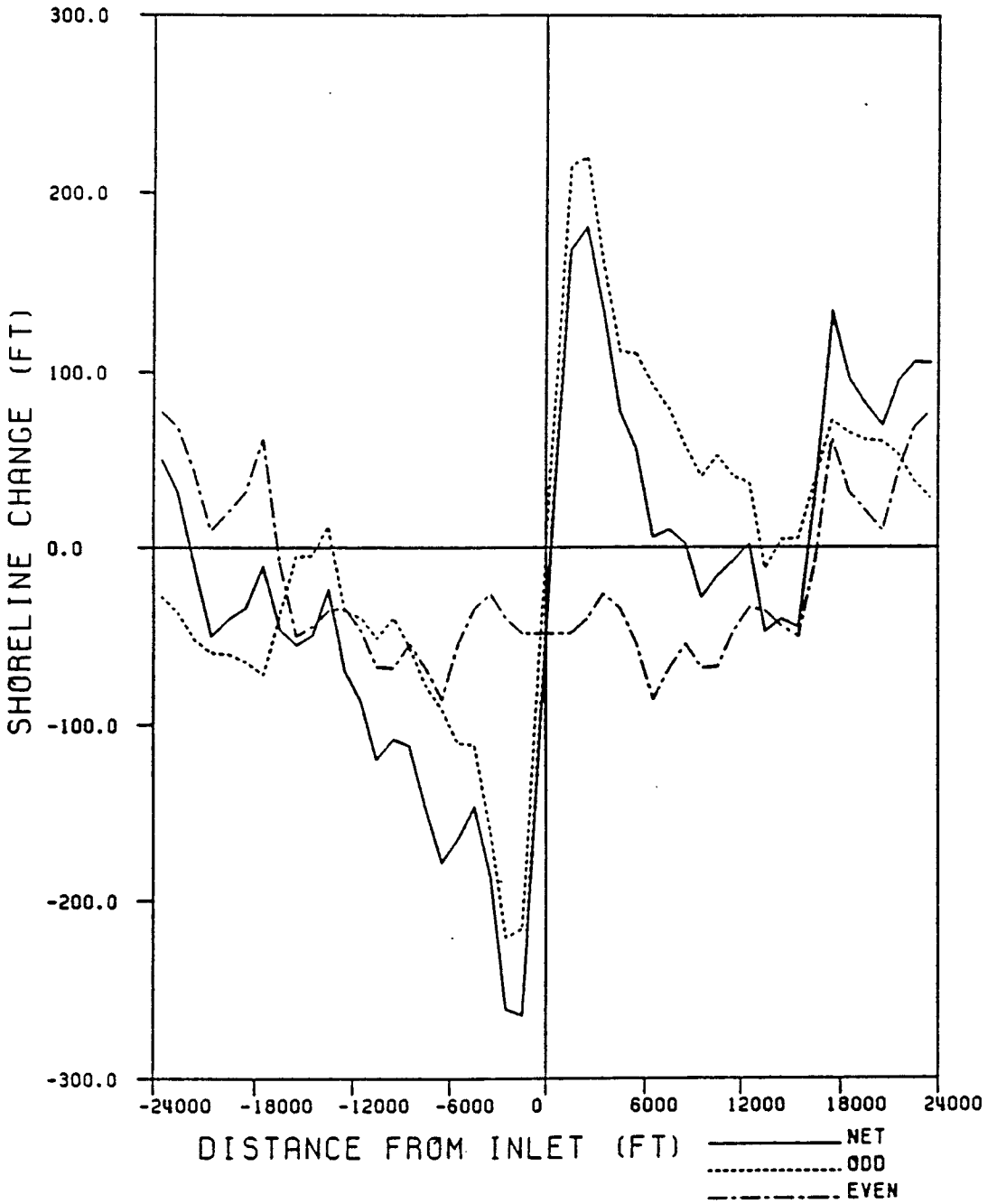

Figure 6.22: Shoreline Changes for St. Andrews Bay Entrance 1934 to 1977

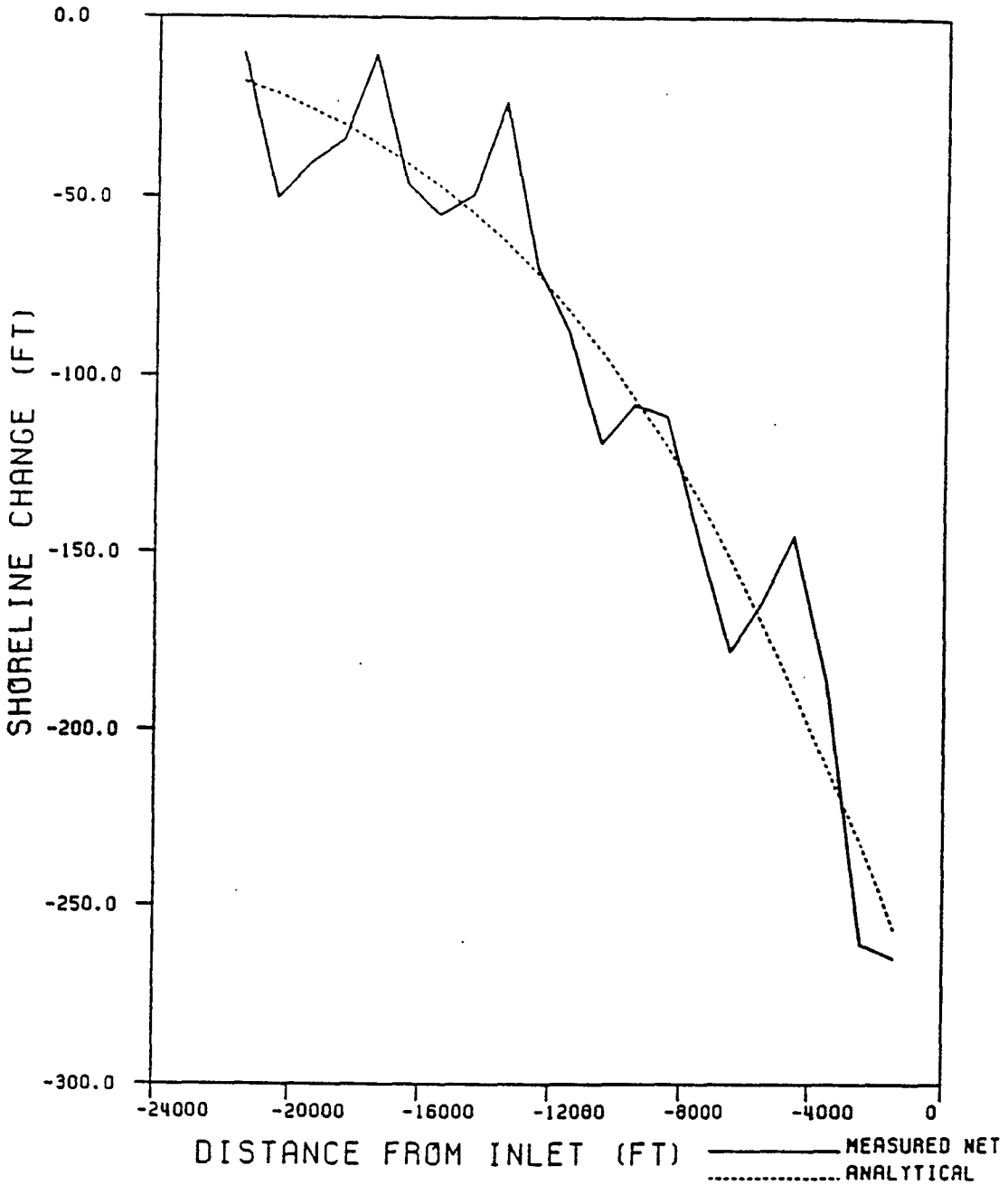

Figure 6.23: Predicted Shoreline Change for St. Andrews Bay Entrance 1934 to 1977

CHAPTER 7
NUMERICAL MODEL RESULTS

Ft. Pierce Inlet is a complex physical system which will provide examples of many coastal processes which occur at inlets. The shoreline change data showed that the maximum erosion at Ft. Pierce was located 5000 feet south of the inlet. This zone immediately south of the inlet exhibited signs that it was sheltered from wave attack. It was initially thought that this sheltered zone was the result of wave diffraction around the jetties. A literature review (Marino and Mehta, 1986) indicated that a sizable ebb shoal had formed after the inlet cut. Also a shore parallel reef was found offshore. Several model runs were made that included refraction and diffraction to attempt to predict this shoreline change.

Table 7 presents the breaking wave heights and wave angles used in the model study of Ft. Pierce inlet. The breaking angles for the littoral drift roses resulted in a net average transport of 0.0531 ft^3/sec while the measured shoreline changes showed a transport of 0.0986 ft^3/sec. The LDR angles were modified with a K value of 0.25, this resulted in a modified mean value of 69.26 degrees. The shore normal for this area is 70 degrees.

The first feature that was investigated at this inlet was the sheltered zone south of the inlet. It was believed that diffraction coupled with refraction over the ebb tidal shoal would account for the presence of this feature. Diffraction can only play a dominant role in the shadow zone in the lee of the jetty. This zone is cast behind the jetty and caused by the difference in the jetty orientation and the incoming wave angle. At Ft. Pierce the northern jetty is 1800 feet long and the southern jetty is 1200 feet long, both jetties are approximately shore normal (70 degrees). The shadow zone does not extend far down shore. If a wave approached at a large angle of 20 degrees relative to the shoreline the shadow zone would only extend approximately 400 feet south of the jetty. For the shadow zone to extend the

Table 7.1: Wave Heights and Angles for Ft. Pierce

MONTH	H_b^*	θ_b
JAN	2.75	68.62
FEB	2.49	68.84
MAR	3.09	68.97
APR	2.04	69.89
MAY	2.37	69.25
JUN	1.63	71.04
JUL	1.35	71.74
AUG	1.40	70.29
SEP	1.51	67.24
OCT	2.97	68.25
NOV	2.81	68.53
DEC	2.76	68.52

$$^*H_b = \left(\overline{H_b^{5/2}}\right)^{2/5}$$

full 5000 feet found in the measured data the waves would have to approach the shoreline at 76 degrees off shore normal. This is a totally unrealistic estimate of breaking wave angle. Other processes besides diffraction must be influencing this region.

Next the effects of refraction were investigated. Bathymetric survey data (Coastal and Oceanographic Department, University of Florida, 1957) were reviewed to develop an offshore grid system for a refraction routine. The Bathymetric data from 1930, figure 7.1 revealed a large offshore shoal at 3000 feet to 6000 feet from the shoreline. This shoal was in 20 to 30 feet of water. A reef was also located at about 1250 feet offshore, this reef rose one to two feet above the adjacent region. A trough was also present immediately in front of this reef. The results of using this bathymetry in the model are shown in figure 7.2. The model predicted maximum erosion at the inlet with shoreline changes decreasing as the distance increased away from the jetty. The predicted shoreline matches the measured shoreline changes from 10,000 feet south of the inlet to 25,000 feet south. It was not attempted to model the shorelines farther south than 25,000 feet. This region is experiencing shoreline disturbances not associated with the Ft. Pierce Inlet. The model results under predict

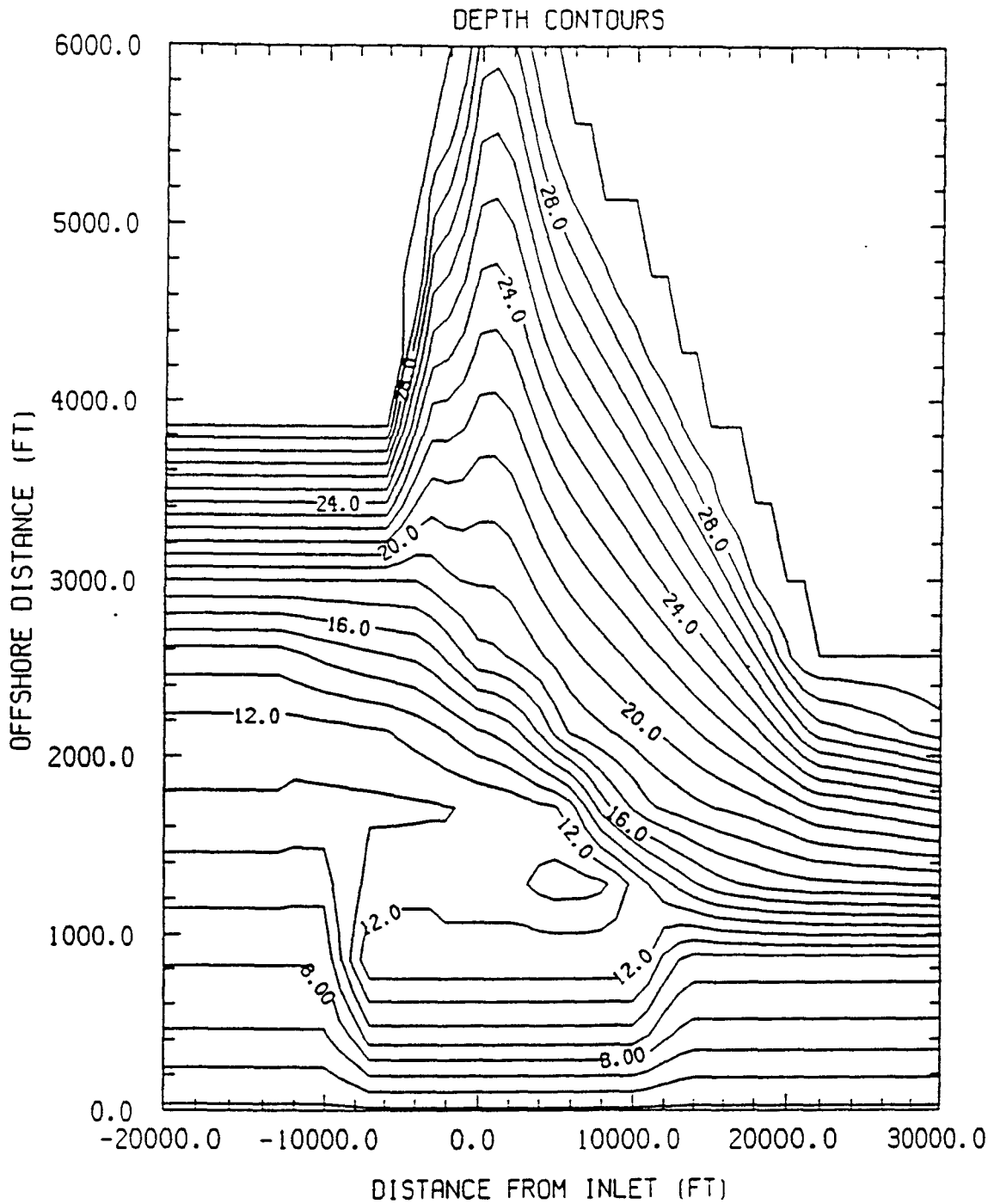

Figure 7.1: 1930 Offshore Contours

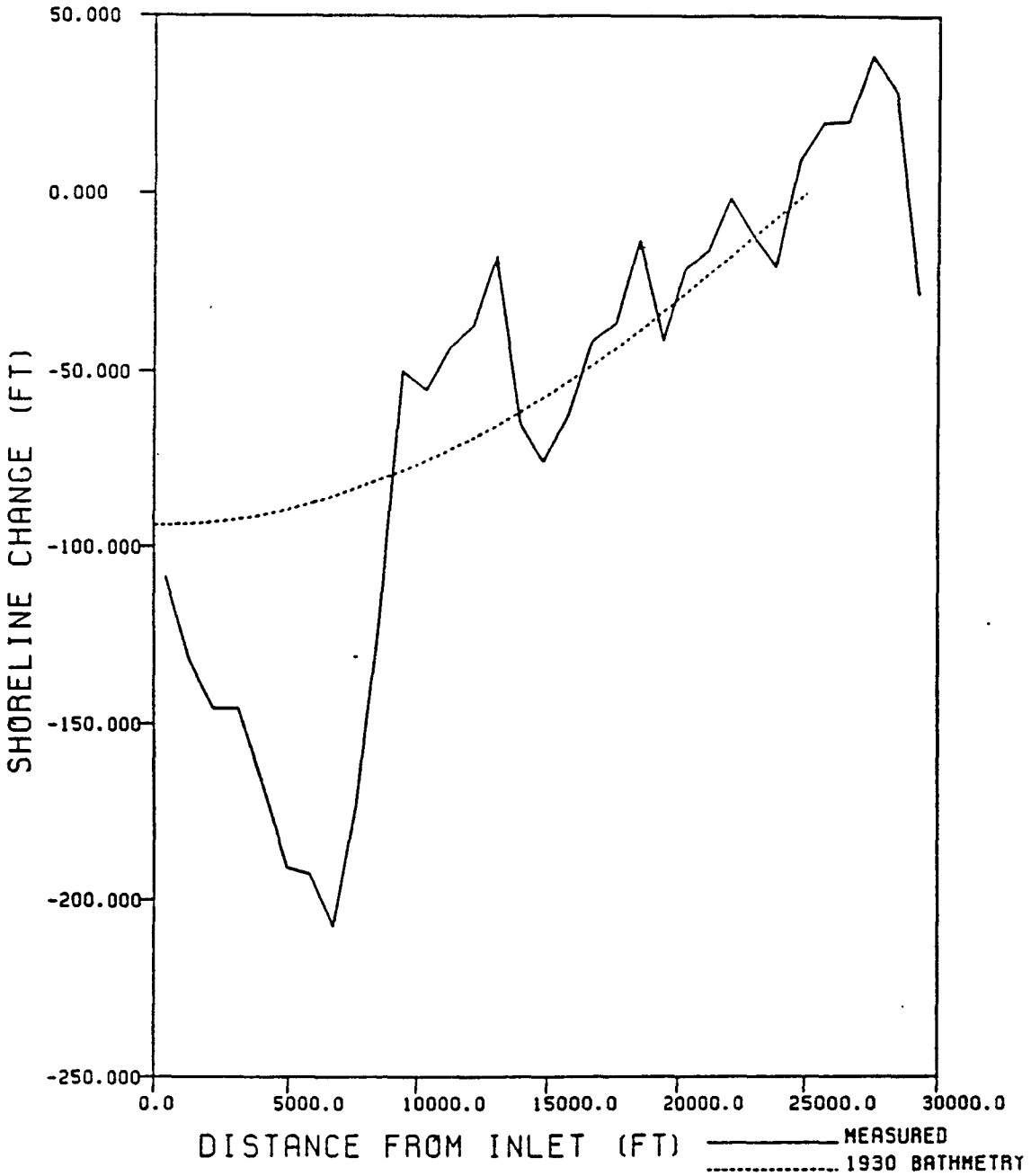

Figure 7.2: Predicted Shoreline for 1930 Bathymetry

the shoreline erosion for the first 5,000 feet south of the inlet. The 1930 Bathymetry is not causing enough erosion to occur at the inlet. Figure 7.3 shows the predicted shoreline positions for 1928 and 1945. The bulge in the shoreline near the inlet is due to the refraction over the large offshore shoal in 20 to 30 feet of water and refraction over the reef in 12 feet of water. This refraction is not great enough to cause the model to predict accurately the erosion adjacent to the inlet.

The bathymetric data also included surveys for 1881 and 1957 and it was found that this offshore shoal was present in all three surveys and stable, in that it did not migrate very much. The model will predict shoreline changes due to a change in the equilibrium state of the region. The changes to the system were the inlet cut which interrupted the longshore transport and the formation of an ebb shoal due to tidal flow. This offshore shoal is an equilibrium feature and the shoreline has adjusted itself to its influences.

It was decided to determine the offshore contour differences from the pre-cut bathymetry and the post-cut bathymetry and use these relative changes as model input. Offshore bathymetry for the 6,12,18, and 30 foot contours was obtained from DNR. These data were interpolated to fit a grid system, and elevation differences were calculated at grid points. The resulting differences indicated a gain of sediment approximately 10,000 feet north of the inlet due to the closure of Indian River Inlet, and a shoal feature of plus 4 feet at the inlet. this shoal was centered at the inlet, with the updrift side having a steeper slope. This shoal feature was smoothed and then superimposed on straight and uniform contours to produce bathymetry which reflected the relative offshore changes due to the inlet cutting (see figure 7.4). Figure 7.5 shows the predicted shoreline compared to the measured changes. The model still does not predict accurately the region immediately south of the jetty. This shoal caused more erosion near the jetty compared to the shoreline changes predicted with the 1930 bathymetry. This shoal, determined from the difference between pre and post cut surveys, is much closer to the shoreline than the shoal in the 1930 survey. The effect of this shoal has been for the diffracted waves to increase transport near the inlet, but the

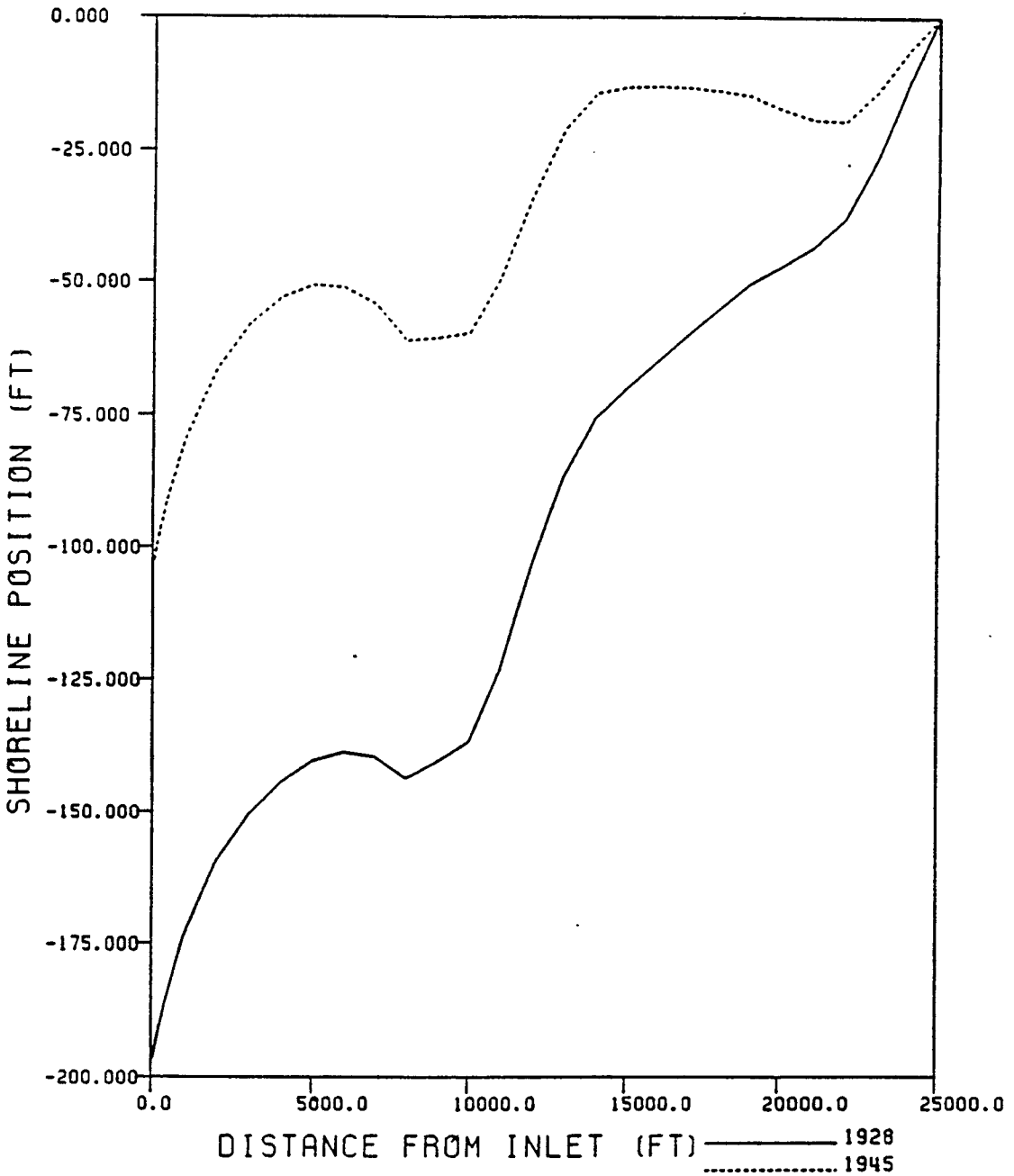

Figure 7.3: Predicted Shoreline Positions From 1930 Bathymetry

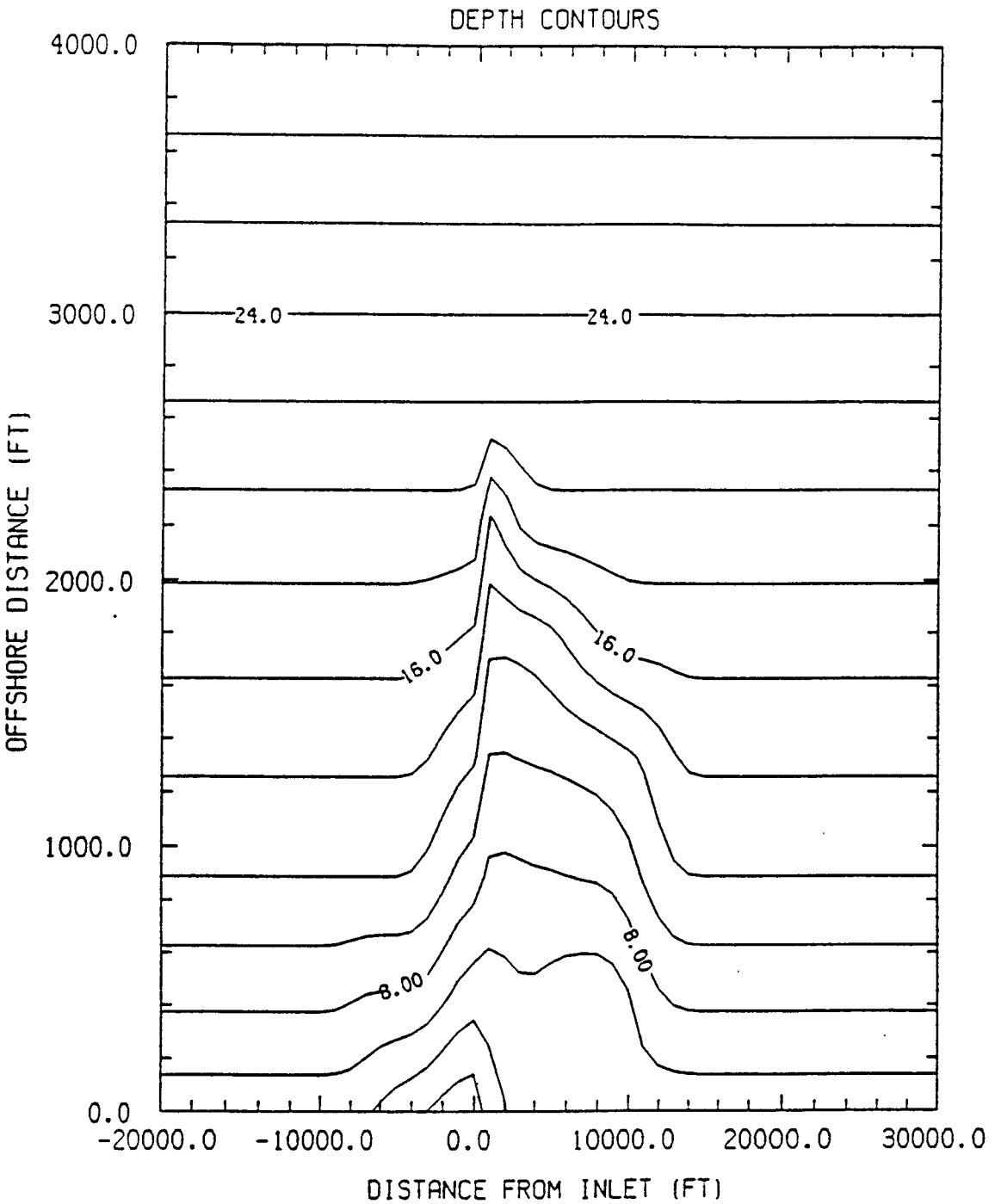

Figure 7.4: Shoal Due to Inlet Cutting

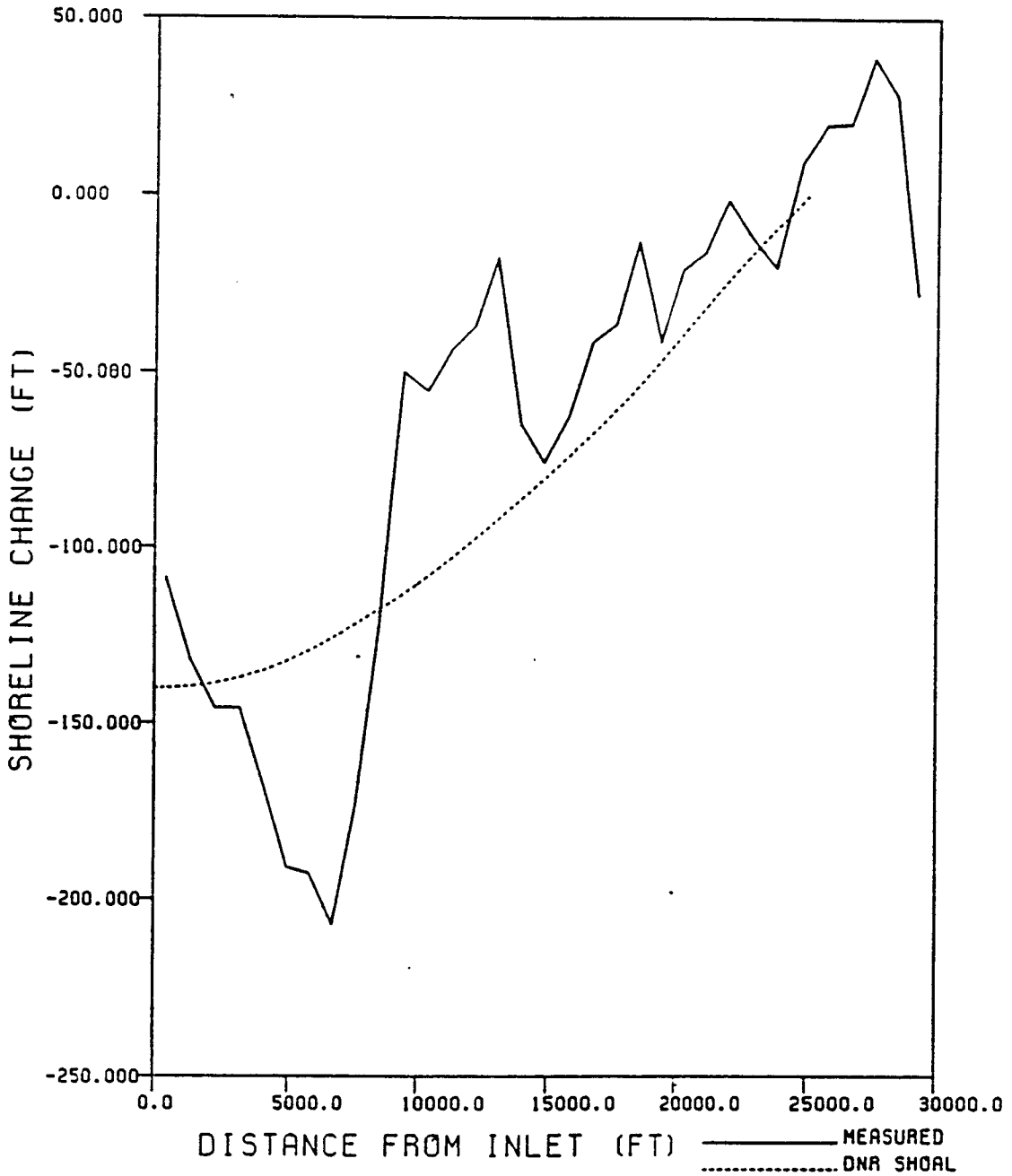

Figure 7.5: Shoreline Change Due to Ebb Shoal

transport from 15,000 feet to 25,000 feet has been affected only slightly. Figure 7.6 shows the predicted shorelines for 1928 and 1945. The shorelines directly south of the inlet have eroded at a rate of one and a half to two times greater than the shorelines predicted by using the 1930 bathymetry. As distance is increased south of the inlet these shorelines tend to approach the shorelines predicted by the 1930 bathymetry. The shorelines predicted from the two different input bathymetrys do have the same overall shape.

The last procedure used to predict the measured shoreline used an idealized shoal. This idealized shoal was a smooth elliptical shape of approximately the same dimension as the shoal obtained from the DNR data but could be place alongshore and offshore at specified locations. The rationale was to determine a hypothetical location for a shoal of the same size as the DNR surveys indicated that would produce the measured shoreline changes. Figure 7.7 shows predicted shoreline changes for three idealized shoals. The shoals have the same dimension but were placed at different locations along the shore. Shoal 1 was centered 5000 feet north of the inlet, shoal 2 was centered at the inlet and shoal 3 was centered 9000 feet south of the inlet (see figures 7.8, 7.9, 7.10).

These results are very similar to the predicted changes produced by the shoal determined from pre and post cut surveys.. But these model runs still do not predict accurately the measured shoreline changes. The model predicts maximum erosion at the inlet and the erosion decreases away from the inlet. Refraction and diffraction are included in the model, yet these processes do not seem to be predicting the sheltered zone south of the inlet. Altering the location of the offshore shoal, therefore moving the zone of sheltering behind it along the shoreline did not predict the sheltered zone. This may be due to that the CDN wave data were average values. The highest wave height was 3.09 feet, even with refraction this wave height will not break on the shoal. This sheltered zone is most likely due to the effects of the jetty coupled with wave breaking on the ebb shoal. The result would be a shadow zone of lowered wave height in the lee of the ebb shoal, that could extend one mile downdrift.

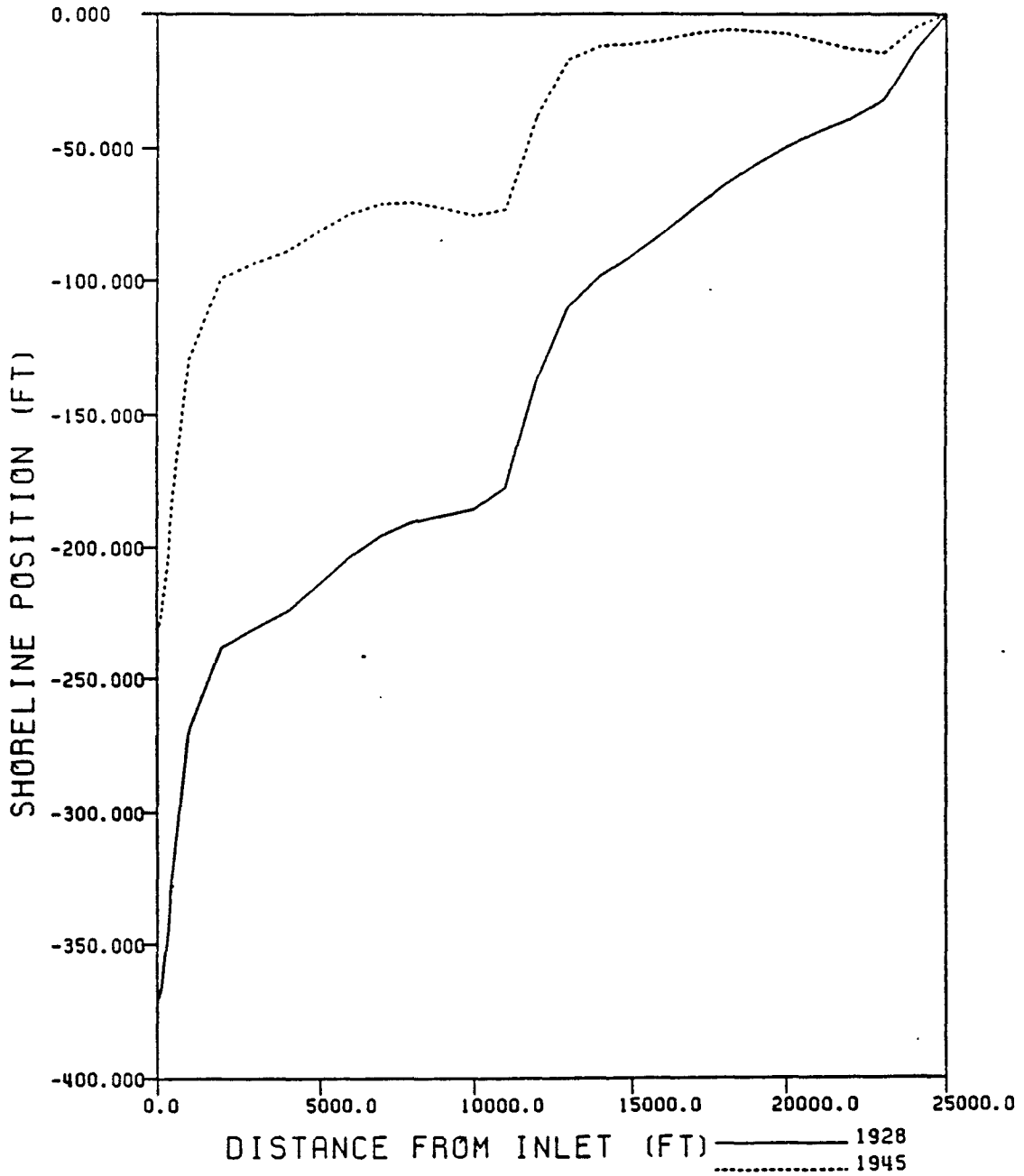

Figure 7.6: Predicted Shoreline Positions From Ebb Shoal

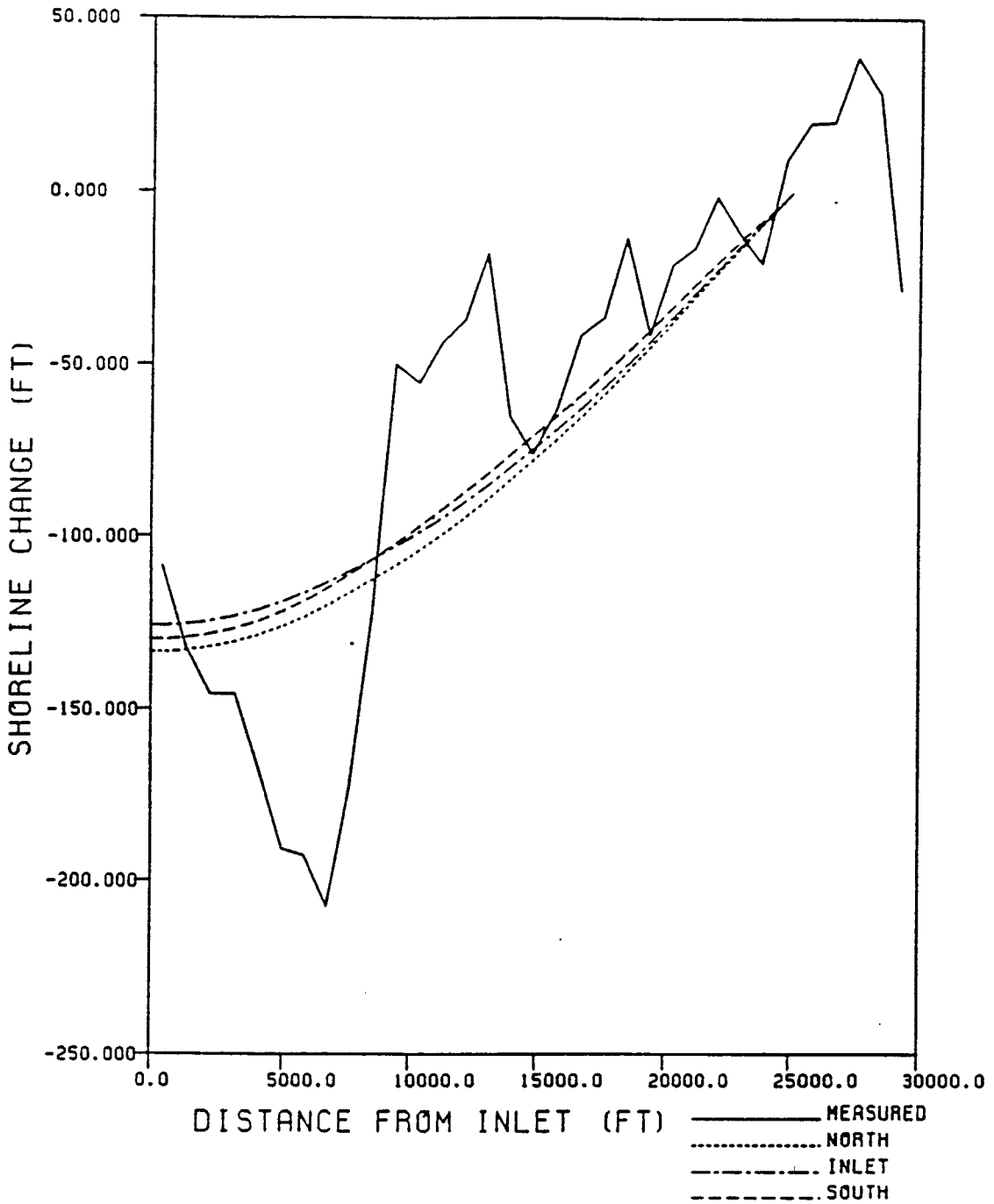

Figure 7.7: Predicted Shoreline Change for Ft. Pierce

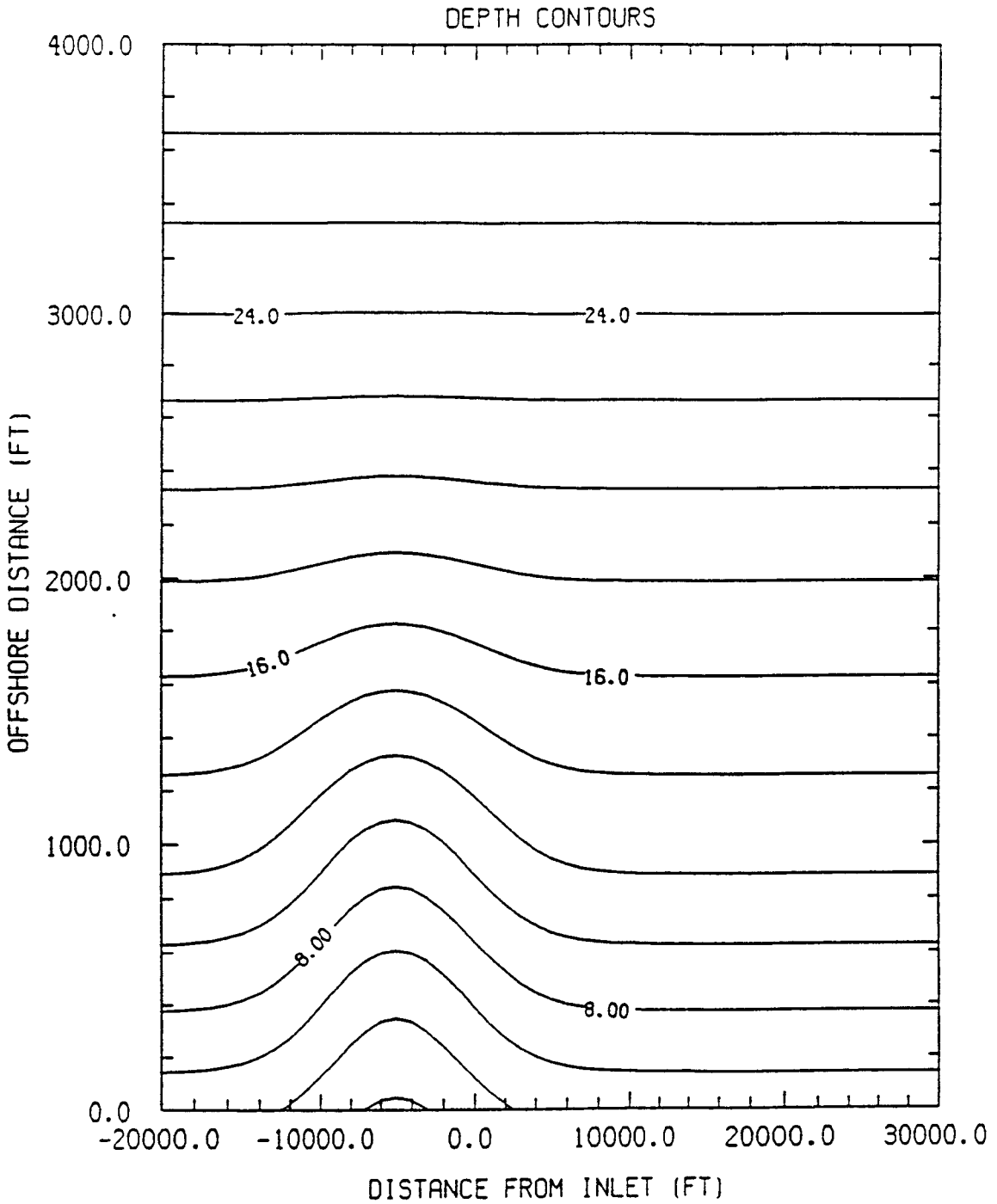

Figure 7.8: Idealized Shoal at Ft. Pierce, Centered 5000 Feet North of Inlet

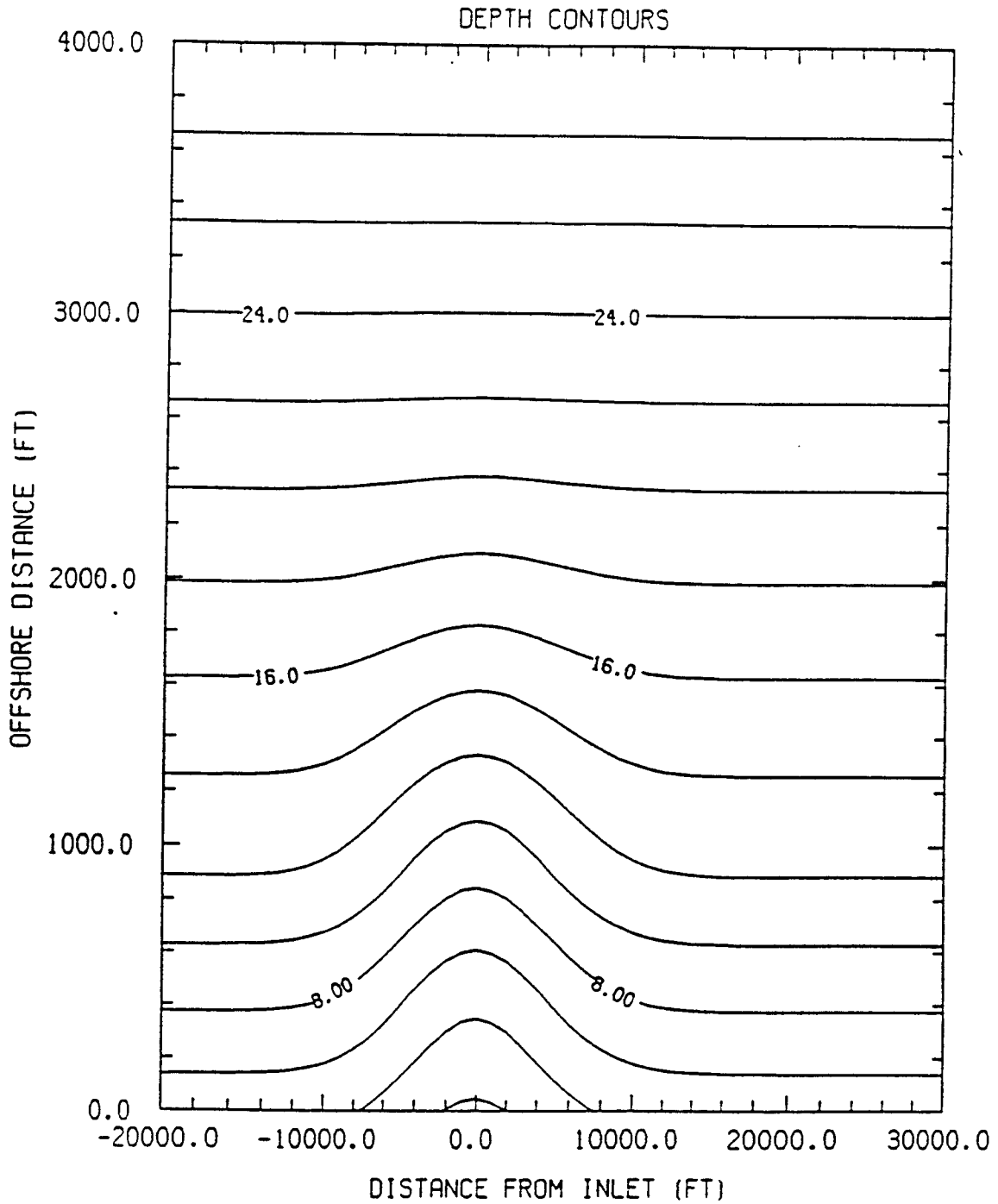

Figure 7.9: Idealized Shoal at Ft. Pierce, Centered at Inlet

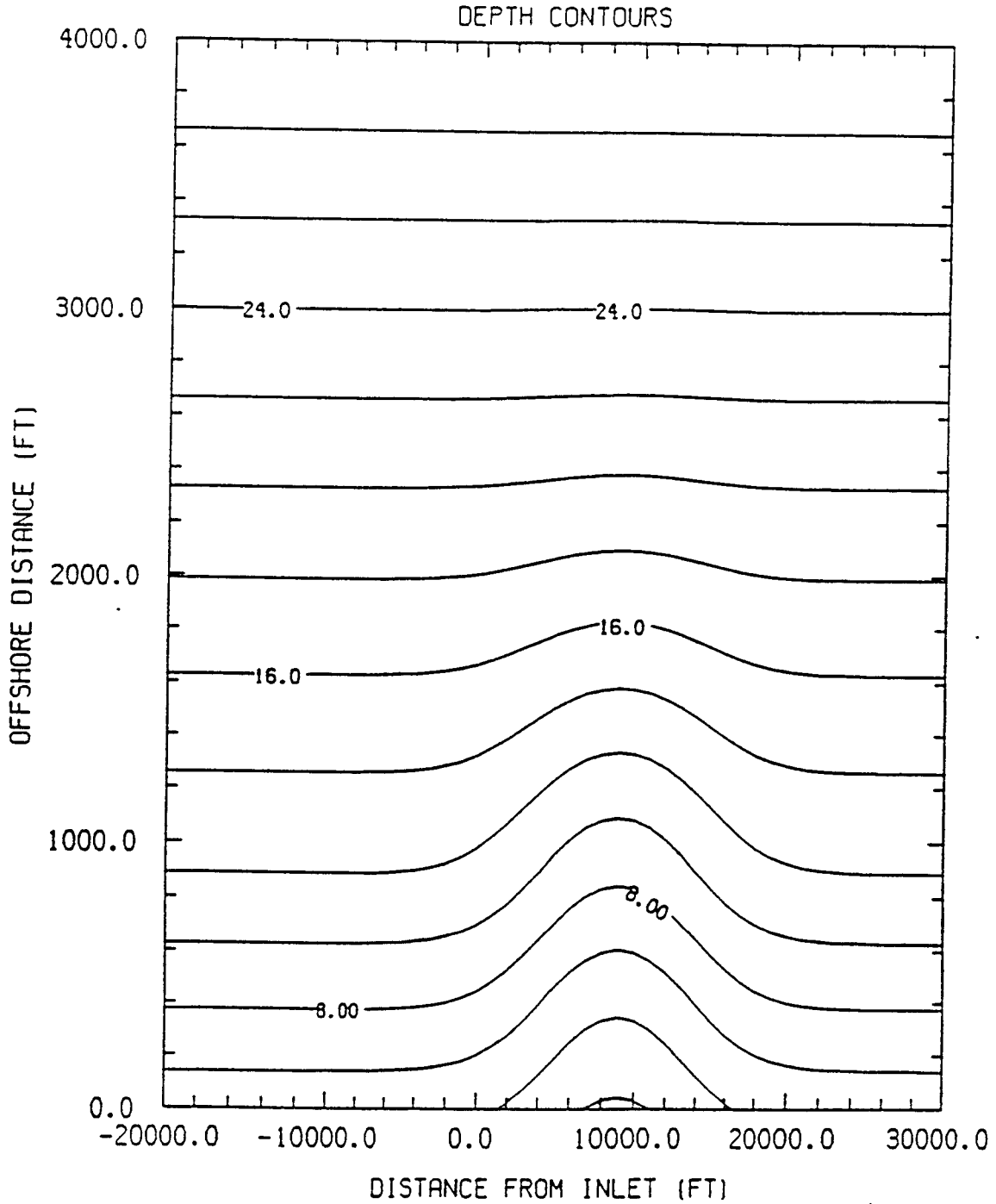

Figure 7.10: Idealized Shoal at Ft. Pierce, Centered 9000 Feet South of Inlet

CHAPTER 8
REFRACTION DUE TO CURRENTS AND VARYING DEPTH

8.1 Tidal Flow Field

This chapter will discuss the combined effects of refraction due to varying fields of tidal currents and depths. A hypothetical tidal flow field was developed, which decreases in magnitude with offshore distance. The tidal velocity is greatest at the inlet mouth for both ebb and flood tide, and decreases with distance from the inlet.

A volumetric transport was specified at the inlet and equations for mass transport in the longshore and offshore directions were developed which satisfy volumetric conservation. It was assumed, for purposes here, that the transport in the offshore direction, q_y, would be similar to a solution of the heat conduction equation, for an initially rectangular area which would then spread with increasing distance offshore.

$$q_y = \frac{q_o}{2}\left(\operatorname{erf}\left[\frac{\ell}{4\sqrt{G'y}}\left(\frac{2x}{\ell}+1\right)\right] - \operatorname{erf}\left[\frac{\ell}{4\sqrt{G'y}}\left(\frac{2x}{\ell}-1\right)\right]\right) \tag{8.1}$$

q_o is the uniform volumetric transport specified at the inlet, ℓ is the half width of the inlet, and G' is a diffusivity term.

A transport conservation equation was then used to determine the mass transport in the alongshore direction, q_x. The mass transport conservation equation is:

$$\frac{\partial q_y}{\partial y} + \frac{\partial q_x}{\partial x} = 0 \tag{8.2}$$

The mass transport in the longshore direction was determined by differentiating the transport in the offshore direction, and then integrating this quantity with respect to longshore direction.

$$q_x = -\int \left(\frac{\mathrm{d}q_y}{\mathrm{d}y}\right) \mathrm{d}x \tag{8.3}$$

The solution of equation 8.3 follows:

$$q_x = \frac{q_o\sqrt{G'}}{2\sqrt{y\pi}}\left(\exp\left(-\left[\frac{\ell}{4\sqrt{G'y}}\left(\frac{2x}{\ell}+1\right)\right]^2\right)-\exp\left(-\left[\frac{\ell}{4\sqrt{G'y}}\left(\frac{2x}{\ell}-1\right)\right]^2\right)\right) \qquad (8.4)$$

For the x and y components of tidal velocity, u and v were the transport components divided by the water depth at that location. These equations are considered to be valid for ebb and flood tide, the only difference being that the sign of the initial transport. There are several limitations to this derivation of the tidal flow. Bottom friction, momentum conservation, turbulence and other factors have been neglected. The objective of this investigation of refraction due to currents was not to develop a methodology to predict the tidal flow, but to investigate the sensitivity of the shoreline response to tidal flow. It was decided as long as the tidal velocity behaved in the same manner as observed tidal velocities that a detailed qualitative study could be conducted.

Figures 8.1 and 8.2 show the velocities that result from equations 8.1 and 8.4. The initial mass transport was 40 ft^2/sec per foot or a velocity of 2.7 ft/sec, the G' diffusivity term was 125 $ft^{1/2}$, and the inlet half width was 500 ft.

The offshore velocity component was symmetric about the inlet, with the maximum value at the inlet centerline. With increasing offshore distance the centerline velocity decreases and adjacent waters about the centerline start to be affected by the current. Figure 8.2 shows the u velocity component for positive x values, the alongshore component is antisymmetric about the inlet centerline. The u component of tidal velocity is zero at the inlet, and has a maximum value that is located at an increasing distance offshore as the longshore distance increases away from the inlet.

The resultant velocity field is shown in figure 8.3, the resultant magnitude is simply the square root of the sum of the squares of the u and v components. The magnitudes represent both an ebb and flood tide, for an ebb tide the flow is directed offshore and for a flood tide the flow is directed towards the shore. The velocity field has a strong core section that is widest at the inlet and decreases with offshore distance.

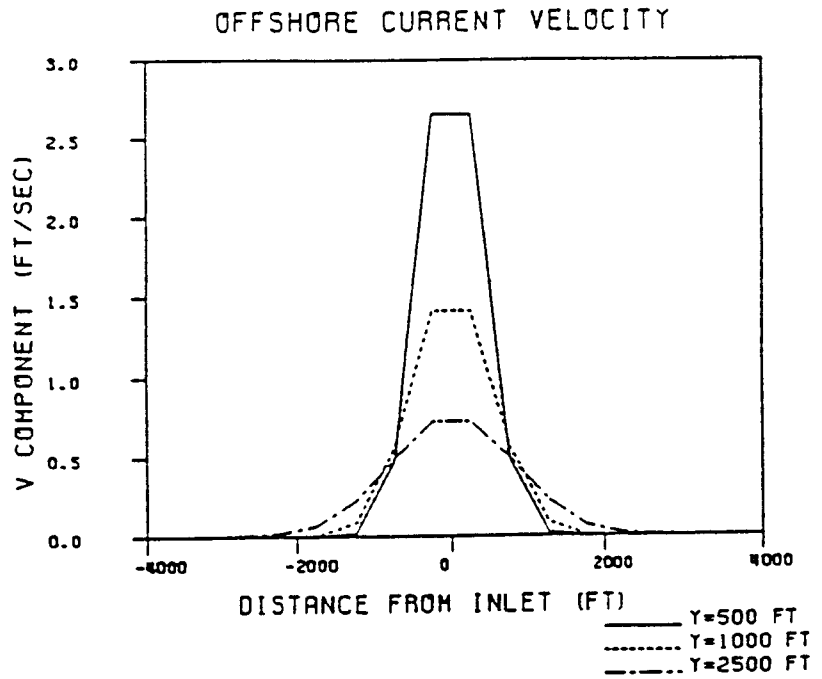

Figure 8.1: Offshore Tidal Velocity Component

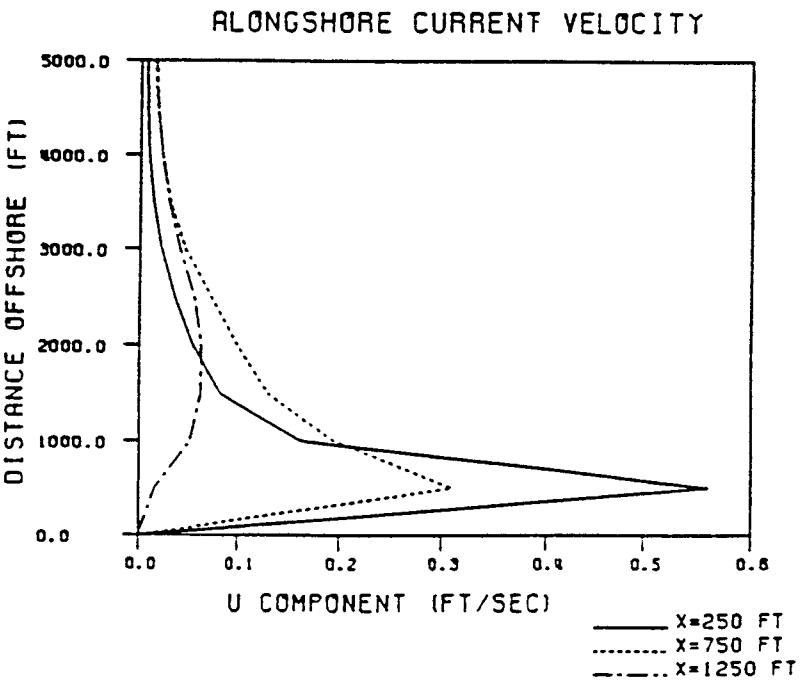

Figure 8.2: Alongshore Tidal Velocity Component

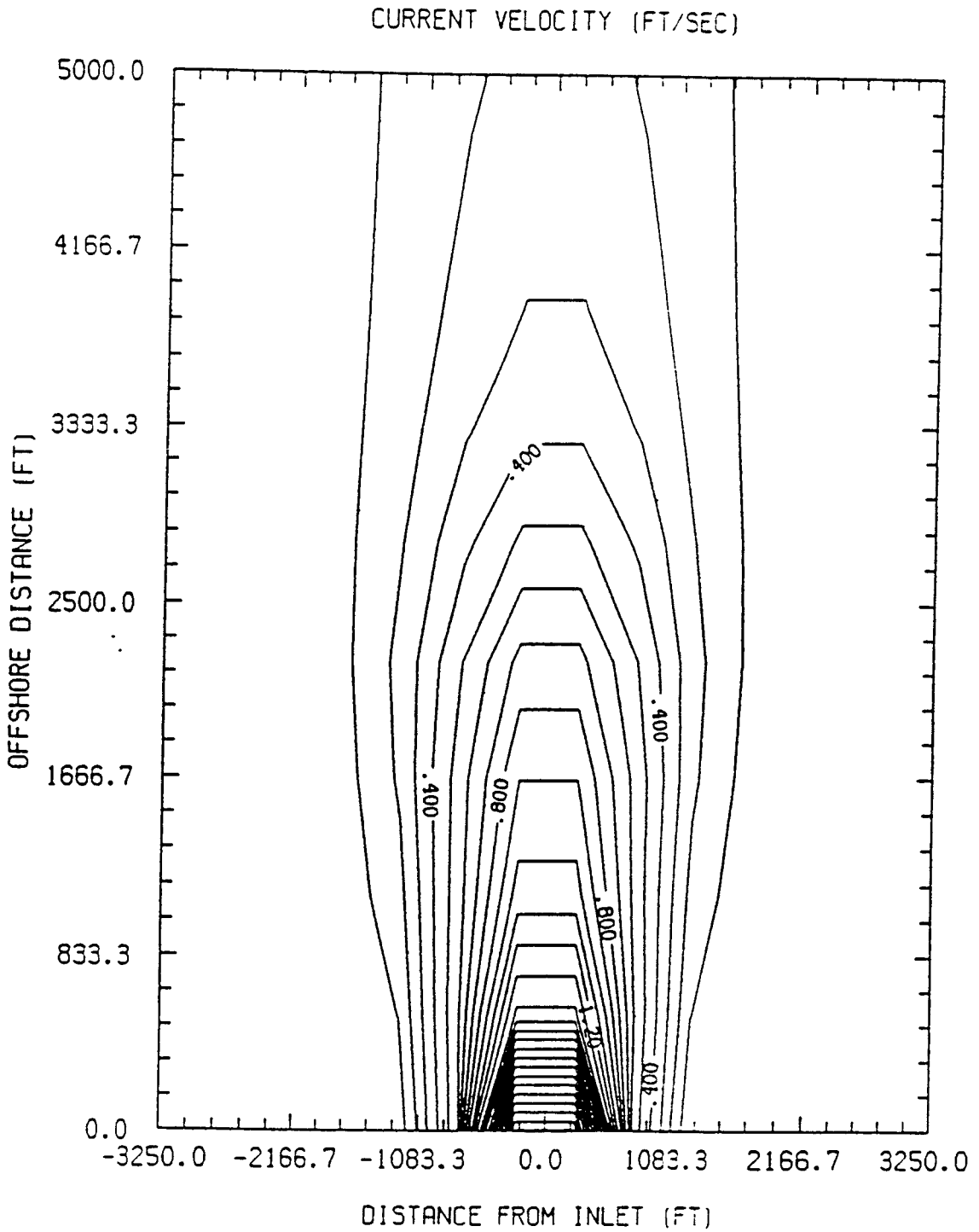

Figure 8.3: Resultant Tidal Velocity Field

8.2 Effects of Refraction on Longshore Transport

The refraction routine which incorporates varying depth and tidal current fields was run with various currents and shoals to investigate the resultant effects to the longshore transport. For an incoming wave which is normal to the shore, the ebb current will increase wave heights and bend waves towards the current centerline, a flood tide will decrease wave heights and cause waves to bend away from the current centerline. This wave energy divergence or convergence will cause gradients in the longshore transport. The ebb current will tend to build sediment up on both sides of an inlet, and the flood current will tend to erode sediment on both sides of an inlet. An idealized case was run to investigate the net effects of refraction due to currents. The longshore transport blockage due to the inlet was not included. The depth contours were made parallel and uniform; no shoal was present. The wave attack was normal to the shoreline. The refraction effects were symmetric about the inlet for both the ebb current and the flood current. The resultant net longshore transport was not equal to zero. The effects of the ebb current dominated over the effects of the flood current, which would cause a build up of sediment on both sides of an inlet. If a shoal is present this effect is accentuated, the shoal will reinforce the refraction from a ebb current and oppose the refraction effects of a flood tide.

8.3 Current Refraction Sensitivity Test

This section will present the results of an investigation of the effects of idealized currents and shoals on longshore transport. Figure 8.4 shows a shoal of 6 feet peak elevation above an equilibrium profile. The shoal is centered 2500 feet offshore of the inlet centerline. Two velocity fields were run with this shoal configuration. For case one the initial volumetric transport was ± 40 ft^2/sec and for case two the initial volumetric transport was ± 20 ft^2/sec. The resultant velocity fields are shown in figures 8.5 and 8.6. The velocity field for case two has velocity magnitudes which are half of the velocities for case one, a comparison of the transport for these two cases will show the sensitivity of the current magnitude. Figure 8.7 shows the resultant transport for ebb and flood tides for cases one and two and

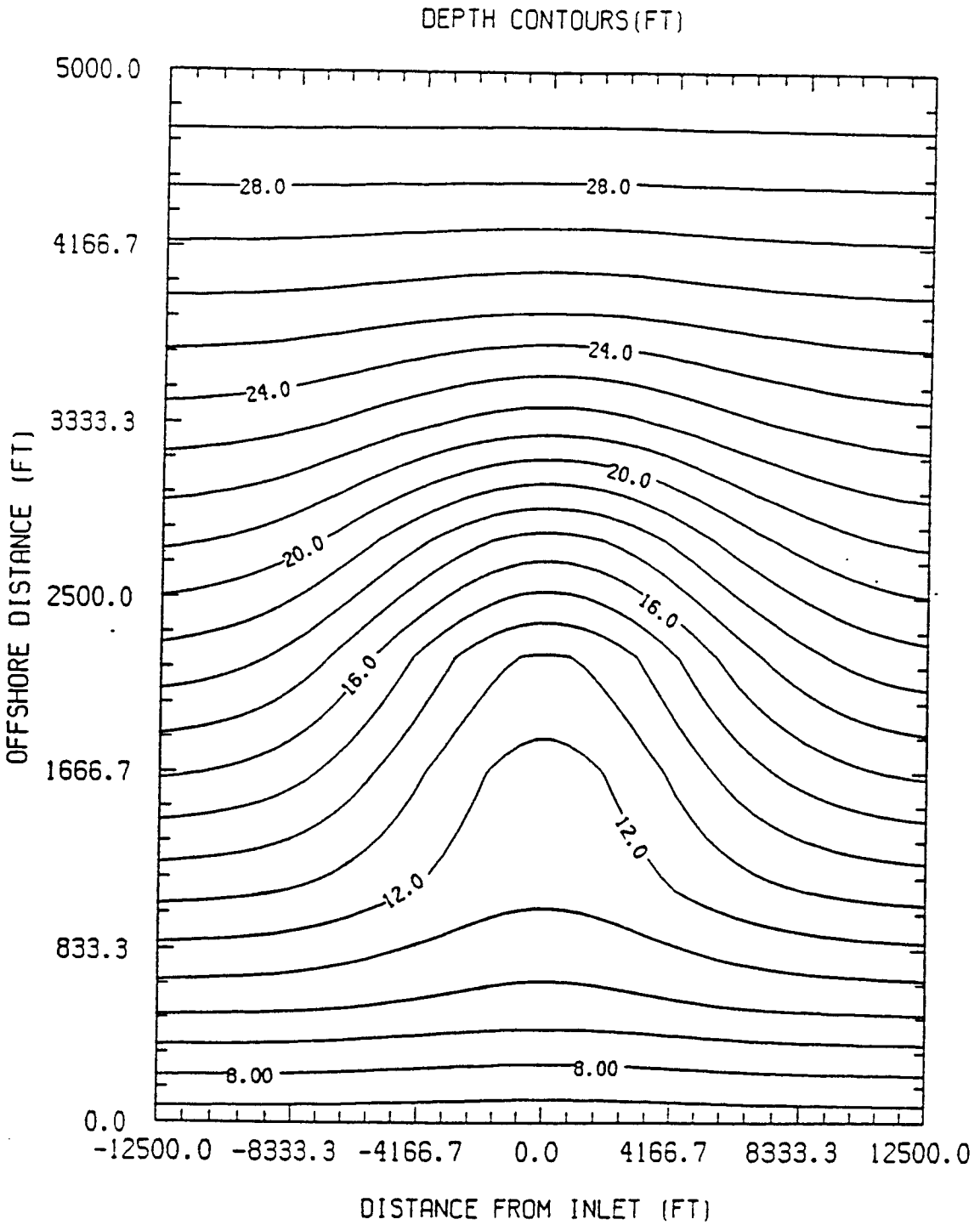

Figure 8.4: Shoal Used for Cases 1 and 2

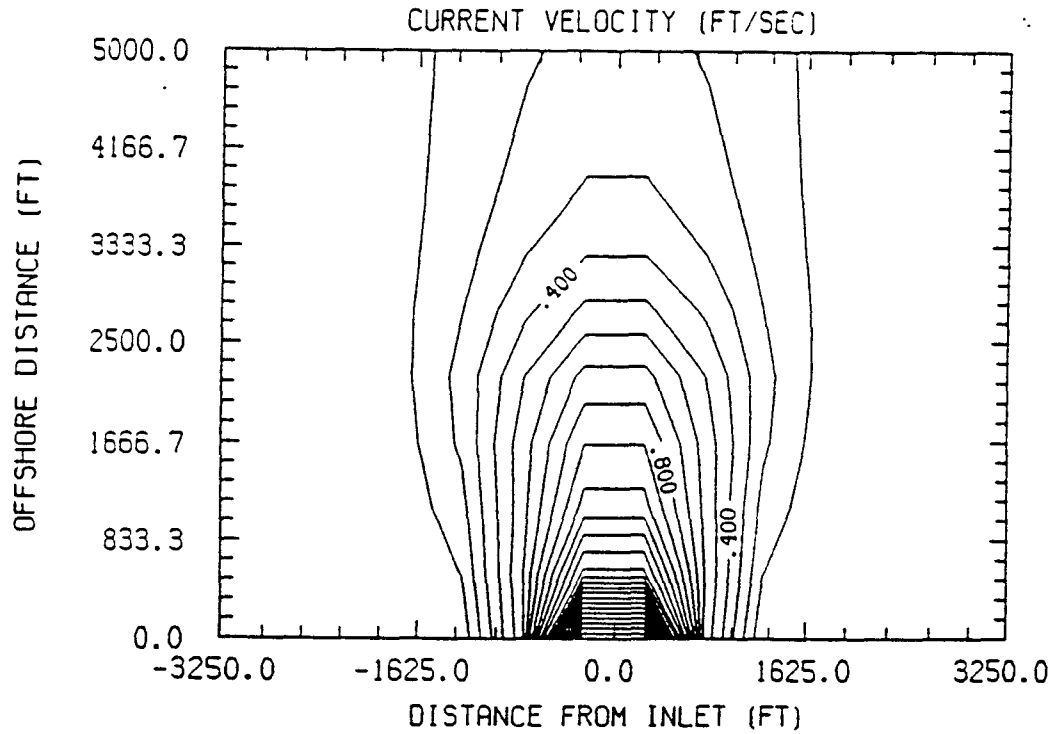

Figure 8.5: Current Velocity Field for Case 1

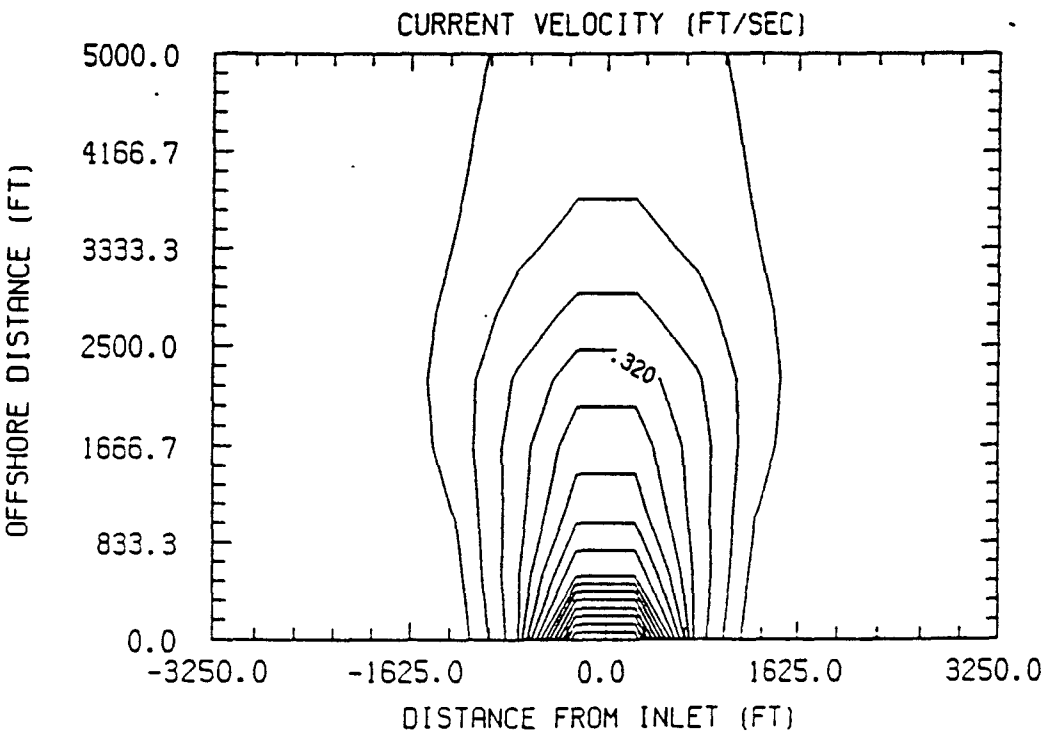

Figure 8.6: Current Velocity Field for Case 2

the transport for the situation of the shoal and no current. As would be expected, the transport from the flood current is in the opposite direction as the transport from the ebb current. The shoal has also caused the transport from the ebb current to be greater than if no shoal existed, and the transport from the flood current to be less than if no shoal was present. Also note the large changes in transport near the inlet caused by the current refraction caused when compared to the case of no current. The currents have influenced the longshore transport for distances of greater then one mile both updrift and downdrift of the inlet. The transport for both cases on flood and ebb tides tend to converge 4000 to 6000 feet away from the inlet. Decreasing the current velocity by a factor of two, decreases the transport by more than a factor of two. This results in the net transport for the ebb and flood tides being much greater for case one than for case two, showing the transport is sensitive to current magnitude.

Refraction sensitivity to shoal size was investigated next. Figure 8.8 shows the shoal configuration used for case three. This shoal has the same maximum displacement of 6 feet, but the lateral dimensions associated with the shoal were reduced by a factor of two. The result is a shoal with the same amplitude but which is smaller and therefore much steeper. Figure 8.9 shows the current velocity field associated with this shoal using the same current parameters that were used for case one. The longshore transport for case one and case three are shown in figure 8.10. The transport near the inlet was basically unaffected by the reduction in shoal size, showing that the current is the dominating influence for this region. The shorelines that were farther than 3000 feet from the inlet were much more sensitive to the size of the shoal. For case one, transport is unaffected by refraction at a distance of 12000 feet away from the inlet, for case three this distance has been reduced to 6000 feet. These regions show that the reduction in shoal size has greatly reduced the effects of refraction on longshore transport. Reducing the current velocity did not affect the distances updrift and downdrift of the inlet that the refraction influenced the longshore transport. Reducing the shoal dimensions by a factor of two reduced the updrift and downdrift influence of

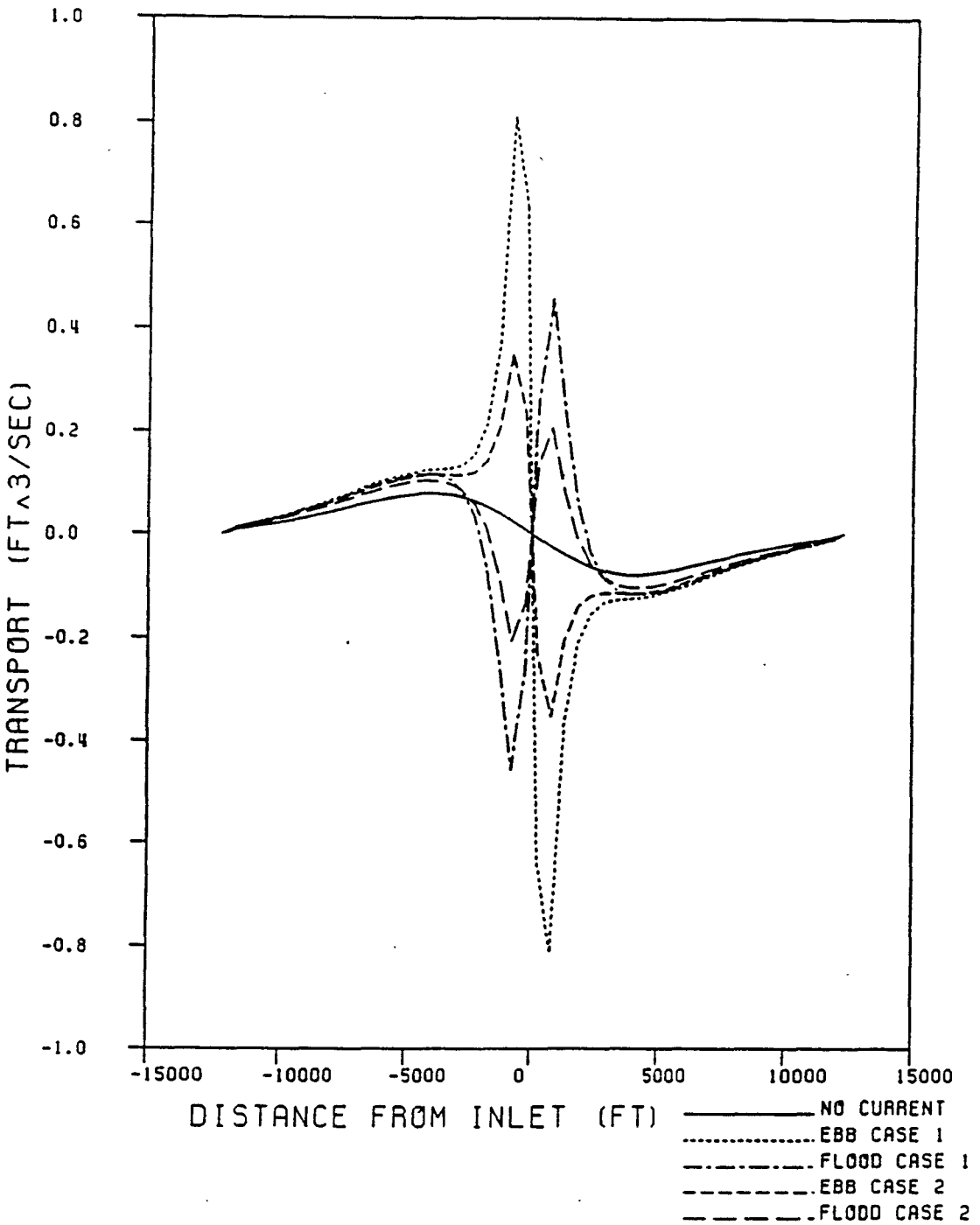

Figure 8.7: Longshore Transport for Cases 1 and 2

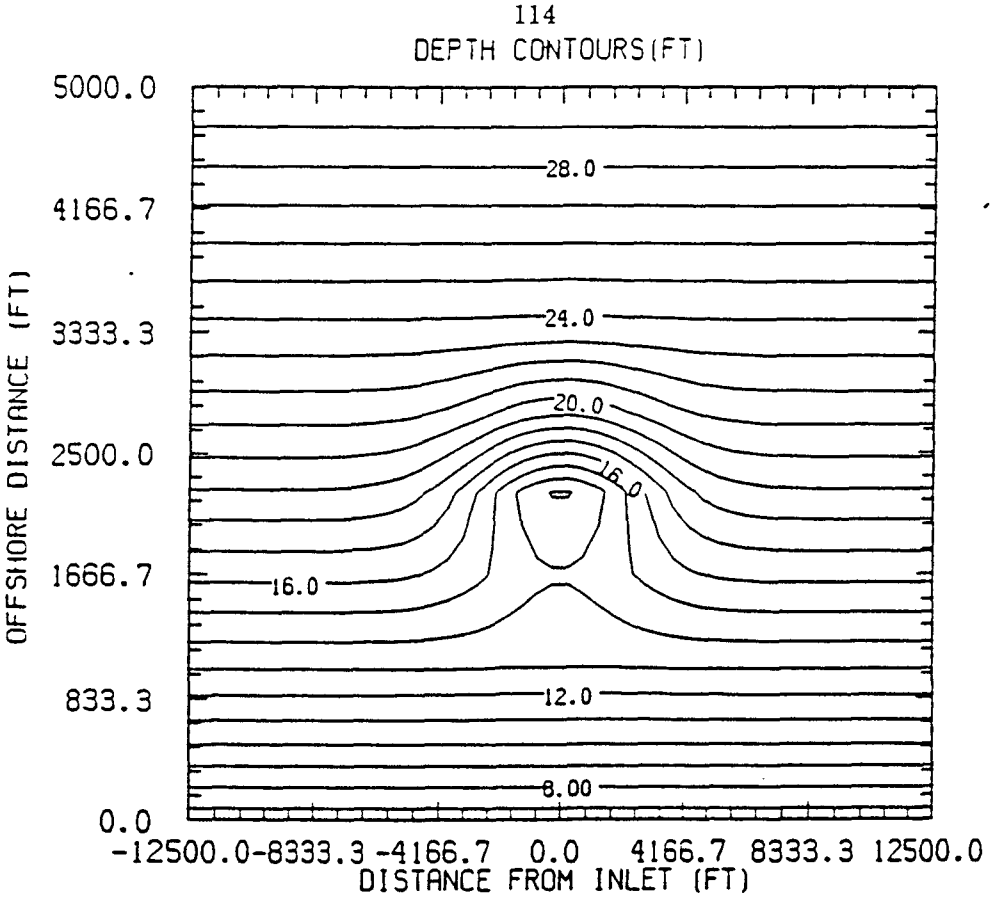

Figure 8.8: Shoal Used for Case 3

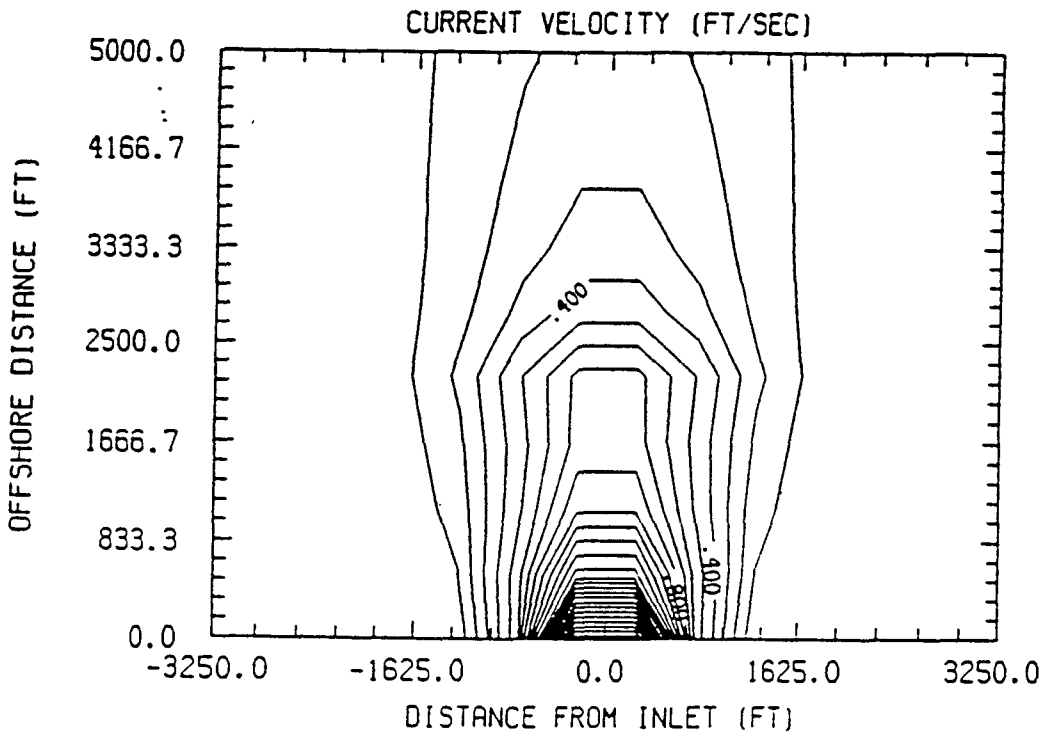

Figure 8.9: Current Velocity Field for Case 3

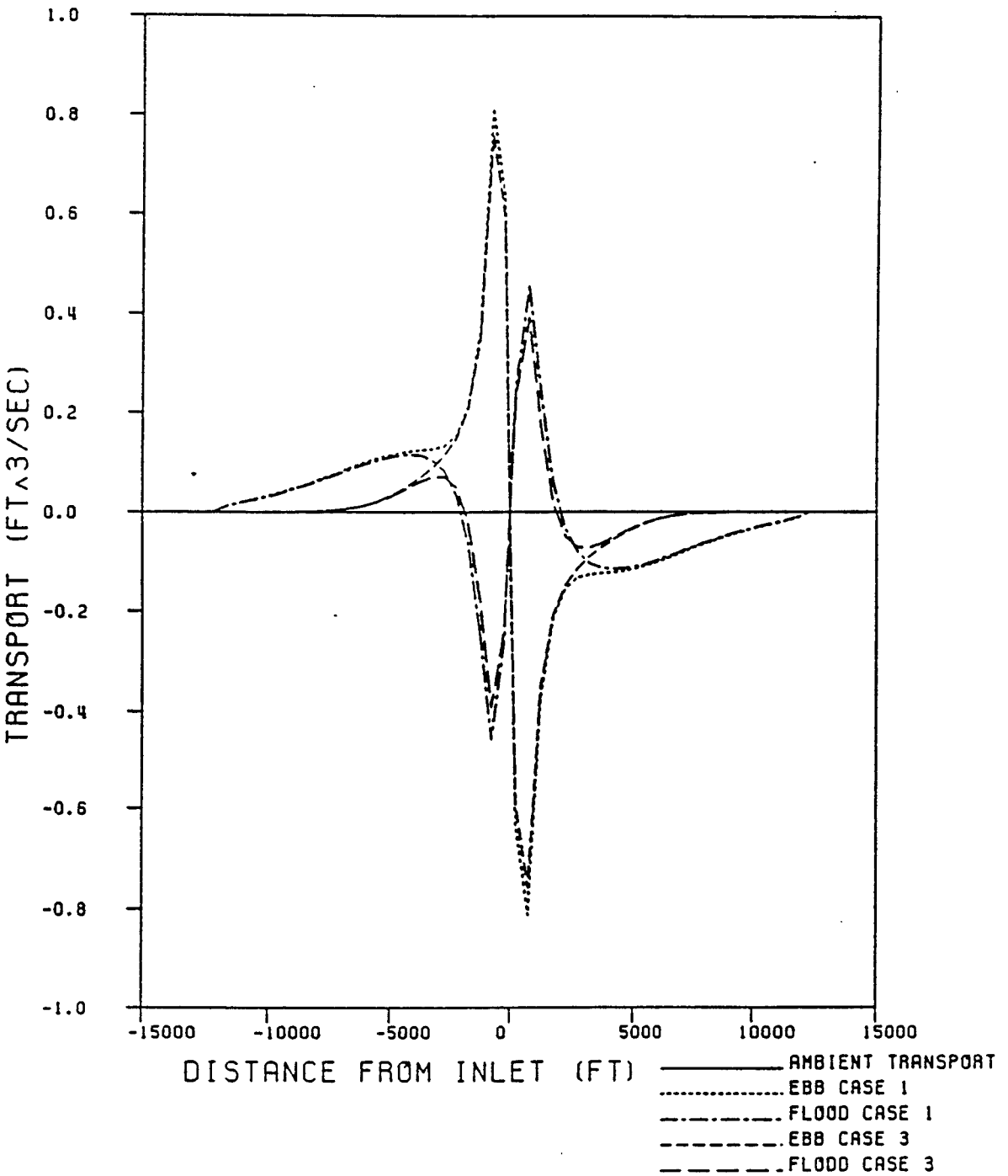

Figure 8.10: Longshore Transport for Cases 1 and 3

refraction on longshore transport approximately by a factor of two. The distances updrift and downdrift of an inlet which the longshore transport is effected by tidal currents is more dependent upon shoal size than the magnitude of tidal velocity.

The last sensitivity test performed was for location of the offshore shoal. Figure 8.11 shows the shoal configuration for case four , this shoal has the same amplitude and dimensions as the shoal for case one but is centered 2750 feet downdrift of the inlet centerline. The same current parameters that were used for case one were also used for case four to produce the current velocity field shown in figure 8.12. The result of the offset to the velocity field was to slightly increase velocity values downdrift of the inlet, because the depth would be less on the downdrift side of the inlet compared to the same location on the updrift side.

Figure 8.13 shows the transport for cases one and four. The transport for case one is antisymmetric about the inlet for both ebb and flood currents. For case 4 the refraction effects of the currents will be approximately antisymmetric about the inlet, but the refraction effects of the shoal will be antisymmetric about a centerline located 2750 feet downdrift of the inlet. The resultant transport which included the combined refraction of the shoal and the currents was not antisymmetric about any point. The ebb tide produced a transport which was greater updrift of the inlet compared to transport downdrift of the inlet, and the flood current produced a slightly larger transport downdrift of the inlet compared to transport updrift. This would result in a net transport updrift of the inlet being greater than the net transport downdrift of the inlet.The ebb and flood currents converged to a larger transport value for case four compared to case one downdrift of the inlet. The ebb and flood currents converged to a larger transport value for case one compared to case four updrift of the inlet. This difference is due to the downdrift shift of the shoal refraction effects.

8.4 Current Refraction Effects on Net Longshore Transport

The previous section presented a sensitivity analysis of current refraction to the longshore transport. This section will present the results of the net effects of refraction due

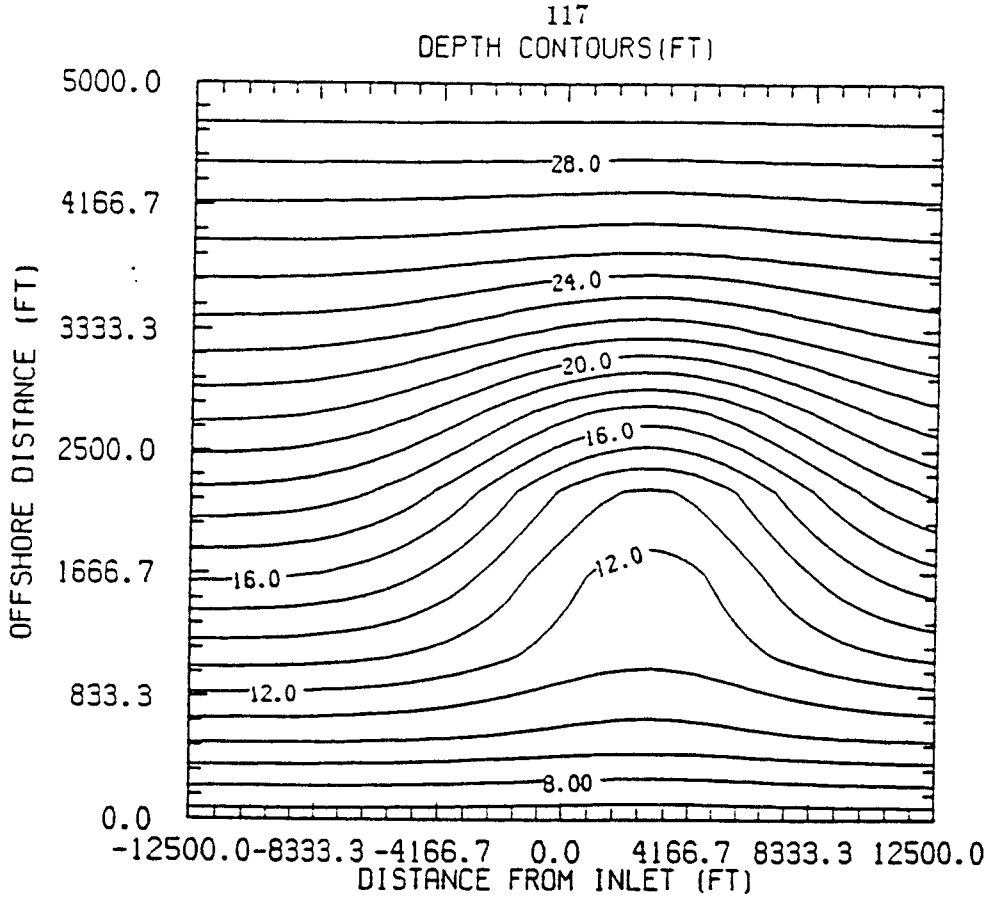

Figure 8.11: Shoal Used for Case 4

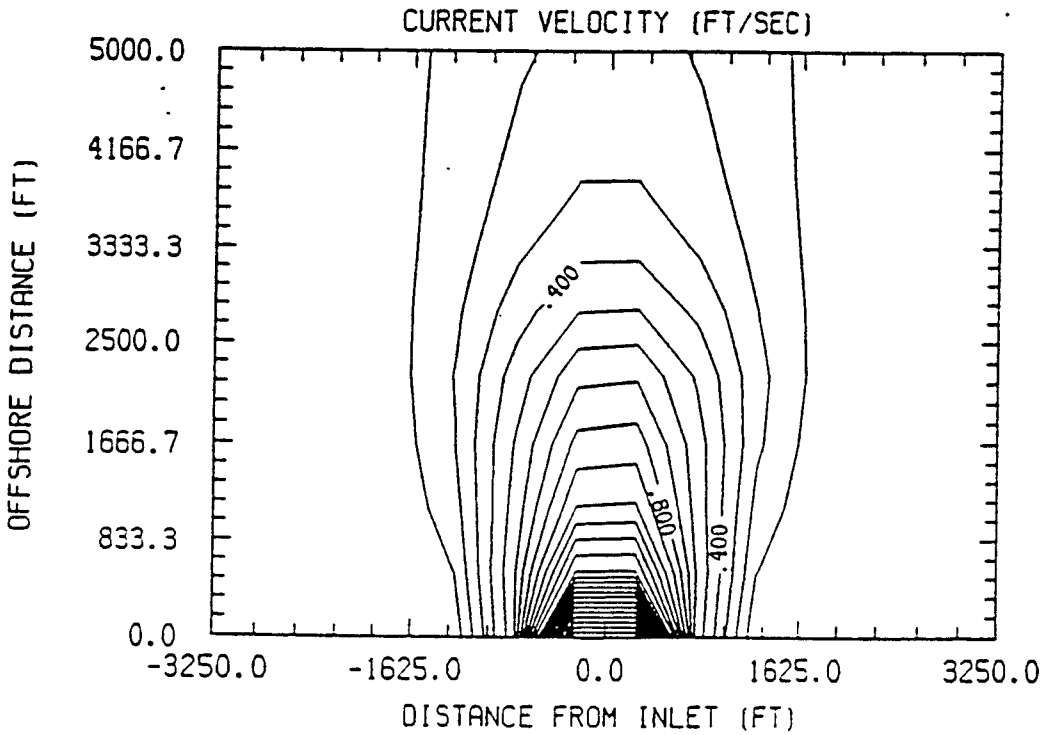

Figure 8.12: Current Velocity Field for Case 4

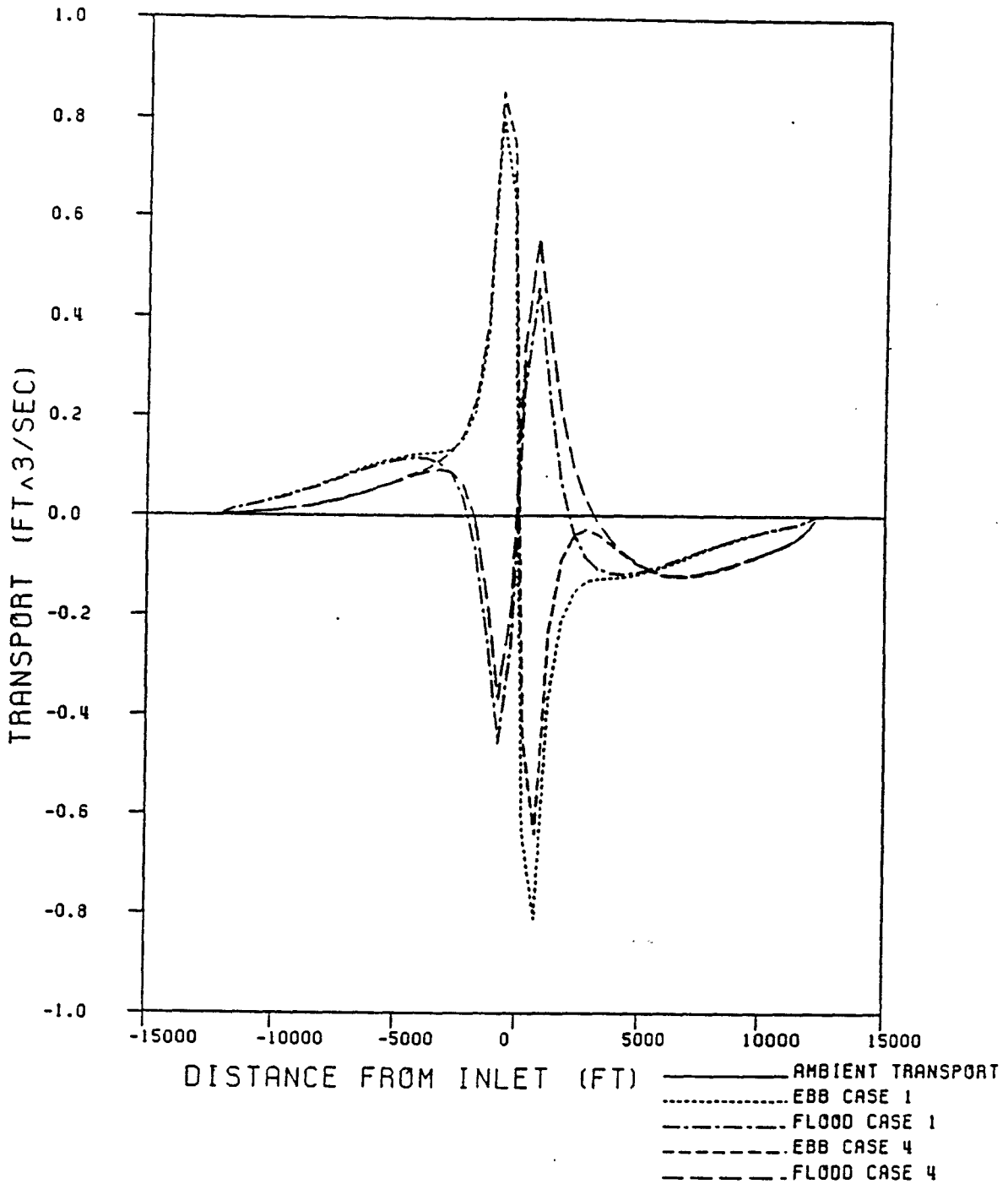

Figure 8.13: Longshore Transport for Cases 1 and 4

to currents on the longshore transport. These reults will show the effects of tidal current refraction on the longshore transport with the influence of the shoal refraction removed.

Figure 8.14 shows the transport for case one and the net transport for one tidal cycle. The net transport for one tidal cycle was determined as the average transport for each grid point if the tide is assumed to be sinusoidal. Each tidal cycle started at a current value equal to zero, then proceeded to the peak flood value then returned to zero. The current then proceeded to the peak ebb value and then returned to zero again. As can be seen in figure 8.14 the net transport is less than the average of the peak flood and ebb transport values; this is due to the sinusoidal nature of the tidal cycle. It would also appear that the net transport does not affect shorelines for a great as distance as the transport for the peak values have indicated. It is important to realize that this plot represents the transport for waves approaching the shoreline normally. The transport is due to refraction only. It could be interpreted that these transport values are the added effect to the ambient longshore transport caused by the current.

Figure 8.15 shows the net transport for one tidal cycle for case one and the difference between the net transport and the transport due to the shoal and no current. This difference then represents the net effect of refraction due to currents relative to the ambient transport. As would be expected this transport difference is less than the net transport for one tidal cycle. It can also be seen that the currents affect the transport for over two miles away from the inlet. The peak values are approximately 87,000 cubic yards per year. The average value from 3,000 to 12,000 feet away from the inlet is approximately 20,000 cubic yards per year. The overall trend for case one, is for the currents to drive sediment towards the inlet.

This same analysis was performed for various scenarios of shoal placement and wave approach. Figure 8.16 shows the net transport and the difference of the net transport and the abient transport for case four. Case four is similar to case one, except the shoal was centered 2,750 feet south of the inlet. The net tidal cycle transport is very complex, because the currents, centered at the inlet are interacting with the shoal which is offset

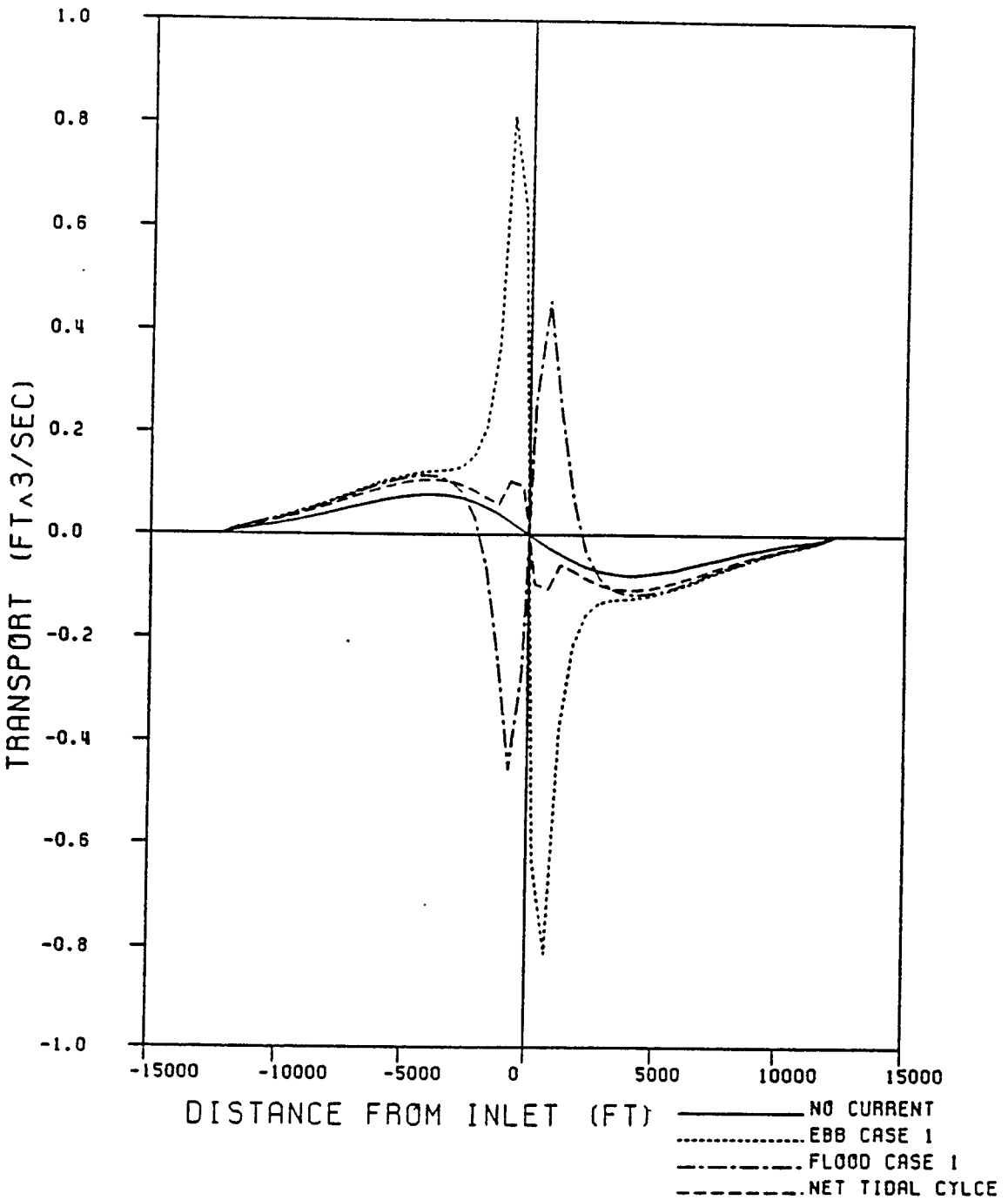

Figure 8.14: Net Transport for Case 1

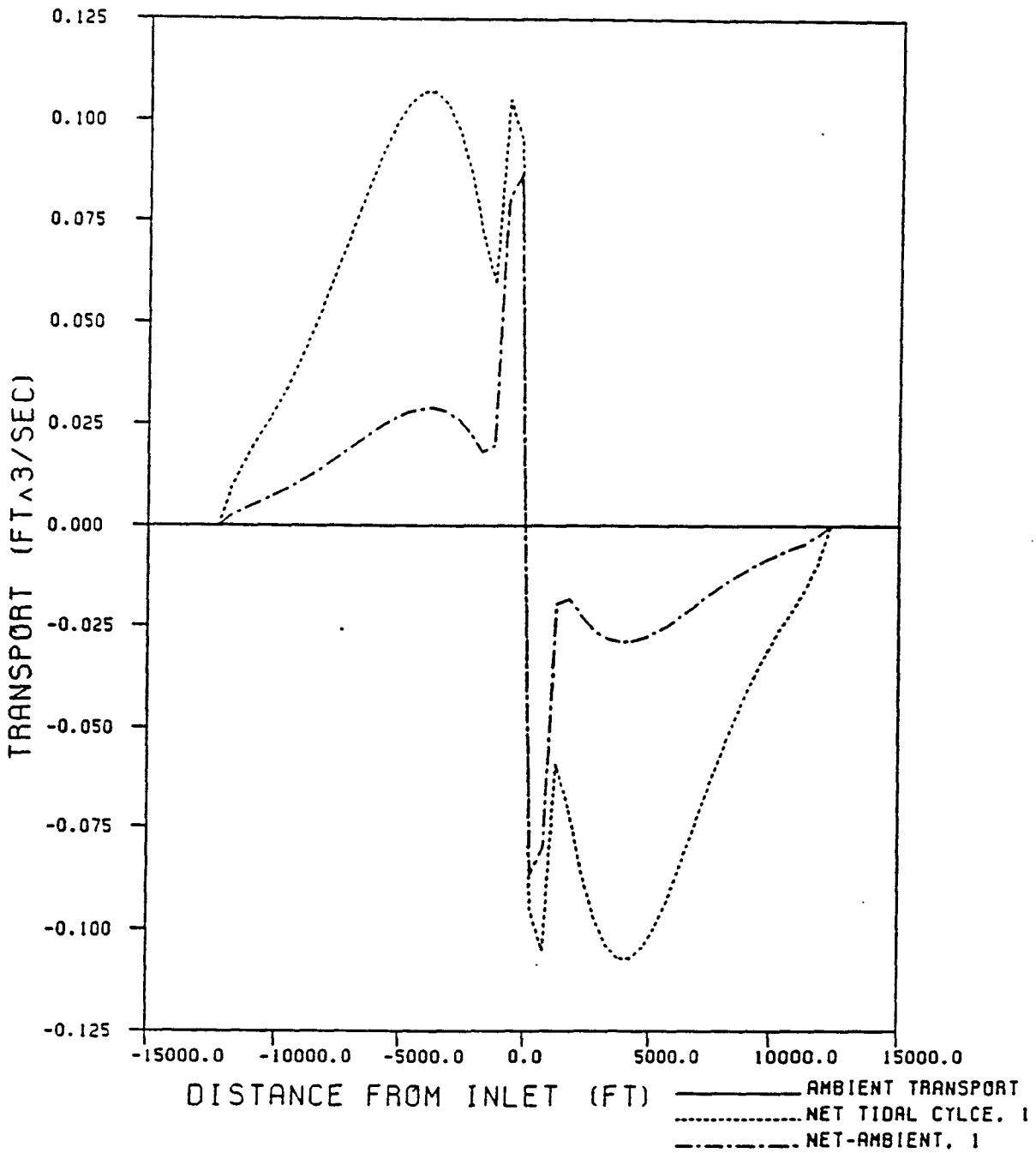

Figure 8.15: Net Transport Relative to Ambient Transport for Case 1

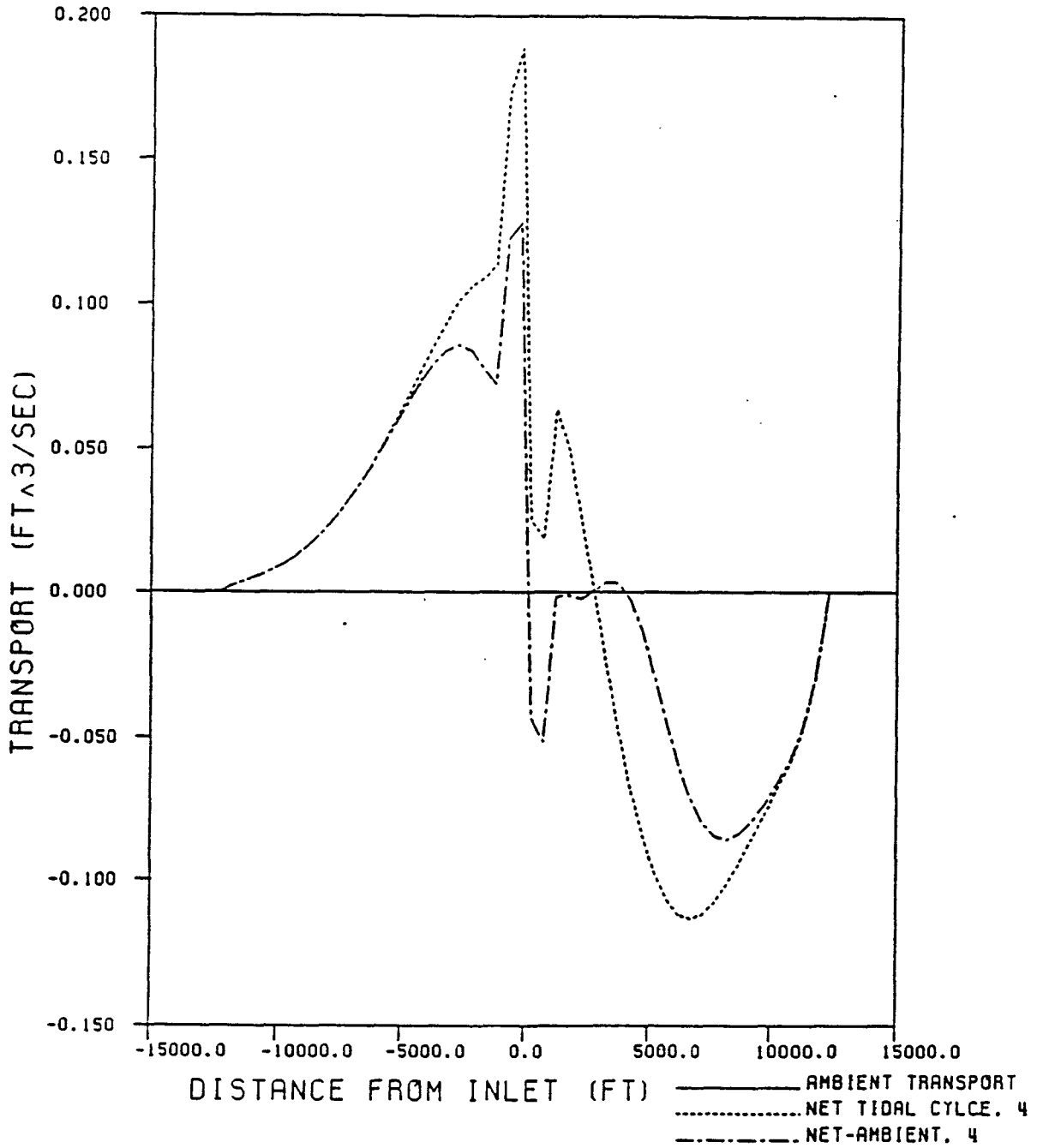

Figure 8.16: Net Transport Relative to Ambient Transport for Case 4

from the inlet. The result of this combination of two processes is that the current transport is reinforced to the north and opposed south of the inlet. This can be seen in the region 3,000 feet south of the inlet. In this region the difference between the net transport and the ambient current is zero. The net transport will tend to build up sediment north of the inlet, and south of the inlet two accretion zones will border an area of very little change.

The next case investigated was for waves approaching the shoreline at an angle. Case five is exactly the same as case one except that the waves approach the shoreline from 10 degrees north of the shore normal. The net transport and the difference between the net and the ambient transport are shown in figure 8.17. This oblique wave approach raises the mean transport from zero to approximately 0.47 ft^3/sec. The net tidal cycle transport is not antisymmetric about the inlet. The transport is greater to the north of the inlet than to the south. The shorelines are affected for the same distances updrift and downdrift as in case one, except that the updrift transport difference is greater and the downdrift transport difference is less.

The last case investigated was for waves approaching at 10 degrees with a shoal centered 2,750 feet to the south of the inlet. The net transport and the difference between the net and the ambient transport is shown in figure 8.18. The results are similar to case four except that the magnitudes immediately updrift and downdrift of the inlet differ by a much larger value for case six. For case six, there is not a zone south of the inlet where the difference between the net transport and the ambient transport is zero. This stable area has been replaced by a zone where the net transport is greater than the ambient transport. This would create two regions of accretion which border an area of erosion. These trends would be superimposed on the ambient transport.

The last scenario investigated, case six, most resembles the processes at a natural inlet. Most inlets have shoals which are elongated in the direction of the net longshore transport. The predominant drift on Florida's East coast is to the south, causing shoals generally to be offset towards the south of an inlet.

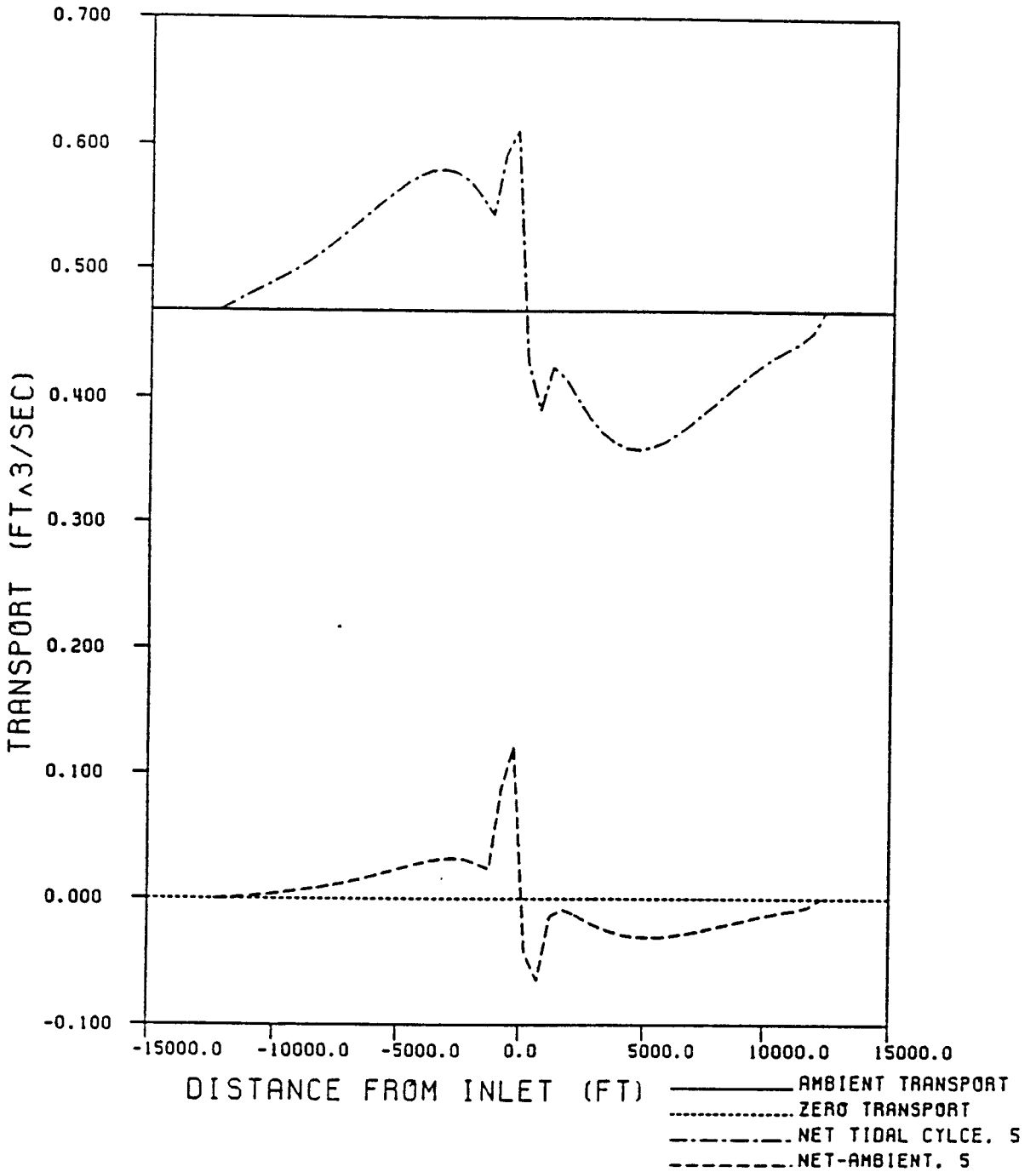

Figure 8.17: Net Transport Relative to Ambient Transport for Case 5

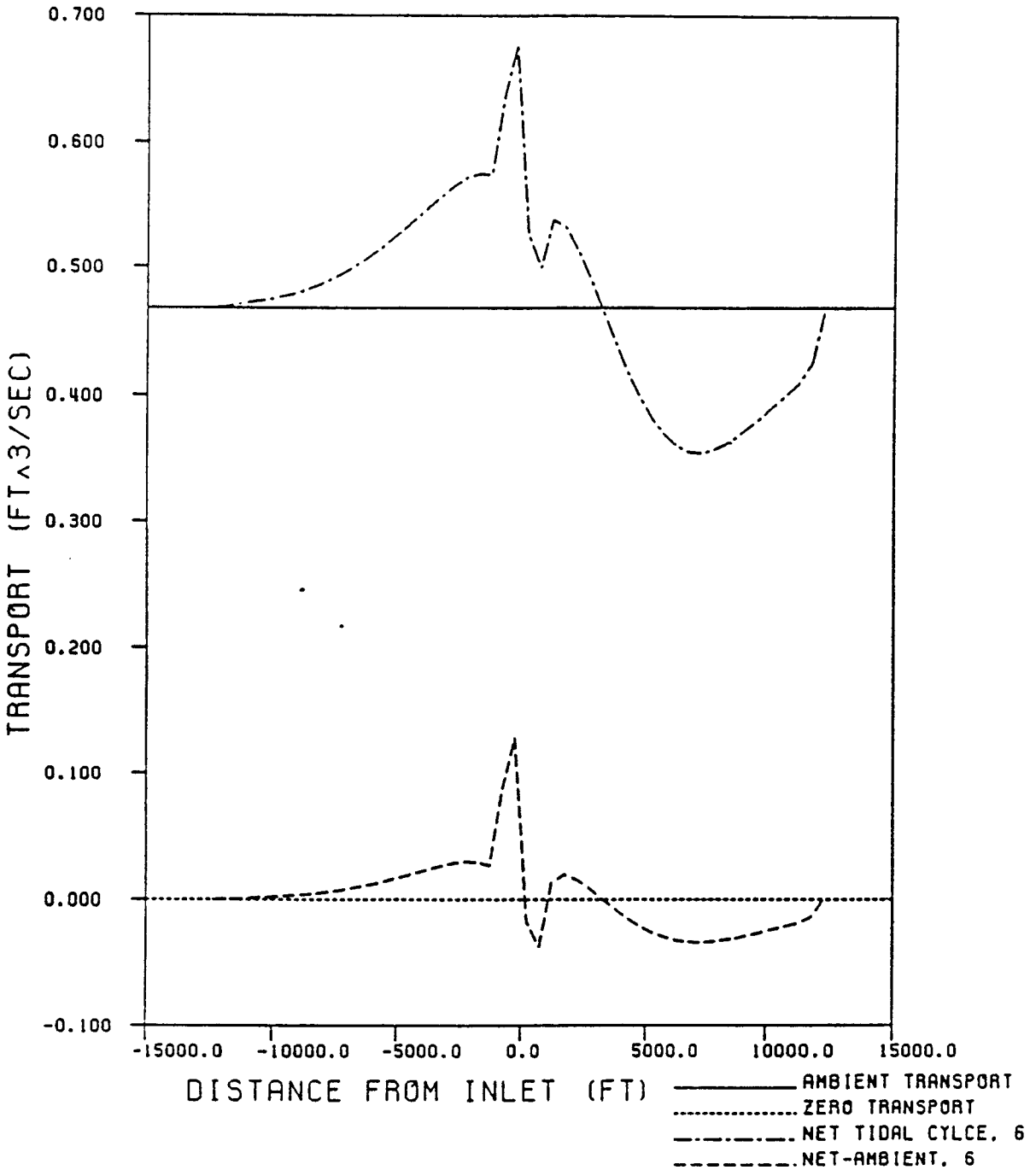

Figure 8.18: Net Transport Relative to Ambient Transport for Case 6

This qualitative analysis of current effects to the longshore transport can be helpful when attempting to interpret shoreline changes near tidal inlets. It was observed in a earlier chapter, that the maximum erosion downdrift of an inlet does not occur at the southern jetty, but is offset some distance downdrift. The analysis in this chapter did not include the effects jetted entrances have on the transport, the inlet then acts as a littoral barrier. This blockage of the longshore drift is the major cause of downdrift erosion. But this analysis has shown that refraction due to the coupling of currents and offshore shoals does drive sediment towards the inlet. This transport mechanism may be one of the major contributors to the downdrift offset of the maximum erosion point.

CHAPTER 9
CONCLUSIONS

It is commonly accepted that tidal inlets block sediment and erode downdrift shorelines. While this statement is true, it tends to over simplify the complex nature of the processes at a tidal inlet. This study has documented the shoreline changes associated at several inlets, and for all inlets the dominant trend was for the downdrift shorelines to be eroding. However, the erosion was different for each inlet, depending upon the processes affecting that particular inlet. Jetty construction, dredging practices, and sand transfer dramatically affected the rate and pattern of erosion. Most inlets were constructed when the needs of the region called for an inlet for navigation purposes or for water quality purposes. These inlets were designed with the objective of maintaining a stable opening; not minimizing the effects to adjacent shorelines. It was only after the adjacent shorelines started to change from their equilibrium state, and become altered by the inlet construction or modification, that inlet improvements designed to affect the shorelines were implemented. The offshore dumping of dredged material has removed sizable amounts of sand from the longshore transport system. With proper sand management practices, the effects of these inlets on adjacent shorelines can be minimized. The goal should be to attempt to pass the net longshore transport of sand across the inlet to the downdrift shorelines.

An analytical method to predict shoreline changes downdrift of shorelines was developed in this study. This analytical method was severely limited by the boundary conditions used in the solution. The solution assumed that the inlet totally blocked all transport to the downdrift shorelines, and used a constant wave height and wave direction. This solution was most accurate at inlets where the inlet itself was the dominant influence to longshore transport. The best results were obtained for inlets such as St. Lucie or St. Andrews.

At some inlets, shoreline changes were influenced by other factors then the inlet and the analytical solution could not predict accurately the shoreline changes.The effects of ebb shoals and wave sheltering could not be included to this analytical method. This solution also predicted maximum erosion directly downdrift of the inlet. This solution would be most useful in predicting the short term shoreline changes after inlet excavation or major modification.

It was shown that the numerical modelling of the shorelines near tidal inlets is a very complex problem. The effects of refraction, diffraction, currents and sand bypassing all need to be considered when modelling the shorelines. This numerical shoreline model would predict changes associated with changes to the natural equilibrium that existed at the inlet, prior to inlet construction or modification. For the continued development of this type of modelling better field data must be obtained. The lack of directional wave height greatly hindered the accuracy of the numerical model presented in this study. The model could predict shoreline changes for Ft. Pierce Inlet for a region farther than approximately one and a half miles downdrift of the southern jetty, but could not accurately predict changes in a sheltered zone near the inlet. This model needs to be adjusted to incorporate wave breaking on offshore shoals.

The effects of currents on the shorelines adjacent to inlets has tended to have been overlooked in the past. This study has shown that refraction due to tidal currents affect the adjacent shorelines for a considerable distance updrift and downdrift. The qualitative analysis of the net effects of current refraction indicate that currents affect the ambient transport for more than one mile away from the inlet. The currents tend to superimpose transport towards the inlet on the ambient transport. The net effect of currents is to cause less erosion immediately downdrift of the inlet, and to add to accretion of sediment updrift. The effects of tidal currents are one of the factors which offset the maximum erosion downdrift of the inlet.

BIBLIOGRAPHY

Abbot, M. B., Numerical Methods, International Course in Coastal Engineering, Delft University, 1971, pp 69-71.

Abramowitz, M. and I. Stegun, eds., Handbook of Mathematical Functions, Dover Press, New York, New York, 1965.

Arthur V. Strock & Associates, Inc., "Preliminary Report, Boca Raton Inlet and Adjacent Beaches," Deerfield Beach, Florida, 1979.

Bruun, P. and F. Gerritsen, "Natural Bypassing of Sand at Inlets," Journal of The Waterways and Harbor Division, A.S.C.E., 1959.

Coastal and Oceanographic Engineering Department, " Beach Erosion and Stabilization Considerations for Bal Harbour Village," Florida Engineering and Industrial Experiment Station, University of Florida, 1969.

Coastal Engineering Laboratory, "Coastal Engineering Study at Bakers's Haulover," University of Florida, 1958.

Coastal Engineering Laboratory Staff, "Coastal Engineering Study of Fort Pierce Beach," Florida Engineering and Industrial Experiment Station, Technical Progress Report No. 7, University of Florida, 1957.

Dean, R.G., and R.A. Dalrymple, Water Wave Mechanics for Engineers and Scientists, Prentice-Hall, Inc., Englewood Cliffs, New Jersey, 1984.

Dean, R.G., and T.L. Walton, " Sediment Transport Processes in Vicinity of Inlets with Special Reference to Sand Trapping," Estuarine Research, 11, L.E. Cronin, ed., New York Academic Press, 1973, pp 129-149.

Fluet, J.E., "The Proposed Improvement of Boca Raton Inlet, A Preliminary Investigation," Department of Ocean Engineering, Florida Atlantic University, 1973.

Marino, J.N., and A.J. Mehta, "Sediment Trapping at Florida's East Coast Inlets," Lecture Notes on Coastal and Esturaine Studies, vol. 29, D. Aubrey and L. Weishar, eds., Springer-Verlag, New York, 1989, pp 284-296.

Marino, J.N., and A.J. Mehta, "Sediment Volumes Around Florida's East Coast Tidal Inlets," Coastal and Oceanographic Engineering Department, University of Florida, 1986.

Mehta, A.J., Adams, W.D., and C.P. Jones, "Sebastian Inlet, Glossary of Inlets Report No. 3," Florida Sea Grant Program, 1976.

Mei C.C., The Applied Dynamics of Ocean Surface Waves, New York, New York, John Wiley & Sons, Inc., 1983.

O'Brien, M.P., "Equilibrium Flow Area of Inlets on Sandy Coasts," Journal of Waterways and Harbors, vol. 95, No. WW 1, A.S.C.E., 1966, pp 43-52.

Pelnard-Considere, R., "Essai de Theorie l'Evolution des Formes de Rivage en Plaaques de Sabe et de Galets," 4th Journees de l'Hydraulique, Les Engergies de la Mer, Question III, Rapport No. 1, 1956.

Penny, W.G., and A.T. Price, "The Diffraction Theory of Sea Waves and Shelter Afforded by Breakwaters," Philosophical Transactions of the Royal Society, Series A, 244, March 1952, pp 236-253.

Perlin, M., "A Numerical Model to Predict Beach Planforms in the Vicinity of Littoral Barriers," M.S. Thesis, University of Delaware, 1978.

Phlegar, W.S., "Performance Prediction of Beach Nourshiment Projects," M.S. Thesis, University of Florida, 1989.

Stauble, D.K., "Guidelines of Beach Restoration Projects, Part II Engineering," Florida Sea Grant College, Report No. 77, 1986.

U.S. Army Corps of Engineers, Jacksonville District, "Beach Erosion Control Study for Sarasota County with Environmental Impact Statement," 1984.

U.S. Army Corps of Engineers, South Atlantic Division, "National Shoreline Study Regional Inventory Report South Atlantic-Gulf Region, Puerto Rico, and The Virgin Islands," 1971.

U.S. Army Corps of Engineers, Jacksonville District, "Beach Erosion Control Study on Martin County," 1968.

U.S. Army Corps of Engineers, Beach Erosion Board, " A Study of Sand Movement at South Lake Worth Inlet, Florida," Tech. Memo No. 42, 1953.

U.S.Army Corps of Engineers, "St. Andrew Bay (St. Andrews Bay), Fla.," House Doc. 559, 80th Congress 2nd Session, 1948.

U.S. Army Corps of Engineers, "Beach Erosion Study of Baker's Haulover Inlet, Fla.," House Doc. 527, 79th Congress 2nd Session, 1946.

Walton, T.L., "Fort Pierce Inlet, Glossary of Inlets report No. 2," Florida Sea Grant Program, Report No. 3, 1974.

Walton, T.L., "Littoral Drift Computations Along The Coast of Florida by means of Ship Wave Observations," Coastal and Oceanographic Engineering Laboratory, University of Florida, Tech. Report No. 15, 1973.

Walton, T.L., and W.D. Adams, "Capacity of Inlet Outer Bars to Store Sand," Proc. 15th Coastal Engineering Conference, A.S.C.E, Honolulu, Hawaii, pp 1919-1937, 1976.